University of Calgary

PRISM Repository **https://prism.ucalgary.ca**

The Vault Open Theses and Dissertations

2018-06-26

Cold, Hot and Steam Assistant Solvent Injection Processes for Heavy Oil Recovery

Wang, Qiong

Wang, Q. (2018). Cold, Hot and Steam Assisted Solvent Injection Processes for Heavy Oil Recovery (Doctoral thesis, University of Calgary, Calgary, Canada). Retrieved from https://prism.ucalgary.ca. doi:10.11575/PRISM/32299

http://hdl.handle.net/1880/107077

Downloaded from PRISM Repository, University of Calgary

UNIVERSITY OF CALGARY

Cold, Hot and Steam Assisted Solvent Injection Processes for Heavy Oil Recovery

by

Qiong Wang

A THESIS

SUBMITTED TO THE FACULTY OF GRADUATE STUDIES

IN PARTIAL FULFILMENT OF THE REQUIREMENTS FOR THE

DEGREE OF DOCTOR OF PHILOSOPHY

GRADUATE PROGRAM IN CHEMICAL AND PETROLEUM ENGINEERING

CALGARY, ALBERTA

JUNE, 2018

© Qiong Wang 2018

ABSTRACT

Solvent-based processes such as vapor extraction (VAPEX) can be another technology that has potential to enhance heavy oil recovery in a more cost-efficient and environment friendly way. Extensive experimental and simulation studies have been conducted to evaluate VAPEX. However, theoretical modeling has not gained much progress in the past two decades. This thesis aims at adopting a series of mathematical models for a new theoretical analysis of comprehensively evaluating solvent-based recovery processes and also attempts to develop a new process to enhance production.

This thesis first develops a comprehensive theoretical analysis method for VAPEX, which considers all the major recovery mechanisms such as dynamic mass transfer, gravity drainage, multiphase flow, and boundary movement in the model. Both constant and variable diffusivity have been studied in this model, and the latter justified in the progressive change of properties such as viscosity in the media within the diffusion layer. A hot solvent injection process takes advantages of both thermal recovery processes (quick heat conduction and large viscosity reduction) and solvent-based processes (lower energy consumption and less green-house gas emission). This thesis then develops a transient mass transfer model to analyze the cold heavy oil–hot solvent mixing process during a hot solvent injection process. This mass transfer model is then incorporated into the VAPEX model to evaluate the performance of a hot solvent injection process. Key indicators such as oil production profile, injection pressure, injection temperature, solvent oil ratio, etc. have been studied to find out a quantitatively correlation.

A new hybrid process, SAVE, is proposed to enhance heavy oil recovery. In this process, a short-slug steam and a long-slug solvent are alternately injected to extract heavy oil. Simulation results show that the cumulative steam-oil ratio of SAVE is 37.26% of that of SAGD. In comparison with VAPEX, SAVE produces oil 8.4 times faster than VAPEX and its cumulative solvent-oil ratio of SAVE is only 26% of that of VAPEX. SAVE performs relatively better in thinner formations than in thicker ones.

ACKNOWLEDGMENTS

I would like to sincerely acknowledge the following individuals or organizations:

- Dr. Zhangxing Chen at the University of Calgary, my academic advisor for his guidance, patience, support, and continuous encouragement throughout the entire years of this research work;
- Dr. Jalal Abedi, Dr. Pedro Pereira Almao, Dr. Yingxu Wang, Dr. Brij Maini at the University of Calgary, and Dr. Giovanni Grasselli at the University of Toronto as the committee members of my dissertation defense for their valuable comments and constructive suggestions for the technical improvement of my research;
- NSERC/Energi Simulation and Alberta Innovates Chairs Funds/Imperial Oil Research Award for research funding;
- My parents, my sister and my niece for their love, care, concern, and support all the time.

DEDICATION

To my parents and my sister

Contents

NOMENCLATURE

Notations

A, B	coefficients
c	solvent concentration in the solvent-diluted heavy oil, vol.%
c^*	solvent saturation concentration, vol.%
c_D	dimensionless concentration, dimensionless
c_{max}	maximum solvent concentration, vol.%
c_{min}	minimum solvent concentration, vol.%
cSOR	cumulative solvent-oil ratio
D	diffusivity, m^2/s
D_{app}	apparent diffusivity in the Das–Butler model, m^2/s
D_D	dimensionless diffusivity, dimensionless
D_{eff}	effective diffusivity, m^2/s
f_o, f_s	volume fractions of oil and solvent in Lederer's equation, dimensionless
g	gravity acceleration, m/s^2
h	vertical distance, m
H	model height, m
k	permeability, m^2
k_{abs}	absolute permeability, m^2
k_{ro}, k_{rg}	relative permeability of oil phase and gas phase, dimensionless
K	K-value
L	length of the horizontal section of a horizontal well, m
l	length of a transition-zone segment, m
$n_{s,chamber}$	amount of solvent vapor in the chamber, mol
N	number of transition-zone segments
N_s, N_{s1}, N_{s2}	dimensionless number in the Butler–Morkys VAPEX model
P	pressure, kPa
q	drainage rate, m^3/s
q_o	oil production rate, m^3/s

q_{in} flowrate of solvent-diluted heavy oil entering a transition-zone segment, m^3/s

q_{out} flowrate of solvent-diluted heavy oil leaving a transition-zone segment, m^3/s

Q_o cumulative oil production, m^3/s

Q_{cal} calculated cumulative oil production, m^3/s

Q_{exp} experimentally measured cumulative oil production, m^3/s

Q_s cumulative oil injection, m^3

$Q_{s,chamber}$ amount of solvent vapor in the chamber, m^3

$Q_{s,dissolved}$ amount of solvent dissolved in oil, m^3

$Q_{s,produced}$ amount of solvent produced with oil, m^3

s Laplacian operator

S_o, S_g saturation of oil phase and gas phase, vol.%

S^* normalized saturation, vol.%

S_{oi} initial oil saturation, vol.%

S_{or} residual oil saturation, vol.%

S_{wc} connate water saturation, vol.%

t time variable, s

t_D dimensionless distance

T temperature, °C

U transition-zone boundary moving velocity, m/s

V_p pore volume, m^3

V_s sand volume, m^3

V_w water volume, m^3

$V_{m,s}$, $V_{m,o}$ molar volume of solvent and oil, m^3/mol

W model width, m

x space variable in horizontal direction, m

X location in horizontal direction, m

y space variable in vertical direction, m

Y location in vertical direction, m

Greek Symbols

α coefficient of viscosity

β coefficient of viscosity

γ specific gravity, dimensionless

γ_o, γ_s specific gravities of crude oil and liquid solvent, dimensionless

δ transition-zone thickness, m

θ inclination angle of transition zone, degree

λ weight factor in Shu's equation, dimensionless

μ viscosity of the solvent-diluted heavy oil, mPa·s

μ_o, μ_s viscosities of crude heavy oil and liquid solvent, mPa·s

ξ distance from the boundary between the solvent chamber and transition-zone to an arbitrary point in the transition zone, m

ξ_0 location of the transition-zone boundary at the beginning of a time step, m

ξ_{max} location of the transition-zone boundary next to the solvent chamber, m

ξ_{min} location of the transition-zone boundary next to the untouched heavy oil zone, m

ξ_{mv} distance of a transition-zone segment moved over a time step, m

ρ density of solvent-diluted heavy oil, kg/m^3

ρ_o, ρ_s densities of crude oil and liquid solvent, kg/m^3

τ time, s

ϕ porosity, vol.%

Ω cementation factor, dimensionless

Subscripts

app	apparent
D	dimensionless
dew	dew point
o	oil
oi	initial oil
or	residual oil
out	outflow
i	the i^{th} time interval
in	inflow
max	maximum
min	minimum
mv	movement
p	pore
s	solvent
τ	time

Abbreviations

ARC	Alberta Research Council
CHOPS	Cold Heavy Oil Production with Sands
CMG	Computer Modelling Group
CPCSI	Cyclic Production with Continuous Solvent Injection
CSI	Cyclic Solvent Injection
CSS	Cyclic Steam Stimulation
CT	Computer Tomography
DPDVA	Dynamic Pendant Drop Volume Analysis
EOR	Enhanced Oil Recovery
DSP	Dynamic solvent process
GEM	Generalized Equation of State Model Reservoir Simulator
ISC	In Situ Combustion
OOIP	Original-Oil-In-Place
RF	Recovery Factor
SAGD	Steam-Assisted Gravity Drainage
SAS	Steam Alternating Solvent
SOR	Solvent–Oil Ratio
SRC	Saskatchewan Research Council
STARS	Steam, Thermal and Advanced Reservoir Simulator
VAPEX	Vapor Extraction

Units

°API	American Petroleum Institute gravity
°C	Celsius
bbl	barrel
cc	cubic centimeter
cm	centimeter
D	Darcy
dm	decimeter
g	gram
hr	hour
kg	kilogram
kPa	kilopascal
MPa	megapascal
m	meter
min	minute
ml	milliliter
mol	mole
MPa	megapascal
mPa·s	milipascal-second
s	second

TABLES

FIGURES

CHAPTER 1 INTRODUCTION

1.1 Heavy Oil Resources

Crude oil is a major type of fossil resources that is made up of hydrocarbons with the addition of certain other substances, primarily Sulphur. Crude oil can be classified as light, medium, heavy, or extra heavy by using the American Petroleum Institute (API) gravity in the following criteria: light – API > 31.1, medium – API between 22.3 and 31.1, heavy – API < 22.3, and extra Heavy – API < 10.0. Besides low API gravity, the crude heavy and extra heavy oil are also featured by high viscosity: higher than 100 mPa·s for heavy oil and 10,000 mPa·s for bitumen [Speight, 1991]. With the new energy emerging and international oil market fluctuation, effective and economical recovery of heavy and extra heavy oil resources has become a key technical challenge.

The heavy and extra heavy crude oil resources are approximately six to eight trillion barrels (bbls), making up more than 66% of the total oil resources in the world [Dusseault, 2001]. Most of these unconventional heavy and extra heavy oil reserves are located in two regions, Canada and Venezuela, where each of them possesses two to three trillion barrels. In Canada, heavy oil and bitumen resources are mainly found in Alberta, Saskatchewan and British Columbia with an estimated original-oil-in-place (OOIP) of 2.5 trillion barrels [Dusseault, 2001; Farouq Ali, 2003]. In particularly, most of western Canadian crude heavy oil deposits are located in the three major basins in Alberta: Athabasca, Cold Lake, and Peace River.

1.2 Heavy Oil Recovery Techniques

Primary production techniques, such as cold heavy oil production with sand (CHOPS), can only recover 5–15% of the original-oil-in-place (OOIP) from western Canadian reservoirs due to reservoir pressure depletion and/or water encroachment to production wells [Ivory et al., 2010]. Second recovery techniques, such as water flooding and chemical flooding can produce some additional oil. However, the overall incremental

recovery using such flooding processes is low due to the high mobility ratio and quick water breakthrough.

1.2.1 Thermal recovery processes

Thermal-based methods, such as steam-assisted gravity drainage (SAGD), cyclic steam stimulation (CSS), and in-situ combustion (ISC) [Butler et al., 1981; Vittoratos et al., 1990; Moore et al., 1995] have been successfully applied to recover heavy oil in-situ. CSS can boost the heavy oil recovery up to 20% and a subsequent steam flooding process is required to extract the remaining oil in the reservoir [Das and Butler, 1998; Talbi and Maini, 2003], whereas ISC is not suitable for producing highly viscous crude oil [Moore et al., 1995]. SAGD is the most commercially viable and technically feasible technique to recover oil sand reservoirs with a thickness larger than 15 m. For heavy oil reservoirs thinner than that, the above-mentioned thermal techniques usually become uneconomical due to large heat losses to the overburden and underburden. Solvent-based techniques, such as solvent vapor extraction (VAPEX) [Butler and Mokrys, 1991; Das, 1998], have emerged as a promising follow-up process and attracted significant research attentions.

1.2.2 VAPEX process

The VAPEX process was first proposed and analyzed as a direct experimental and theoretical analog of SAGD [Butler and Mokrys, 1989]. In a VAPEX process, a pair of parallel horizontal wells is used to extract heavy oil with an injector above a producer. Vaporized solvent, such as light alkane (propane, butane, pentane, hexane, etc.), together with a carrier gas (methane, ethane, carbon dioxide, etc.), is injected to extract heavy oil. The major oil recovery mechanisms in this process consist of viscosity reduction through solvent dissolution (molecular diffusion and convective dispersion), possible asphaltene precipitation, and gravity drainage of the solvent-diluted heavy oil.

VAPEX, as a solvent-based process, has some distinct advantages over its counterpart SAGD. It has little need for steam generation and water treatment, and thus reduces carbon dioxide emissions and fuel costs [Butler and Mokrys, 1991; Frauenfeld et al., 1998; Luhning et al., 2003; Upreti et al., 2007]. In addition, VAPEX can upgrade crude heavy oil in situ due to asphaltene precipitation, which is beneficial for the subsequent oil

transportation and processing. Major disadvantages of VAPEX are its low oil production rate, especially in some thin heavy oil reservoirs because of slow mass transfer and inadequate gravity drainage.

1.3 Problem Statement and Research Objectives

1.3.1 Physical modeling of VAPEX

Extensive lab-scale experimental studies have been conducted in the literature to explore the potential of the VAPEX process. Various types of physical models, oil and solvent samples, and operating schemes have been investigated. Physical modeling can lead to better observed oil production but it is difficult to evaluate a specific factor since it may involve too many mechanisms. In addition, laboratory experiments have some inherent limitations such as wall effect and pressure gradient modeling. Moreover, it is difficult to upscale experimental results among different scales and especially from lab-scales to field scales.

1.3.2 Analytical modeling of VAPEX

Unlike physical modeling, a theoretical study of VAPEX has not gained much progress in the past two decades. The existing analytical models of VAPEX over-simplify some physical phenomenon, such as a constant boundary moving velocity and steady-state mass transfer. Besides, they are unable to describe the dynamic solvent chamber evolution in space and are unreliable for oil production prediction in either lab-scale or field-scale cases [Jia et al., 2014; Baytex, 2005].

1.3.3 Numerical modeling of VAPEX

Numerical simulation is another important tool to analyze the VAPEX process. It is able to handle both laboratory experiment and real field implementation. However, the reliability of simulation results is bothered by numerical dispersion which is inherent to numerical methods. For example, numerical dispersion can be much larger than physical dispersion. In particular, numerical simulation models usually use a gridblock size that is much larger than the transition zone thickness, making it difficult to accurately capture fluid properties inside the transition zone.

1.3.4 Research objectives

Aiming at the aforementioned technical issues with VAPEX, this thesis is expected to achieve the following objectives:

1. To model the solvent chamber evolution during the solvent chamber spreading and falling phases;
2. To characterize the mass transfer process in the solvent chamber boundary;
3. To evaluate the performance of warm VAPEX processes; and
4. To propose a new technique that is able to improve an oil production rate and lower solvent consumption.

1.4 Thesis Outline

This thesis is composed of seven chapters. Specifically, Chapter 1 gives an introduction to the thesis research topic together with the purpose and scope of this study. Chapter 2 provides an up-to-date literature review on the VAPEX theoretical modeling methods. Chapter 3 describes a new analytical study of the VAPEX process. The mathematical models, solution procedures, as well as a numerical model for the purpose of comparison are presented in this chapter. Chapter 4 describes a new method to determine the effective diffusivity between heavy oil and vaporized solvent through the newly-developed VAPEX theoretical model. Chapter 5 evaluates the performance of a hot solvent injection process including its oil production rate, chamber development, as well as solvent retention and a solvent-oil ratio. Chapter 6 simulates a novel heavy oil recovery process: steam-assisted vapor extraction (SAVE) for enhancing heavy oil recovery. Chapter 7 summarizes the major scientific findings of this thesis and provides some technical recommendations for future studies.

CHAPTER 2 LITERATURE REVIEW

This chapter comprehensively reviews a solvent-based heavy oil recovery process, namely, VAPEX and its variants in the literature, including experimental, simulation, and theoretical studies. Major conclusions from experimental studies of VAPEX are summarized, and merits and limitations of simulation and theoretical studies are clarified.

2.1 VAPEX Concept and Mechanisms

Butler and Mokrys [1989] first proposed the concept of VAPEX as a direct solvent-analogy of SAGD. In a typical VAPEX process, a pair of parallel horizontal wells is used. A solvent vapor (typically a lighter hydrocarbon gas) with or without a carrier gas is injected into a reservoir through the upper horizontal injection well, and heavy oil is diluted by the solvent, drained downward by gravity, and produced from the lower horizontal well (**Figure 2.1**). Three zones are formed during this process: a solvent vapor chamber, an intact heavy oil zone, and a transition zone in between.

2.2 VAPEX Modeling

2.2.1 Physical modeling

Since its first appearance, VAPEX has attracted tremendous research attention and has been studied extensively, especially in Canada. **Table 2.1** summarizes the laboratory experimental analysis of the VAPEX processes in the literature. It can be seen that a variety of solvent vapors (mainly light alkanes such as propane, butane, pentane, carbon dioxide, toluene, etc.) and carrier gases (usually non-condensable gases including methane, ethane, nitrogen, carbon dioxide, steam, etc.) have been attempted to extract more than ten different heavy oil and bitumen samples from western Canadian petroleum reservoirs. Three types of physical models, i.e., micromodels, Hele-Shaw models, and sandpacked models, are utilized to analyze effects of a number of petrophysical and operating conditions on the VAPEX performance. Main conclusions from these studies are summarized below:

:

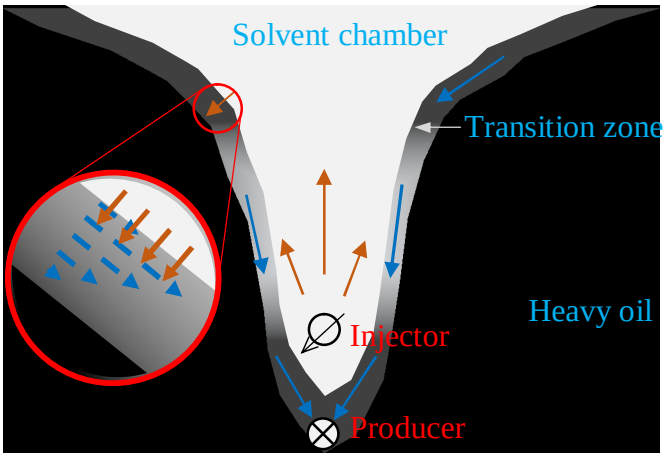

Figure 2.1 Schematics of VAPEX.

Table 2.1 Summary of VAPEX experimental studies in the literature.

Bitumen	Solvent	Model Type	Permeability Darcy	Objectives	Reference
AB	Toluene	Hele–Shaw	64–19600	VAPEX mechanisms, permeability	Butler and Mokrys, 1989
LM	C_3	Hele–Shaw	1356	Propane co-injection with hot water	Butler and Mokrys, 1991
LM	C_2, C_3	Sandpack	81030	Solvent type, asphaltene precipitation	Butler and Mokrys, 1993
AB	C_3, C_4, N_2	Sandpack	217	Solvent mixture, well configuration, solvent injection rate	Jiang and Butler, 1997
LM	C_4	Sandpack	217	Thin low-permeability layers and lenses	Jiang and Butler, 1996
PR, CL, LM	C_3, C_4, N_2	Sandpack	43.5, 191.1–195.8	Carrier gas, upward leaching	Das and Butler, 1995
PR, CL, LM	C_3	Hele-Shaw	830	Asphaltene precipitation	Das and Butler, 1994
DV, PN	C_3	Hele-Shaw	5376	Interfacial mass transfer	Boustani and Maini, 2000
NCL	C_3	Sandpack	—	Visualization (Magnetic Resonance Imaging)	Fisher et al., 2000
LM	Toluene	Sandpack	8, 88, 90	Dispersive mass transfer, visualization (CT scanning)	Cuthiell et al., 2003
—	C_1, C_4	Sandpack	220, 330, 640	Upscaling	Karmaker and Maini, 2003
—	CO_2	Sandpack	640	CO_2-based VAPEX	Talbi and Maini, 2003
—	C_4	Micromodel	—	Pore-scale mechanisms (mass transfer, deasphalting, drainage, capillarity)	James and Chatzis, 2004
DA, EP	C_4	Sandpack	220, 330, 640	Upscaling (model height), bitumen types, physical model shape	Yazdani and Maini, 2005
KB	C_4	Sandpack	2.9/4.3, 90, 400	Bottom water	Frauenfeld et al., 2006
FL	C_4	Sandpack	10	Connate water	Etminan and Maini, 2007
LM	C_1, C_2, C_3, steam	Sandpack	250	Solvent mixture, solvent and steam, electrically heated injector	Frauenfeld et al., 2007
LM	C_3, C_4	Sandpack	7, ~130, ~420	Permeability	Zhang and Gu, 2007
AB-1	C_3, CO_2	Sandpack	640	Solvent and carrier gas	Zedah and Maini, 2008

Table 2.1 Summary of VAPEX experimental studies in the literature (Cont'd)

Bitumen	Solvent	Model Type	Permeability (Darcy)	Objective	Reference
EP	C_3, toluene	Sandpack	2.7	Asphaltene precipitation in porous media	Haghighat and Maini, 2010
CL, LM	nC_5	Sandpack	220, 830	Solvent temperature (superheated solvent), asphaltene precipitation	Rezaei et al., 2010
Glycerol	Ethanol	Sandpack	43	Oil drainage rates	Alkindi et al., 2012
heavy oil	C_1, nC_4	Sandpack	<10, 30, 301, 2960	3D physical model, waterflooding, Visualization (excavation)	Knorr and Imran, 2012
LM	C_3	Sandpack	4.3-5.7	Foamy oil	Jia et al., 2013
Glycerol	Ethanol	Sandpack	10, 150	Sandpack heterogeneity	Al-Hadhrami et al., 2014
Mineral oil	C_5, toluene	Sandpack	—	Visualization (laser)	Fang and Babadagli, 2014
LM	C_3, C_4, CO_2	sandpack	5.12-9.63	Effect of model size	Mohammad and Torabi, 2015

Note: Abbreviation for bitumen sources

AB-1/AB-2	Athabasca/Atlee Buffalo
BL	Burnt Lake
CL	Cold Lake
DA	Dina
DV	Dover
EP	Elk Point
FL	Frog Lake
KB	Kerrobert
LM	Lloydminster
LD	Lindbergh
NCL	North Cactus Lake
PN	Panny
PR	Piece River
KM	Kuhe-Mond

- *Solvent types.* A variety of gases (ethane, propane, butane, heptane, carbon dioxide, toluene, etc.) have been used as a pure single solvent or a solvent mixture. Methane, carbon dioxide and nitrogen are used as non-condensable carrier gases in the VAPEX process. It is found that vaporized solvent performs better than liquid solvent due to larger gravity drainage forces. Under similar conditions, propane works better as a pure solvent, and a propane and carbon dioxide mixture leads to a higher oil production rate than other pure or mixed solvents.
- *Solvent Injection temperature.* In most studies, the solvent injection temperature is set the same as a reservoir temperature. However, it is found that injection of heated solvent or co-injection of solvent and steam can lead to a higher oil production rate while keeping heat losses within an acceptable range.
- *Solvent Injection pressure.* A higher oil production rate can be obtained when the operating pressure is set close to and slightly below its dew point pressure for a pure solvent or a saturation pressure for a solvent mixture.
- *Sandpack heterogeneity.* An effect of matrix heterogeneity on VAPEX performance is complicated. Thin low-permeability layers or lenses can affect the solvent chamber evolution, oil flow paths and thus the oil production rate. Generally, low permeability zones can reduce the overall arithmetic mean permeability as well as oil production.

2.2.2 Mathematical modeling

Table 2.2 lists the theoretical studies or mathematical models of the VAPEX process in the literature, including the model types, principal presumptions, functions, and limitations. The following sections describe some of these models in slightly more details. Butler and Mokrys [1989] developed the first analytical model to predict the oil production rate of their VAPEX experiments in a Hele−Shaw cell. This model assumes pseudo-steady state mass transfer between solvent and bitumen, a constant interface advancing velocity, and uniform viscosity/density/diffusivity distribution across a transition zone, and ignores interfacial tension and the drainage of undiluted bitumen. A stabilized oil production rate is derived by coupling Fick's 1st Law, the Darcy equation, and mass balance equation:

$$q_o = 2L\sqrt{2kg\phi\Delta S_o N_s H} \tag{2.1}$$

$$N_s = \int_{c_{min}}^{c_{max}} \frac{\Delta\rho(1-c)D}{\mu c} dc \tag{2.2}$$

where q_o is the oil production rate, m^2/s; k is the permeability, Darcy; g is the gravitational acceleration, m/s^2; ϕ is the porosity, vol.%; $\Delta S_o = S_{oi} - S_{or}$ is the oil saturation change in the solvent chamber; S_{oi} is the initial oil saturation and S_{or} is the residual oil saturation; H is the height of the sand-packed physical model, m; N_s is the dimensionless number and in the integrand $\Delta\rho$ is the density difference of the solvent-diluted heavy oil and the liquid solvent, kg/m^3; μ is the viscosity, mPa.s; D is the diffusion coefficient, m^2/s; This analytical model indicates that the stabilized oil production rate is a constant in a given reservoir.

Das [1995] investigated the VAPEX process in porous media and found that the oil production rate in a sandpack was three to five times higher than that predicted by using the Butler−Mokrys model. He attributed the higher production in porous media to capillary imbibition, an enlarged bitumen–solvent contact area, increased solvent solubility, and enhanced surface renewal at the interface. Das modified the Butler–Mokrys model by introducing an apparent diffusion coefficient to replace the earlier intrinsic molecular diffusion coefficient:

$$D_{app} = D\phi^{\Omega} \tag{2.3}$$

where Ω is a cementation factor that expresses the consolidation of particles in the matrix. The experimental measurement of Ω is between 1.3 and 2.2, and it changes with the rock lithology. With D_{app}, following the same derivation procedures, Das obtained a new formula to estimate the oil production rate in a sandpack:

$$q_o = 2L\sqrt{2kg\phi^{1-\Omega}\Delta S_o N_s (h-y)} \tag{2.4}$$

Table 2.2 Summary of VAPEX theoretical modeling studies in the literature.

Type	Major Assumptions	Prediction	Limitation	Reference
Analytical	• Pseudo-steady state mass transfer • Constant boundary moving velocity	• Oil prod rate in bulk phase	• Chamber development • Multi-phase flow	Butler and Mokrys, 1989
Analytical	• Same as those in B–M model[1] • Apparent diffusion coefficient	• Oil prod rate in porous media	• Same as those in B–M model	Das and Butler, 1996
Empirical		• Oil prod rate as a function of drainage height	• Same as B–M model • Regressed coefficient valid to specific cases	Yazdani and Maini, 2006
Analytical	• Same as those in B–M model • Concentration-dependent diffusivity	• Oil prod rate in porous media	• Same as those in B–M model	Heidari, 2008
Analytical	• Parallelogram transition zone • Linear drainage velocity across TZ	• Oil prod rate in porous media • Solvent chamber evolution during spreading and falling phases	• Mass transfer process • Multi-phase flow	Moghadam et al., 2008
Analytical	• Multi-phase flow • Pressure gradient in fluid flow	• Oil prod rate in lateral well configuration	• Chamber development	Knorr and Imran, 2012
Semi-analytical	• Single phase flow in TZ	• Oil prod rate in porous media • Chamber evolution during spreading and falling phases	• Multi-phase flow	Jia et al., 2013
Analytical	• Circular solvent chamber boundary	• Oil prod rate in porous media • Chamber evolution during rising/spreading/falling phases	• Mass transfer process • Multi-phase flow	Lin et al., 2014
Analytical	• Parabolic solvent chamber	• Oil prod rate in porous media • Chamber evolution during spreading/falling phases	• Mass transfer process • Multi-phase flow	Ma et al., 2017

Note: [1]Butler–Mokrys Model [1989]
[2]Transition zone

Yazdani and Maini [2007] examined the effect of oil drainage height on stabilized oil drainage rates. Through a series of VAPEX tests in physical models of three different heights, they regressed two empirical correlations to upscale oil production rates:

$$q_o = 0.0174 H^{1.26} \sqrt{k\phi^{\Omega}} \tag{2.5}$$

$$q_o = 0.0288 H^{1.13} \sqrt{k\phi^{\Omega}} \tag{2.6}$$

The constant coefficient in the above equation represented the combined effect of the gravity drainage, mass transfer, residual oil saturation, and original oil viscosity. They found that the oil production rate is a function of the drainage height to the power of 1.13–1.26 rather than 0.5 as predicted in the previous models. Although the empirical coefficients are still uncertain for a general application, this model indicates that the relationship between an oil production rate and drainage height can be more complicated than expected.

Moghadam et al. [2008] developed a new theoretical VAPEX model to predict oil production and solvent chamber evolution during the rising and spreading phases. They assumed the transition zone having two straight-line boundaries with a space varying with time, and also they considered the gravity drainage velocity to be a linear function of the transverse distance from the interface (**Figure 2.2**). Cumulative oil production rates during the solvent chamber spreading and falling phases were derived by coupling the Darcy equation and some geometric relations:

$$Q_o = H^2 \phi \Delta S_o \cot\theta \text{ (for the spreading phase)} \tag{2.7}$$

$$Q_o = HW\phi \Delta S_o \left(2 - \cot\theta_s \tan\theta\right) \text{ (for the falling phase)} \tag{2.8}$$

where Q_o is the cumulative oil production rate, m^2; W is the model width, m; θ is the inclination angle, degree; θ_s is the inclination angle of the transition zone at the end of the solvent chamber spreading phase. Transition zone thickness is used as a tuning parameter and determined by the best fitting between theoretically predicted and experimentally measured cumulative oil production data.

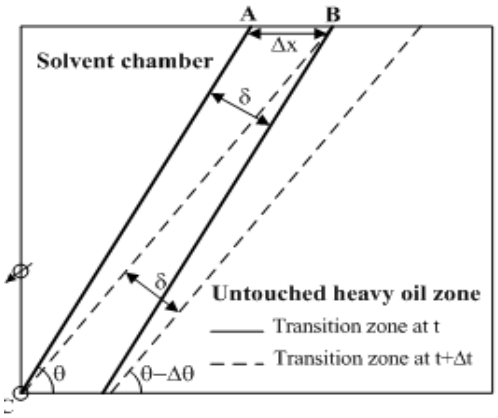

(a)

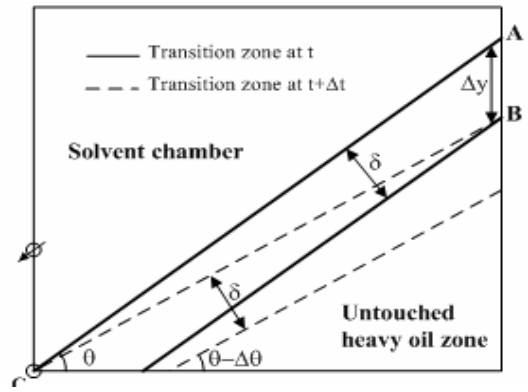

(b)

Figure 2.2 Approximation of solvent chamber as a linear profile [Moghadam et al., 2008].

Knorr and Imran [2012] considered a different well configuration, an injector and a producer are placed laterally apart, and they named this process as solvent vapor extraction (SVX). They extended the Das and Butler model by including more mechanisms (such as multi-phase flow, pressure gradient-driving drainage, and convective dispersion) into a new analytical model to predict an oil production rate:

$$Q_o = 2\sqrt{2\phi\Delta S_o k_{abs}\left(\frac{\Delta p}{H}N_{s1} + gN_{s2}\right)H} \tag{2.9}$$

$$N_{s1} = \int_{c_m}^{c_i} \frac{Dk_{ro}}{\mu} d\frac{c(1-c)}{c} \tag{2.10}$$

$$N_{s2} = \int_{c_m}^{c_i} \frac{\Delta\rho Dk_{ro}}{\mu} d\frac{c(1-c)}{c} \tag{2.11}$$

where k_{abs} is the absolute permeability, Darcy; Δp is the pressure difference between an injector and a producer, Pa; k_{ro} is the oil-phase relative permeability, unity; N_{s1} and N_{s2} are two dimensionless integration terms.

Jia et al. [2014] developed a mathematical model for a VAPEX transition zone. This model approximates the transition zone as a series of segments with a piecewise linear boundary. Various mechanisms including transient mass transfer, gravity drainage, and a moving boundary problem are considered in this model. Fick's 2nd law, mass balance equation, and the Darcy equation are coupled together to describe the solvent chamber evolution during its rising and spreading periods. However, this model is unable to deal with either multiphase flow in a mobile layer or mass transfer during the rising phase.

Lin et al. [2014] assumed the solvent chamber has a circular shape throughout the entire VAPEX process. Based on this presumption, they developed a mathematical model to predict an oil production rate during the solvent chamber rising, spreading, and falling phases:

$$q = \frac{\pi}{4}\Delta S_o \phi H^2 \text{ (for rising phase)} \tag{2.12}$$

$$q = \Delta S_o \phi d H^2 \frac{\pi - \theta + \sin\theta\cos\theta}{(1+\cos\theta)^2} \text{ (for spreading phase)} \tag{2.13}$$

$$q = \Delta S_o \phi d L^2 \left[\frac{\pi - \theta}{4 \sin^2 \theta} + \frac{H}{L} - \frac{2 + \cos\theta}{4 \sin\theta} \right] \text{ (for falling phase)} \quad (2.14)$$

An objective function is developed and minimized by adjusting the transition zone thickness in their model. It is found that the prediction of the solvent chamber shape is fairly consistent with their experimental observation in high permeability scenarios, but poorly matched in low permeability scenarios.

2.2.3 Numerical simulation

Table 2.3 shows a summary of the VAPEX simulation studies in the past twenty years, including each study's bitumen and solvent types, simulators applied, model scales, and conclusions made from these simulation studies.

First, regarding the simulation tool for VAPEX, there are mainly two simulators used in the literature, a semi-compositional simulator Steam, Thermal and Advanced Reservoir Simulator (STARS), and a fully compositional simulator Generalized Equation of State Model Reservoir Simulator (GEM). Although GEM seems more accurate in simulating the mass transfer process in VAPEX, it is usually time-consuming and unable to handle non-equilibrium solvent solubility. STARS simplifies the gas-bitumen system by using vapor-liquid K-values. It is much more flexible than GEM since it does not require additional fitting to obtain an adequate equation-of-state description of fluids.

Second, simulation studies have been performed in the literature to either study the effects of the reservoir/fluid properties and operating parameters or simulate and validate the laboratory tests. All the major aspects of the VAPEX process have been investigated through simulation studies, such as asphaltene precipitation, molecular diffusion and convective dispersion, operating temperature and pressure, solvent composition and bitumen types, fingering in early VAPEX, upscaling, and multi-phase flow (relative permeability). Some simulation results are reasonable and can provide a better understanding or an optimal design of the VAPEX process, while others are difficult to comprehend or even erroneous due to numerical dispersion inherent to the finite difference method.

Table 2.3 Summary of VAPEX simulation studies in the literature.

Bitumen	Solvent	Simulator	Height	Understanding	Reference
LD	C_3, CO_2	Compositional model	20	• Asphaltene is modeled as a solid phase • Dispersivity is important for history matching	Nghiem et al., 2001
LM	toluene	STARS	0.3	• Match viscous fingering, breakthrough time, oil rates	Cuthiell et al., 2003
	C_3	GEM	20	• High diffusion coefficient is used for history match • Reducing gridblock size for mobile layer	Das, 2005
LM	C_3	STARS	0.698	• Asphaltene precipitation does no harm to fluid flow • Operating pressure and gas rate control are critical • Linear relative permeability curves is suitable	Wu et al., 2005
—	C_4	COMSOL	1	• Finite element model can match VAPEX oil rate • Effect of mesh size on oil rates in within 15%	Tam, 2007
KM	C_3	GEM	0.673, 30	• Solvent flows quicker in fractured reservoir due to faster communication through fracture networks;	Rahnema et al., 2008
DA, EP	C_4	GEM	0.6	• Transition-zone thickness is about 0.3–1.5 cm • Gridblock size needs to be 1/5–1/10 of TZ thickness • Dynamic gridding refinement can be an option • Numerical dispersion is larger than physical dispersion	Yazdani and Maini, 2009
LM	C_3	Compositional model	0.698	• Boundary layer can be captured with one coarse gridblock • Three-phase flow can be characterized in one gridblock	Nourozieh et al., 2011
LM	C_1, C_4	STARS	0.1, 0.52	• Early stage of VAPEX is difficult to match • Wall effects explains time lag in 3D experiments	Xu et al., 2012
DA, EP	C_4	Tetrad	0.15, 0.3, 1	• Mechanical dispersivity can be 10 times of molecular diffusivity in lab tests, but molecular diffusivity may dominate mass transfer in field operation • Oil rate increases near-linearly with model height	Cuthiell et al., 2013
—	C_3, C_4	STARS	25	• Different solvent injection schemes • Economic analysis for hot solvent selection • Solvent-heat combination can be profitable	Leyva and Babadagli, 2017

Third, like experimental or theoretical studies, simulation has its own limitations that need more attentions to be paid for the following issues: (1) Due to the extremely small physical diffusion coefficient between solvent and heavy oil, the adjusting of an effective diffusion coefficient in a simulator needs to be reasonably constrained, as the numerical dispersion may affect simulation results to a larger extent than the physical diffusion/dispersion. (2) Given that the transition zone is rather thin (about 1 cm wide in lab-scale tests), a gridblock size and a time step need to be reasonably set in order to effectively reduce numerical dispersion and accurately capture the transition zone. (3) There is still lack of sound rules for the tuning of relative permeability and capillary pressure for history match.

2.3 Warm VAPEX

In a warm VAPEX process, a solvent is heated so that it condenses in situ and the liquid essentially strips heavy oil/bitumen. In such a process, a heated solvent carries sensible heat to the VAPEX interface where it condenses at the bitumen surface. The bitumen viscosity is reduced due to solvent dissolution (both diffusion and convection). The sensible heat transfers from the solvent to the bitumen via thermal diffusion. Farouq Ali and Snyder [1973] and Wang and Farouq Ali [1980] suggested hot miscible displacement using heated solvents. Butler and Jiang [2000] and Karnaker and Maini [2003] examined the effect of an increased reservoir temperature. Butler and Jiang [2000] conducted VAPEX experiments in a large rectangular packed glass bead model saturated with an Atlee Buffalo heavy oil with a viscosity of 870 mPa·s. Using propane as the solvent, production rates increased 21.5% when the operating temperature was elevated from T = 21°C to T = 27°C. Karnaker and Maini [2003] conducted a VAPEX test with a sandpack permeability of k = 340 Darcy and a bitumen viscosity of μ_o = 40,000 mPa·s (at 10°C), and observed an 18% increase in oil production when the operating temperature was increased from 10°C to 19°C. Nsolv injects moderately heated (30–50°C) and pure solvent (propane, butane) to produce heavy oil [Nenniger, 2002].

2.4 Hybrid VAPEX

In a hybrid VAPEX process, also known as solvent-assisted SAGD processes, steam and solvent or non-condensable gas are simultaneously co-injected. Gupta et al. [2002, 2005, 2007] proposed solvent-aided process (SAP), in which butane, as an additive, is co-injected with steam in a SAGD process. Field pilot tests reported encouraging results with an accelerated oil production rate and improved economics. Nasr et al. [2003, 2006] suggested that using C_7–C_{12} as an additive to steam, injected at 1400 kPa can reduce the solvent content from 10 to 5 vol.%. Léauté [2002, 2005, 2007] proposed Liquid Addition to Steam for Enhancing Recovery (LASER) to uplift an oil-steam ratio and evaluate the diluent recovery. In this process, a small amount of a liquid hydrocarbon (C_{5+}) (3–10 vol.%) is injected with steam at certain stages of a CSS process. The solvent used is a light-hydrocarbon condensate or diluent, which is the same solvent used for mixing with the bitumen to produce a sale blend to meet pipeline specifications. The solvent co-injection ranges from a low concentration of a heavy solvent (e.g., hexane and pentane) to a high concentration of light solvent (e.g., propane and butane).

2.5 Key Issues

2.5.1 Mass transfer

Diffusion equation

A heavy oil viscosity reduction through sufficient solvent dissolution is one of the most important mechanisms of VAPEX. This process is essentially a mass-transfer process between the solvent and heavy oil, and is described by Fick's 2nd Law [Fick, 1955]:

$$\frac{\partial c}{\partial t} = \frac{\partial}{\partial x}\left(D \frac{\partial c}{\partial x} \right) \tag{2.15}$$

where c is the solvent concentration in heavy oil, vol.%; D is the diffusion coefficient, m^2/s; x is the space variable, m; t is the time variable, s.

Diffusion coefficient

A diffusion coefficient is a transport property that is used to calculate the mass-transfer rate between solvent and heavy oil. There are two categories of diffusion coefficients in

the literature: a concentration-independent constant value and a concentration-dependent variable value.

A diffusion coefficient is assumed as a constant value when the solubility of a solvent in a heavy oil is small under the test conditions. Most of molecular diffusivity between light hydrocarbon or carbon dioxide and a heavy oil is measured with various methods and calculated as a constant value. [Schmidt, 1985; Upreti and Mehrotra, 2000, 2002; Tharanivasan et al., 2006; Yang and Gu, 2006; Etminan et al., 2010]. **Table 2.4** lists some measured diffusivity through laboratory tests.

On the other hand, Hayduk and Cheng [1971] concluded that the diffusion coefficient of a solvent-oil system (ethane in n-hexane, heptanes, octane, dodecane, and hexadecane, or carbon dioxide in hexadecane) can be dependent on the mixture's viscosity, which was commonly expressed as:

$$D(\mu) = \alpha\mu^{-\beta}, \tag{2.16}$$

where α and β are constants depending on the crude oil and solvent properties as well as the operating conditions; μ is the viscosity of heavy oil−solvent mixture, mPa·s. β is less than 1. Based on this general form, Equation (2.16), a number of variable diffusion coefficients are proposed. Some examples are shown below,

$$D = 0.591\times10^{-10}\,\mu^{-0.545} \text{ (propane-hexane/heptane [Hayduk et al, 1973])} \tag{2.17}$$

$$D = 13.06\times10^{-10}\,\mu^{-0.46} \text{ (for propane-bitumen [Das and Butler, 1996])} \tag{2.18}$$

$$D = 4.13\times10^{-10}\,\mu^{-0.46} \text{ (for butane-bitumen [Das and Butler, 1996])} \tag{2.19}$$

It is worthwhile to note that in the actual VAPEX process, the solvent-diluted heavy oil drains down along the transition zone and thus the upward-moving solvent keeps contacting the fresh heavy oil. In this case, both the molecular diffusion and convective dispersion of the solvent in the heavy oil contribute to the mass transfer between a heavy oil and solvent. The back-calculated effective diffusion coefficient by Das and Butler contained both of the effects [Boustani and Maini, 2001].

Table 2.4 Measured diffusion coefficient for solvent and heavy oil system.

Crude oil	Solvent	Pressure (MPa)	Temperature (°C)	Diffusivity (10^{-9} m^2/s)	Reference
AB-1	C_1	4.0	25	0.08−0.11	Upreti and Mehrotra, 2002
AB-1	C_1	4.0−8.0	25	0.06−0.08	Upreti and Mehrotra, 2002
LM	C_1	4.9−5.0	23.9	0.21−0.22	Tharanivasan et al., 2004
LM	C_1	6.0−14.0	23.9	0.12−0.19	Yang and Gu, 2006
Dodecane	C_1	3.5	45, 65	4.22−5.28	Etminan et al., 2010
AB-1	C_2	4.0	25	0.21−0.38	Upreti and Mehrotra, 2002
LM	C_2	1.5−3.5	23.9	0.13−0.77	Schmidt, 1989
LM	C_3	0.4−0.8	23.9	0.49−0.79	Yang and Gu, 2006
LM	C_3	0.4−0.9	23.9	0.09−0.68	Yang and Gu, 2006
AB-1	CO_2	5.0	20	0.28	Schmidt, 1989
AB-1	CO_2	3.1−4.1	25	0.16−0.22	Upreti and Mehrotra, 2000
AB-1	CO_2	4.0	25	0.12−0.20	Upreti and Mehrotra, 2002
LM	CO_2	3.5−4.2	23.9	0.46−0.55	Tharanivasan, 2004
LM	CO_2	2.0−6.0	23.9	0.22−0.55	Yang and Gu, 2006
AB-1	CO_2	3.2	75	0.5	Etminan et al., 2010
AB-1	C_3	6.0-14.7	20-50	0.49-9.2	Talebi et al.,2017

Heavy oil viscosity

The viscosity of a heavy oil-solvent system is commonly modeled in terms of solvent concentration by using the Lederer–Shu correlation [Lederer, 1933; Shu, 1984]:

$$\mu = \mu_s^{f_s} \mu_o^{f_o} \tag{2.20}$$

$$f_s = \frac{c}{\lambda(1-c)+c}, \quad f_o = 1 - f_s \tag{2.21}$$

$$\lambda = \frac{17.04(\gamma_o - \gamma_s)^{0.5237} \gamma_o^{3.2745} \gamma_s^{1.6316}}{\ln(\mu_o/\mu_s)} \tag{2.22}$$

where μ_o, μ_s, and μ are the viscosities of the crude oil, liquid solvent, and mixture of the two, respectively, mPa·s; f_o and f_s are the weighted volume fractions, vol.%; λ is a weight factor; γ_o and γ_s are the specific gravities of the crude heavy oil and liquid solvent, respectively.

Heavy oil density

The density of a heavy oil-solvent system can be determined by using a mixture rule for an ideal solution [McCain, 1990]:

$$\rho = \frac{1}{(1-c)/\rho_o + c/\rho_s} \tag{2.23}$$

where ρ_o and ρ_s are the densities of the heavy oil and liquid solvent, respectively, kg/m^3; The above equation is applicable only if the volume change due to the solvent dissolution into the heavy oil is negligible. In addition, the solvent is assumed to be a liquid once it dissolves into the heavy oil.

2.5.2 Gravity drainage

Darcy equation

With a known concentration distribution, the concentration-dependent viscosity and density of the solvent-diluted heavy oil can be obtained. Therefore, the gravity drainage velocity across the transition zone can be determined by using Darcy's law:

$$v = -\frac{K}{\mu(c)}\left[\rho(c) - \rho_s\right] g \sin\theta \tag{2.24}$$

where v is the oil drainage velocity, m/s; k is the absolute permeability, m^2; k_{ro} is the oil phase relative permeability, dimensionless; ρ_c and ρ_s are the densities of the solvent-diluted heavy oil and the liquid solvent, kg/m3; g is the gravitational acceleration, m/s^2. It is worthwhile to note that due to the much smaller density of solvent vapor, ρ_s is often omitted in the calculation of v.

Relative permeability and capillary pressure

Most analytical studies of VAPEX assume that only a single liquid phase exists in the transition zone. Therefore, the permeability is often considered as a constant. Vapor-liquid two-phase flow is assumed to take place in the transition zone. Corey's [1954] oil–gas two-phase relative permeability formula is usually adopted to describe this multi-phase flow in the mobile layer of VAPEX:

$$k_{ro} = \left(1 - S_g^*\right)^4 \tag{2.25}$$

$$k_{rg} = \left(S_g^*\right)^4 \left(2 - S_g^*\right) \tag{2.26}$$

where S_g^* is the effective gas saturation, dimensionless. It is defined as:

$$S_g^* = \frac{S_g}{1 - S_{wc}} \tag{2.27}$$

The reason for using Corey's correlations is because Corey's expressions are mathematically simple in comparison with other models. It assumes that the wetting and non-wetting phase-relative permeabilities are independent of the saturations of the other phases, as shown in the above two equations. Also, these correlations are well applicable to well-sorted homogeneous rocks such as unconsolidated oil sands reservoirs. Moreover, Corey's correlations have been widely used in the mathematical modeling of SAGD processes [Lei et al., 2010; Sharma and Gates, 2010; Morte and Hascakir, 2016; Zeidani and Maini, 2016].

The effect of capillary forces is neglected in most VAPEX studies, which is a reasonable assumption when the grain sizes in a model are coarse and permeability is relatively large in Darcy.

2.6 Chapter Summary

From the literature review in this chapter, it can be seen that extensive laboratory experimental studies and numerical simulation studies have been conducted to evaluate and analyze the VAPEX process. However, VAPEX theoretical modeling has not gained as much progress as the other two types of studies. Some analytical models are only able to roughly estimate an oil production rate while others are built up on the basis of questionable assumptions. As a result, the applicability of the existing analytical, empirical, and mathematical models is rather limited. Therefore, a new reliable VAPEX theoretical model is desirable.

CHAPTER 3 MATHEMATICAL MODELING OF VAPEX

This chapter presents a new theoretical analysis method to describe the solvent chamber evolution during a VAPEX heavy oil recovery process. This new method is based on two physical processes: mass transfer and gravity drainage. The mass transfer process is modeled as a transient process with a constant diffusivity. The heavy oil–solvent transition zone in which most of the mass transfer occurs is modeled as a piecewise linear zone that is updated step by step temporally. The boundary of the transition zone is considered as moving with time and calculated on the basis of a material balance equation. This VAPEX model is able not only to describe the distributions of solvent concentration, oil drainage velocity, and diffusivity across the transition zone, but also to predict the solvent chamber evolution and the heavy oil production rate.

3.1 Introduction

A conventional VAPEX process employs a pair of parallel horizontal wells with one placed right above the other in a heavy oil reservoir. The upper horizontal well is used as a solvent injector and the lower one as an oil producer. Throughout a VAPEX process, first, the two wells are communicated by implementing a big pressure difference in-between. Then, a vaporized solvent (typically a light hydrocarbon gas) with or without a carrier gas is injected into the heavy oil reservoir. Finally, the heavy oil is diluted through solvent dissolution, drained downward by gravity, and pumped out from the producer at the bottom of the reservoir (**Figure 3.1**).

In literature studies, VAPEX processes have been intensively modeled through laboratory physical experiments. A variety of factors, such as fluid properties and operating conditions, have been analyzed and the corresponding conclusions have been made. In contrast, theoretical modeling of the VAPEX processes has not gained much progress in the past two decades. **Table 2.3** summarizes the VAPEX theoretical studies in the literature. It is found that the existing theoretical models are neither able to accurately

describe fluid properties in the transition zone nor reasonably characterize solvent chamber development.

As a powerful diagnostic tool, various numerical simulators (STARS, GEM, and COMSOL) have been employed to analyze VAEPX processes [Nghiem et al., 2001; Cuthiell et al., 2003; Das, 2005; Wu et al., 2005; Tam, 2007; Rahnema et al., 2008; Yazdani and Maini, 2009; Nourozieh et al., 2011; Xu et al., 2012; Cuthiell et al., 2013]. Mostly, simulation studies are resorted to simulate and validate the laboratory experimental data. Some simulation results are reasonable while others are unreliable and difficult to comprehend or even erroneous. The principal reason is the numerical dispersion that is inherent in finite difference methods, and others lie in the physical properties of the VAPEX process. For example, due to an extremely small physical diffusion coefficient between heavy oil and solvent, the mixing zone is too thin (about 1 cm) to be precisely captured by conventional gridblock sizes in simulation. In short, the applicability of the existing analytical, empirical, and mathematical models is rather limited. Therefore, a new reliable VAPEX theoretical model is desirable.

This chapter formulates a new semi-analytical mathematical model to simulate the solvent chamber evolution of a VAPEX process. In this model, a transition zone or a solvent chamber boundary is approximated as a piecewise linear profile that is updated stepwise. Major production mechanisms of VAPEX such as dynamic mass transfer, gravity drainage, surface renewal or a moving boundary, and multiple phase flow are accounted for in the model. Modeling results are compared with the previous experimental data, as well as with simulation data at both laboratory and field scales.

3.2 MATHEMATICAL MODEL

3.2.1 Assumptions

In a VAPEX process, most of the mixing of heavy oil and solvent and the drainage of the solvent-diluted heavy oil take place at a solvent chamber boundary or a transition zone (**Figure 3.1**). Across the transition zone, solvent concentration decreases gradually from a maximum value (saturation concentration) to nearly zero. Also, the depletion of oil from

the transition zone leads to the expansion of the solvent chamber. Therefore, this study focuses on the transition zone and simplifies it as a piecewise linear profile (**Figure 3.2**). Some assumptions for the model and fluid properties are made below:

1. Uniform porosity and permeability distribution,
2. Line-source solvent injection at a constant pressure and a constant temperature,
3. Pure gravity drainage of the solvent-diluted heavy oil, and
4. Linear dependence of gas-phase saturation on solvent concentration in the transition zone.

It is worthwhile to mention that due to the complexity in recovery mechanisms and minor contribution to oil production [Zhang et al., 2006], the rising phase of a solvent chamber is not considered in this study.

3.2.2 Dynamic mass transfer

The transient heavy oil–solvent mixing process within the transition zone can be described by using Fick's 2nd law. Initially, the heavy oil is free of any solvent. The oil at the left boundary is fully saturated with solvent and the right boundary is impermeable. Thus, the heavy oil–solvent mass transfer model can be developed as

$$\frac{\partial c}{\partial t} = D\frac{\partial^2 c}{\partial x^2} \tag{3.1}$$

$$c\left(x, t=0\right) = 0 \tag{3.2}$$

$$c\left[x = s\left(t\right), t\right] = c_{\max} \tag{3.3}$$

$$\frac{\partial c}{\partial x}\left(x = L, t\right) = 0 \tag{3.4}$$

Here D is defined as an effective diffusion coefficient that incorporates all the mechanisms contributing to heavy oil–solvent mixing such as molecular diffusion, convective dispersion, improved interfacial contact, and enhanced surface renewal by capillary imbibition [Upreti, et al., 2007].

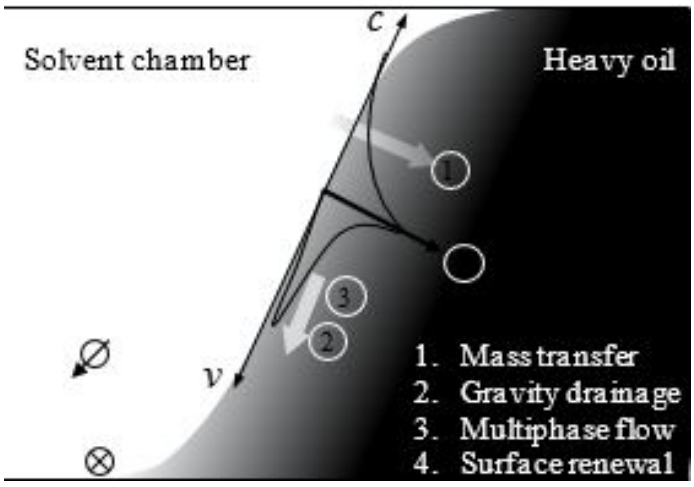

Figure 3.1 Schematics of VAPEX mechanisms.

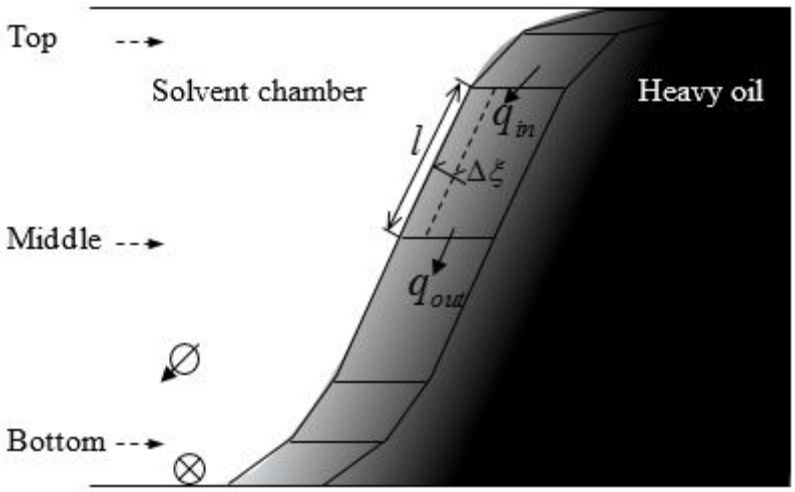

Figure 3.2 Approximation of oil depletion and boundary movement of a transition zone.

It should be noted that $x = s(t)$ represents the position of the left boundary of a transition-zone segment that advances towards the untouched heavy oil zone due to the depletion of solvent-diluted heavy oil. This makes the mathematical model a moving boundary problem or a Stephen problem [Crank, 1984]. To solve such a problem, there are generally three categories of methods: front tracking, front fixing, and fixed domain methods [Joshi et al., 2006]. This study uses a front tracking method, in which a new coordinate is defined to immobilize the front:

$$\xi = x - \int_0^t U(t)\,dt \tag{3.5}$$

where U is the boundary moving velocity normal to the solvent chamber boundary, m/s. Applying the chain rule to obtain the first- and second-order derivatives of c with respect to ζ, respectively, and replacing them into Equations (3.1–4) result in a transformed mass transfer model in the new coordinate system:

$$\frac{\partial c}{\partial t} = D\frac{\partial^2 c}{\partial \xi^2} + U\frac{\partial c}{\partial \xi} \tag{3.6}$$

$$c(\xi = 0, t) = c_{\max} \tag{3.7}$$

$$\frac{\partial c}{\partial \xi}(\xi = L, t) = 0 \tag{3.8}$$

$$c(\xi, t = 0) = 0 \tag{3.9}$$

An analytical solution to this model was derived from the general solution given by Carslaw and Jaeger [Carslaw and Jaeger, 1959]:

$$c = c_{\max}\frac{2\pi}{\lambda^2}\sum_{n=1}^{\infty}\frac{n}{1+\frac{n^2\pi^2}{\lambda^2}}\sin(n\pi X)\left[e^{-\left(1+\frac{n^2\pi^2}{\lambda^2}\right)T} - 1\right] \tag{3.10}$$

where

$$\lambda = \frac{UL}{2D},\ X = \frac{\xi}{L},\ T = \frac{U^2 t}{4D} \tag{3.11}$$

are dimensionless terms that were defined by Mohsen and Baluch [1983].

3.2.3 Multiphase gravity drainage

The fluid gravity drainage velocity across the transition zone can be determined by Darcy's law:

$$u = -\frac{Kk_{ro}}{\mu}\left(\rho - \rho_s\right) g \sin\theta \tag{3.12}$$

where g is the gravitational acceleration, m/s^2; θ is the slip angle, degree. A linear relative permeability is expected for the multiphase flow in the transition zone:

$$k_{ro} = \left(1 - S_g^*\right)^4 \tag{3.13}$$

$$S_g^* = \frac{S_g}{1 - S_{wc}} \tag{3.14}$$

where S_g^* is the effective gas saturation and the capillary pressure is neglected given its small magnitude in a large permeability environment [Yazdani and Maini, 2005]. Also, the effective gas saturation is assumed linear with solvent concentration across the transition zone, which is referred from the SAGD modeling [Sharma and Gates, 2010] and can be reasonable since VAPEX is a direct solvent analog of SAGD. The oil drainage rate from a transition-zone segment can be determined by integrating the drainage velocity profile:

$$q_o = \phi W \int_{\xi_{\min}}^{\xi_{\max}} u\left(1 - c\right) \mathrm{d}\xi \tag{3.15}$$

where $\zeta_{\max}$ and $\zeta_{\min}$ are the boundary positions of the transition zone, respectively, m.

3.2.4 Boundary moving velocity

Suppose that oil flows into and drains out of a transition-zone segment at rates of q_{in} and q_{out}, respectively. Within a short period of time, δt, the left boundary of the transition zone moves by $\delta\xi$ due to the depletion of solvent-diluted heavy oil from the segment. Therefore, a mass balance equation can be formulated:

$$\left(q_{out} - q_{in}\right)\delta t = l\phi\left(S_{oi} - S_{or}\right)\delta\xi \tag{3.16}$$

If the time snippet is small enough, it is reasonable to take the segment boundary length of a transition-zone constant and the residual oil saturation in the depleted area uniform. Thereby the boundary moving velocity can be approximated as a constant value over that time interval:

$$U \approx \frac{\delta\xi}{\delta\tau} = \frac{\left(q_{in} - q_{out}\right)}{\phi\left(S_{oi} - S_{or}\right)Wl} \tag{3.17}$$

3.2.5 Solvent chamber evolution

Given a constant boundary moving velocity U during a short time period Δt, the movement of the transition zone can be easily calculated by

$$\Delta\xi_{mv} = U\Delta t \tag{3.18}$$

The respective advancement of a transition-zone segment in the horizontal and vertical directions can be determined by using a trigonometric correlation:

$$\Delta x = \frac{\Delta\xi_{mv}}{\sin\theta},\ \Delta y = \frac{\Delta\xi_{mv}}{\cos\theta} \tag{3.19}$$

The cumulative heavy oil production can be achieved by integrating the oil saturation difference over the solvent vapor chamber in the (x, y) coordinate system and the instantaneous oil production obtained by taking the derivative of Q with respect to t:

$$Q_o = \int_0^W \phi\Delta S_o \left(H - y\right) dx \tag{3.20}$$

3.3 Results and Discussion

3.3.1 Solvent chamber evolution

Table 3.1 lists the model and fluid properties and operating conditions for a base case. Particular parameters for different scenarios in the following sections will be specified. Using the base-case data and following the solution flowchart in **Figure 3.3**, the solvent chamber evolution and oil production rates can be estimated. Previous visualization studies of VAPEX usually indicate that a solvent chamber extends literally during its spreading phase and falls downward after reaching to the right-hand side of a model [Butler and Mokrys, 1989], which agrees well with the theoretical prediction of this study (**Figure 3.4a**). Obviously, the solvent chamber boundary takes an “S” shape and advances faster at the top than at the bottom.

Table 3.1 Approximation of solvent chamber as a base case.

Property	Symbol	Value	Unit
Model			
Dimension (lab-scale)	L×H×W	0.1×0.2×0.02	m×m×m
Dimension (field-scale)	L×H×W	10×20×1	m×m×m
Porosity	ϕ	35	vol.%
Absolute permeability	k	25×10^{-12}	m^2
Initial oil saturation	S_{oi}	90	vol.%
Residual oil saturation	S_{or}	10	vol.%
Heavy oil			
Viscosity @ 20.8°C and 800 kPa	μ_o	126,500	mPa.s
Density @ 20.8°C and 800 kPa	ρ_o	930.5	kg/m^3
Solvent			
Solvent name		Propane	
Viscosity (liquid) @ 20.8°C and 800 kPa	μ_s	0.165	mPa.s
Density (liquid) @ 20.8°C and 800 kPa	ρ_s	547.6	kg/m^3
Binary diffusivity	D	5×10^{-9}	m^2/s
Others			
Injection Temperature	T	21	°C
Injection pressure	P	800	kPa
Gravity acceleration	g	9.8	m/s^2

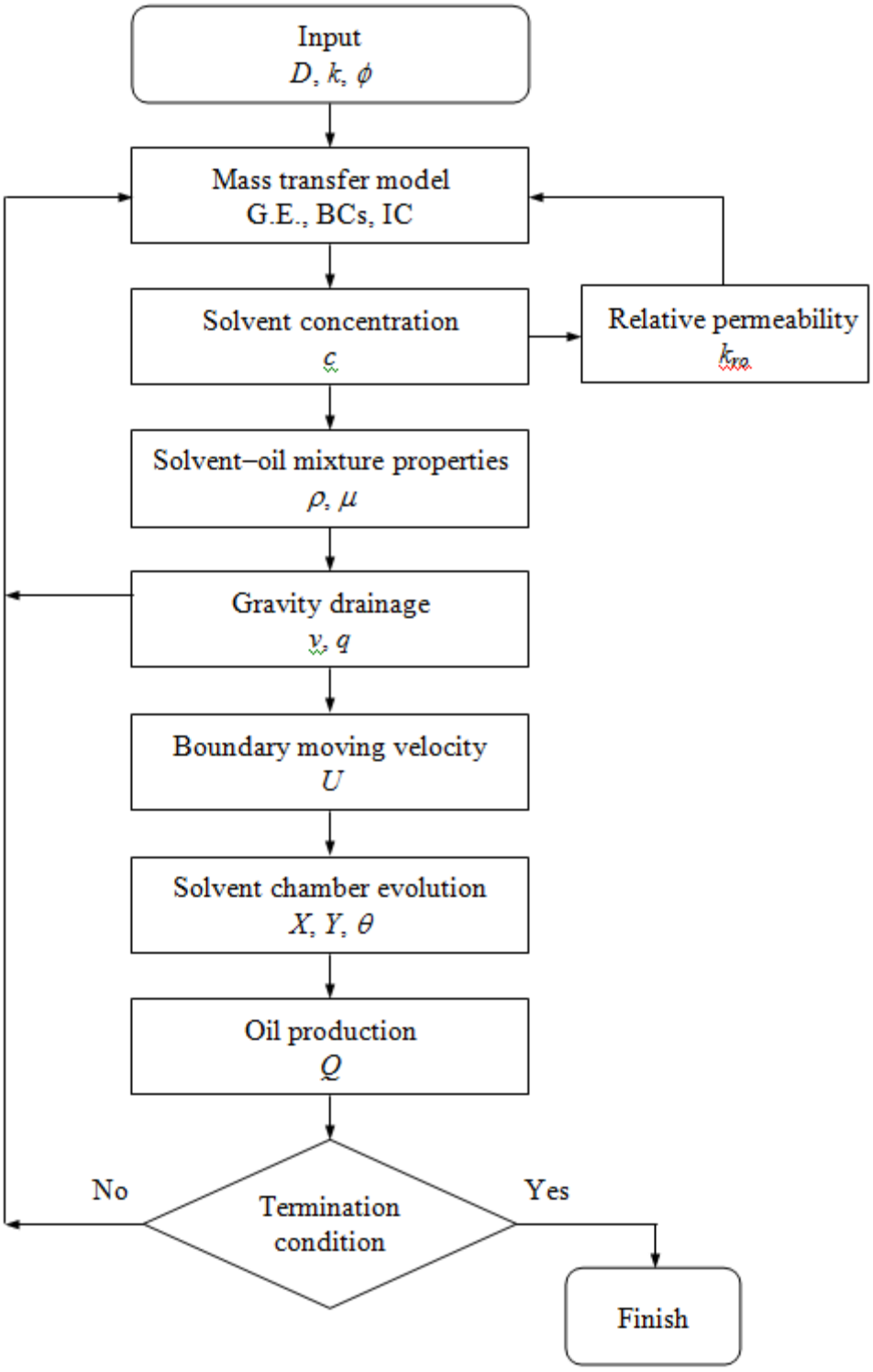

Figure 3.3 Flow chart of the solution to the VAPEX mathematical model.

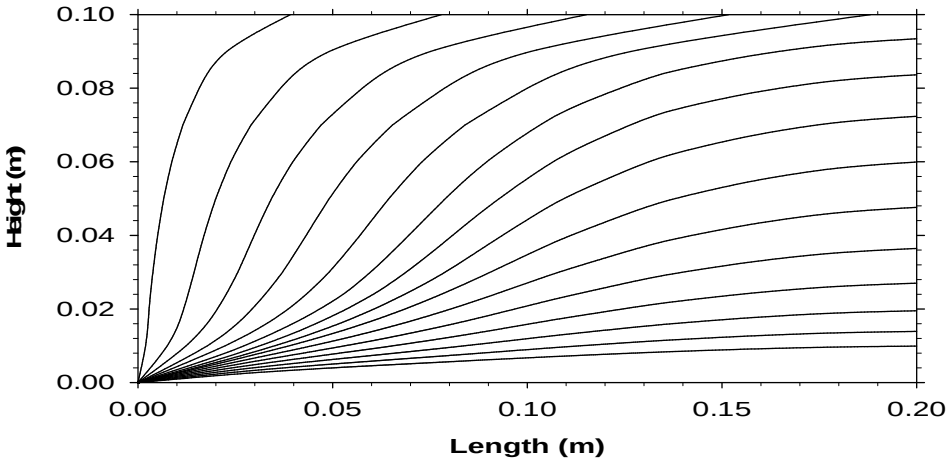

(a)

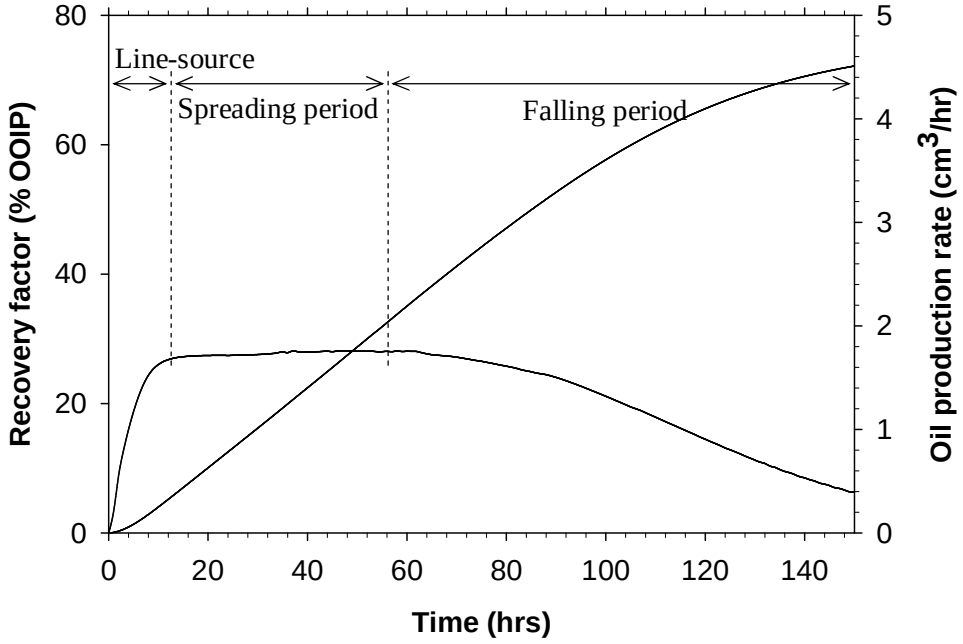

(b)

Figure 3.4 Simulation results of a VAPEX base case: **(a)** evolution of solvent chamber boundary (time interval for adjacent lines is 5 hrs) and **(b)** recovery factor and oil rate.

Figure 3.4b presents the recovery factor and the oil production rate of the base case. In general, the production profile can be identified into three periods: (1) a line-source effect period. It is caused by the line-source solvent injection scheme in this study: Solvent dissolves into heavy oil from a vertical plane at the left-hand side of the model, and no gas solvent breaks through to the producer that is placed at the left-bottom corner; (2) a spreading period in which the oil production rate profile maintains at a relatively constant level, suggesting a stabilized oil production rate; (3) a falling period in which the oil rate drops gradually with time due to the declining slip angle of the solvent chamber boundary and the resultant diminishing gravity force.

3.3.2 Effects of division number and time step

This study approximates the transition zone as a number of piecewise linear segments, and **Figure 3.5** analyzes the effect of the transition-zone division number (n = 5, 10, 15, 20, and 25) on the solvent chamber boundary profile. It is found that the solvent chamber profiles for n = 5, 10 and 15 are rather close to each other at most positions except the first segment at the chamber top (**Figure 3.5a**). This is because the first segment for the case of n = 5 has a larger length, which leads to a smaller moving velocity as indicated in Equation (3.17). **Figure 3.5b** shows that the cumulative oil production for the five division scenarios tends to converge to a certain value. This implies that the modeling results should be reliable given a proper approximation of the transition zone. This study uses a division number of n = 10 in the following calculation.

The solvent chamber profile is updated stepwise during the computation. **Figure 3.6** shows the effects of three time-intervals (Δt = 90s, 180s, and 360ss) on the solvent chamber boundary profiles and cumulative oil production, respectively. It is found that the three profiles almost overlap with one another (**Figure 3.6a**) and the corresponding cumulative oil production data is rather close to each other (**Figure 3.6b**), which suggests the time step plays a minor role in the new developed VAPEX model.

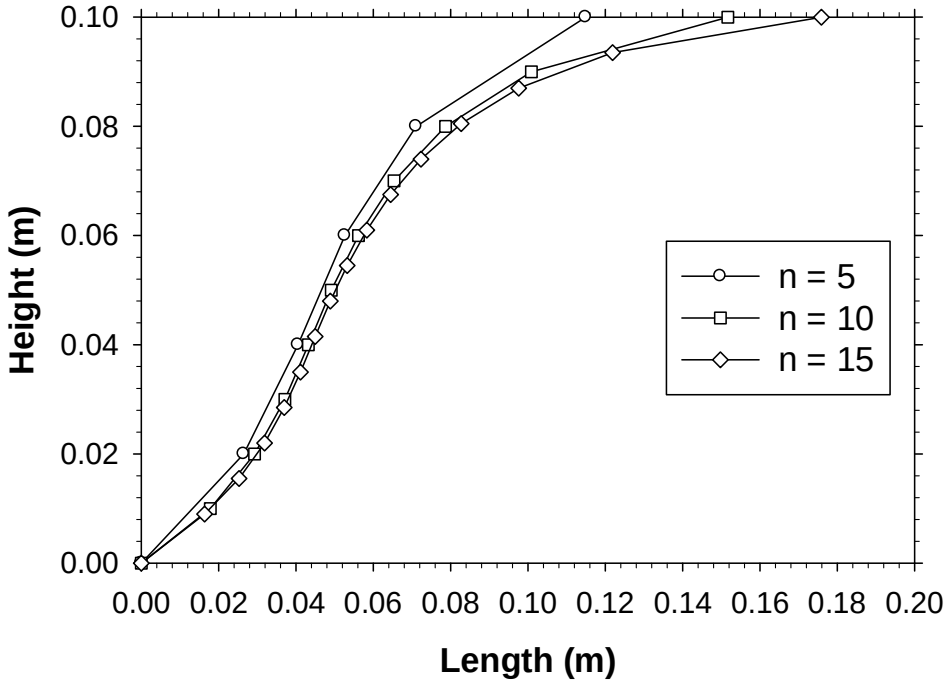

(a)

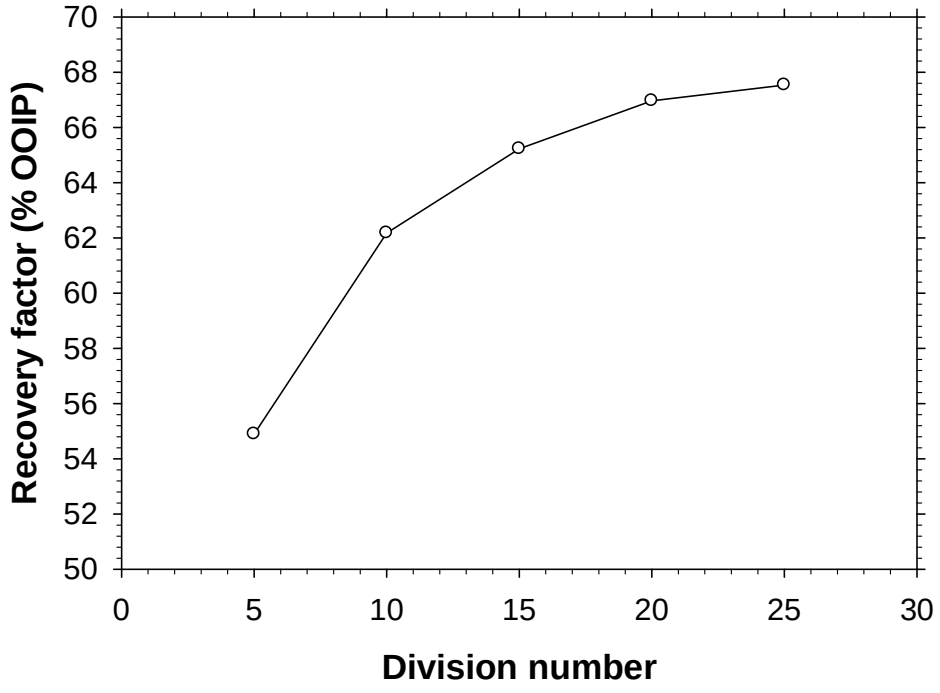

(b)

Figure 3.5 Effects of division number on **(a)** the solvent chamber evolution and **(b)** the recovery factor at t = 40 hrs.

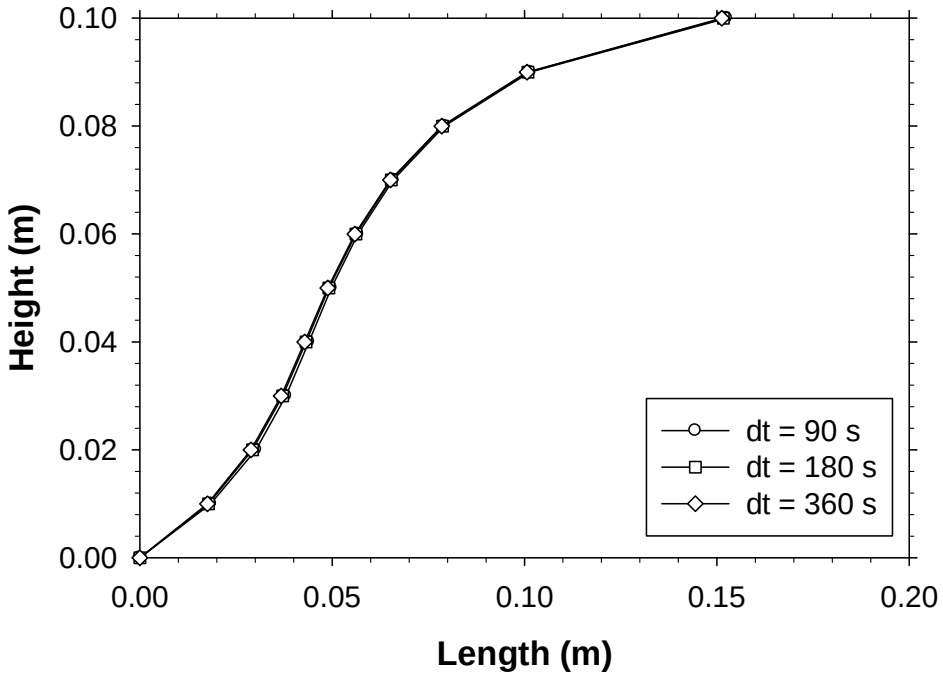

(a)

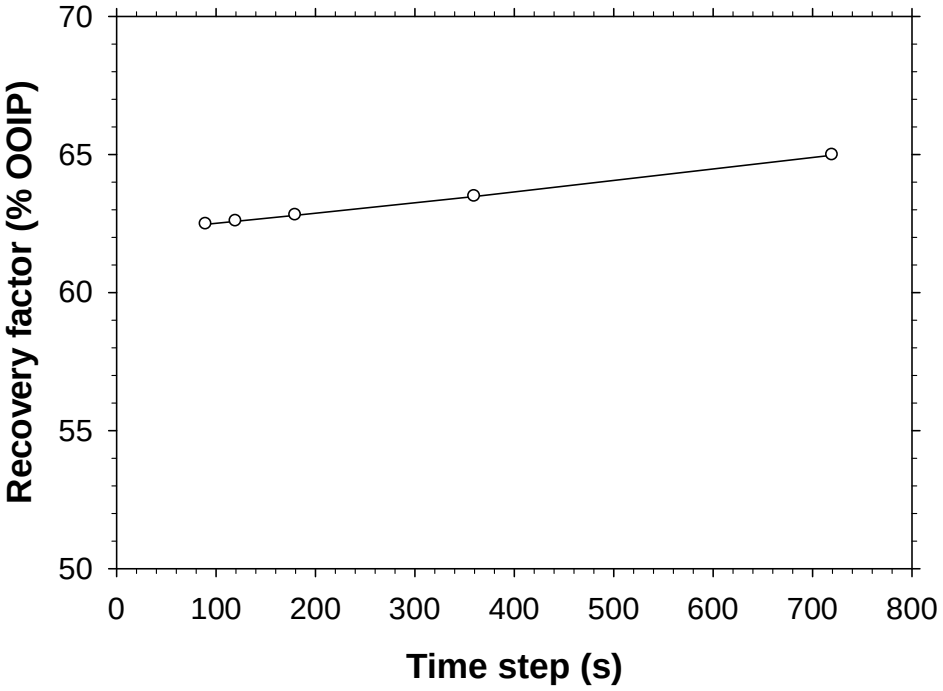

(b)

Figure 3.6 Effects of time interval on **(a)** the solvent chamber evolution and **(b)** the cumulative oil production at t = 40 hrs.

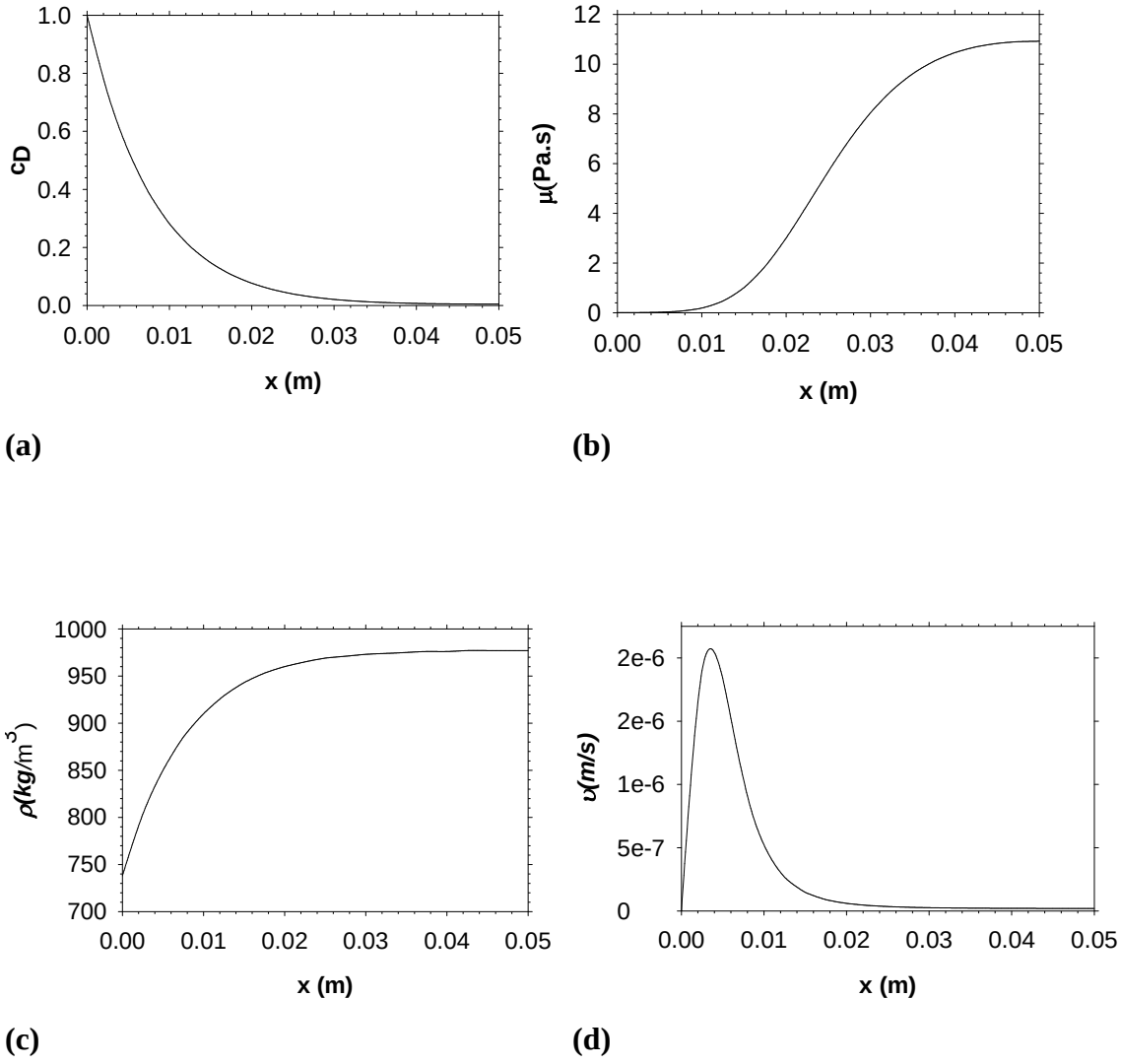

Figure 3.7 Properties of the solvent-diluted heavy oil across the transition zone: **(a)** solvent concentration, **(b)** viscosity, **(c)** density, and **(d)** drainage velocity.

3.3.3 Concentration along interface

Figure 3.7 shows the properties of the solvent-diluted heavy oil within the transition zone: solvent concentration, viscosity, density, and drainage velocity. The oil drainage velocity profile starts from zero at the front and peaks some distance away, which is because the transition zone in this study is considered as a two-phase zone. The dimensionless oil-phase saturation is zero at the front, which leads the oil-phase relative permeability there to zero, as indicated by Equations (3.13) and (3.14).

Along the solvent chamber boundary, the transition zone properties change with position [Mohsen and Baluch, 1983]. **Figure 3.8** shows the concentration distributions at the top, middle, and bottom of the transition zone. It can be seen that the concentration profile at the top grows fast during the spreading phase (**Figure 3.8a**). This is caused by the small inclination angle of the first transition-zone segment, which renders solvent more time to mix with oil rather than to slip down the interface. **Figure 3.8b** shows that at the middle part of the solvent chamber boundary, the concentration grows slowly during the spreading period (before t = 26 hrs), indicating a relatively bigger boundary moving velocity during this period. Subsequently, solvent penetrates deeper and deeper into the oil zone, which is probably caused by the diminishing slip angle during the solvent chamber falling phase. In general, the transition zone at the middle part seems stabilized throughout the spreading and falling phases, which validates the assumption of steady-state mixing and a constant boundary moving velocity in previous analytical modeling. **Figure 3.8c** shows that the solvent concentration profile at the lower part of the model grows quickly and steadily throughout the VAPEX process, which is related to the small slip angle and a closed boundary at the bottom.

3.3.4 This study vs. numerical simulation

This chapter also performs a numerical simulation study of VAPEX with the STARS module [Version 2014, Computer Modeling Group Limited, Canada] for the purpose of comparison with the newly developed mathematical model. Fluid and matrix properties in the numerical model mostly are the same as those listed in **Table 3.1** and **Figure 3.9**.

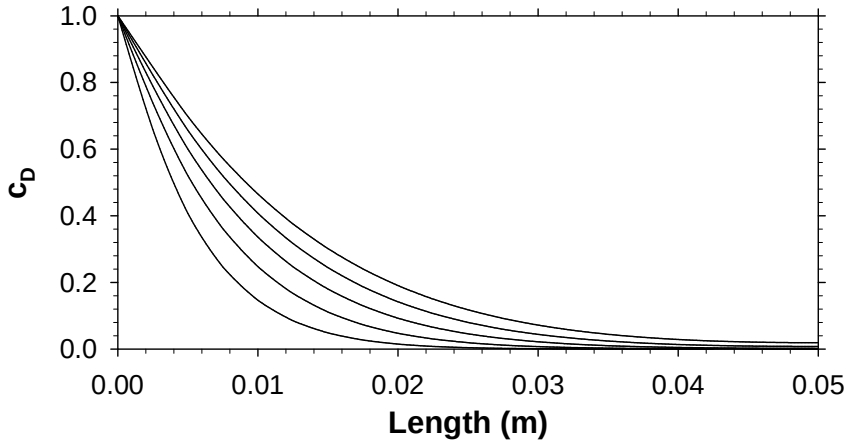

(a)

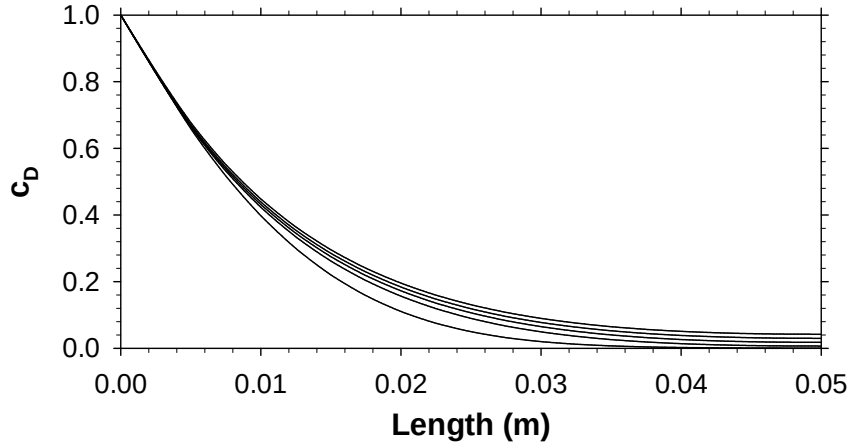

(b)

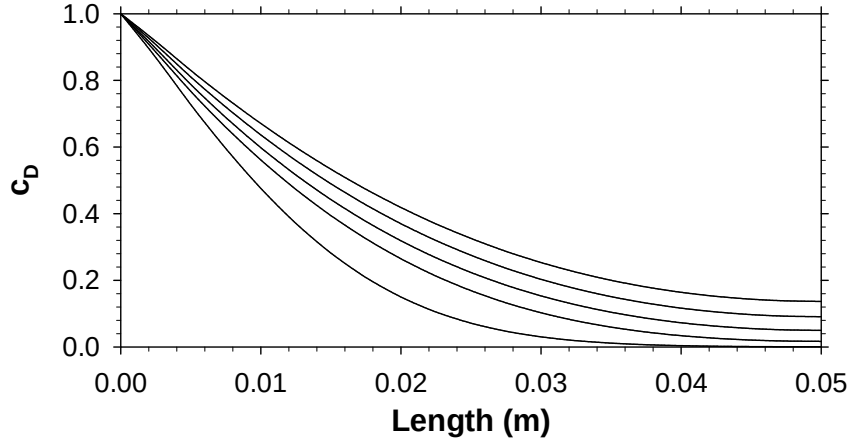

(d)

Figure 3.8 Concentration at the **(a)** top, **(b)** middle, and **(c)** bottom of the transition zone.

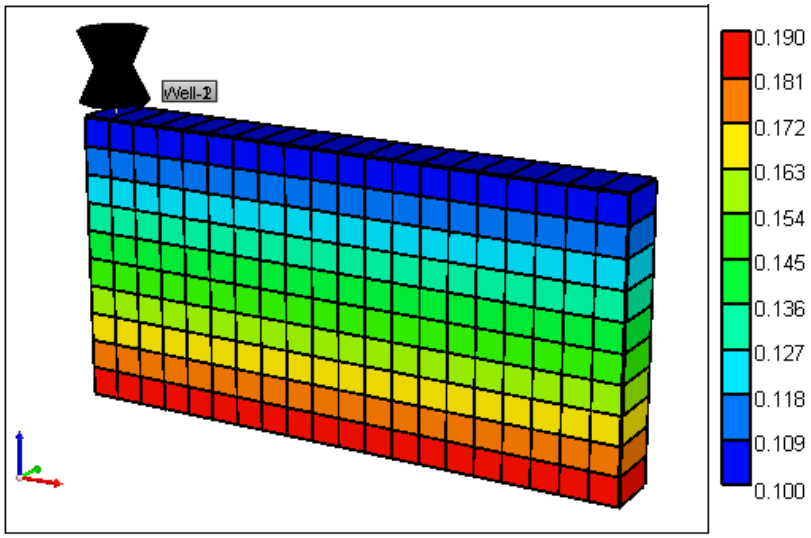

(a)

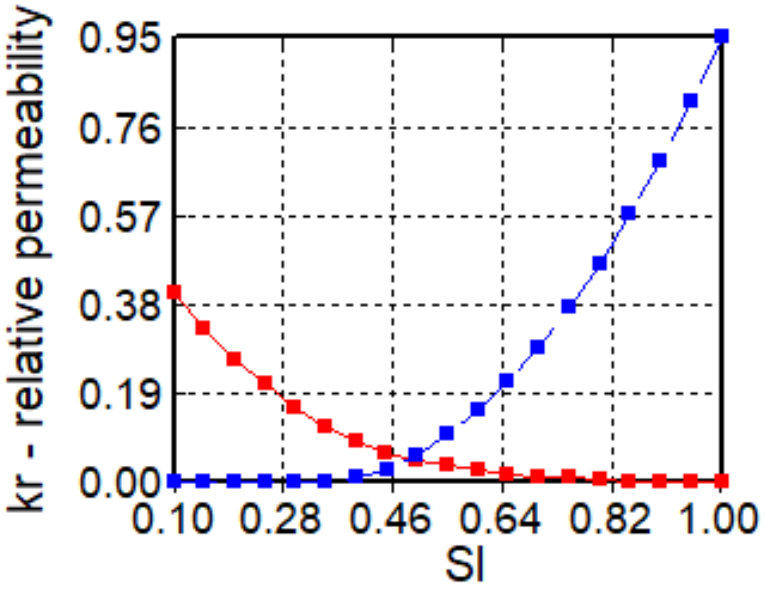

(b)

Figure 3.9 (a) Numerical simulation model, **(b)** relative permeability curve.

Effect of Δx and Δt

Numerical dispersion is caused by the discretization of space and time and is inherent to finite difference methods [Fanchi, 2006]. **Figure 3.10** visually presents the effect of four gridblock sizes on the oil saturation distribution. It can be seen that smaller grid blocks tend to generate a bigger solvent chamber as well as oil production: The difference in oil production between the coarsest and finest gridblocks can be as high as 16.1% at t = 30 hrs. **Figure 3.11** displays the effect of a time step on the relative oil production rate that is defined as the ratio of an oil production rate to the maximum one for a certain range of time steps (Δt = 0.0001, 0.001, 0.01, 0.1, 1, 10 days). It is found that at a lab scale, a four-order difference in the time step results in about 10% discrepancy in the oil production rate, while, at a field scale, a four-order difference in the time step leads to about 33% discrepancy in the oil production rate. These data suggest that the simulation results are less sensitive to time steps than gridblock sizes.

Effect of h

Analytical studies demonstrated that the stabilized oil production rate of VAPEX is proportional to the square root of the gravity drainage height [Butler and Mokrys 1989; Yazdani and Maini, 2005]. However, through a number of physical experimental studies with three models of different heights (h = 0.075, 0.3, and 0.6 m), Yazdani and Maini [2005] found that the stabilized oil production rate is a function of the gravity drainage height to the power of 1.1–1.3 rather than 0.5. The larger exponent was ascribed to a height-dependent effective diffusivity between heavy oil and solvent, and, yet, this guess has not been rigidly proved so far. To further analyze these two statements, this study uses five different model heights from lab- to field-scale (h = 0.1, 0.5, 1.0, 5.0, 10.0 m). The corresponding oil production rates are, respectively, plotted against both $h^{0.5}$ and $h^{1.13}$ to investigate the analytical and empirical correlations. It is found that the calculated results of this study are better fitted with $h^{0.5}$ (**Figure 3.12a**) while the simulated data are more consistent with the empirical correlation (**Figure 3.12b**).

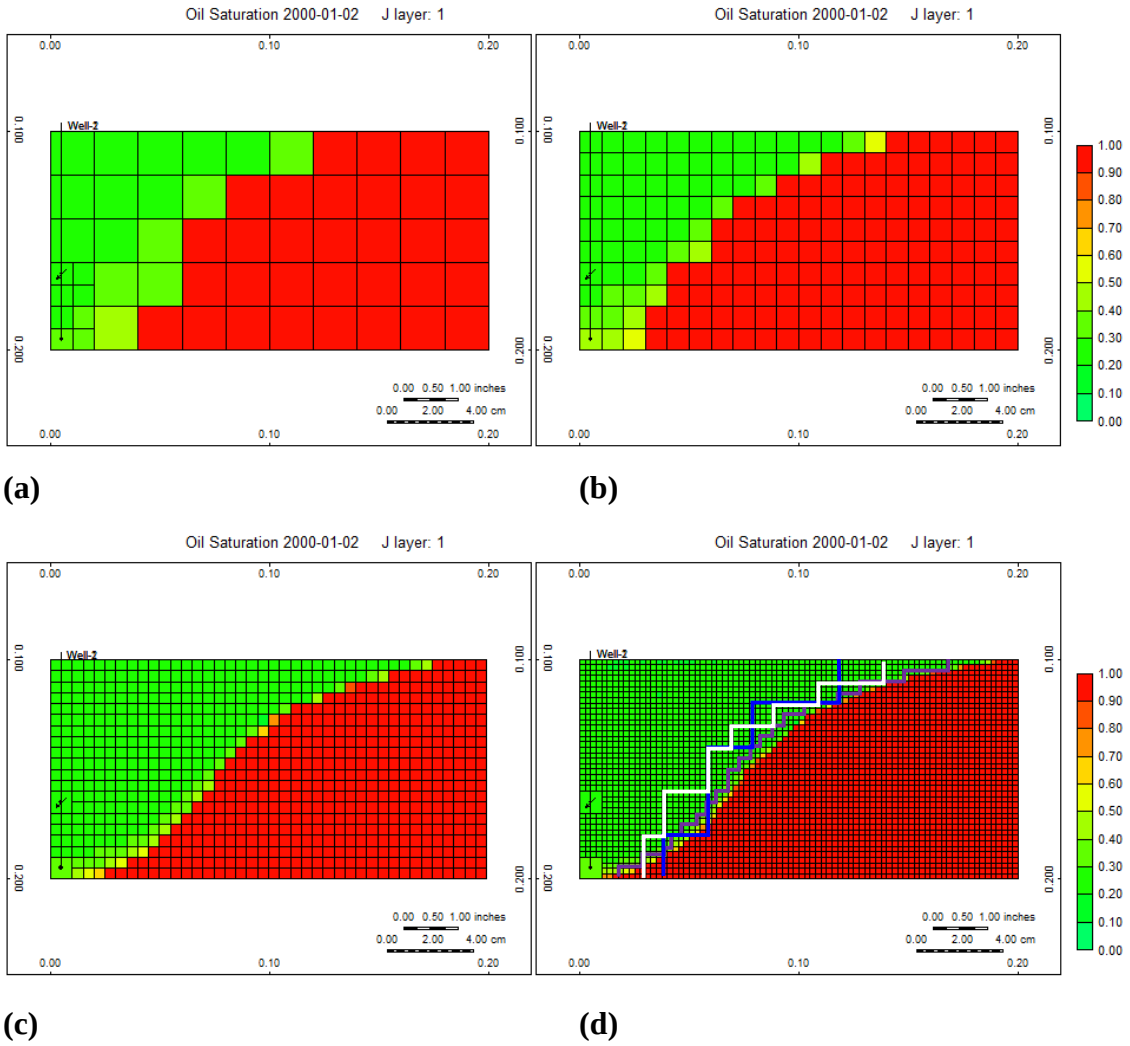

Figure 3.10 Effect of gridblock sizes on the oil saturation profile: **(a)** Δx = 0.02 m, **(b)** Δx = 0.01 m, **(c)** Δx = 0.005 m, and **(d)** Δx = 0.002 m.

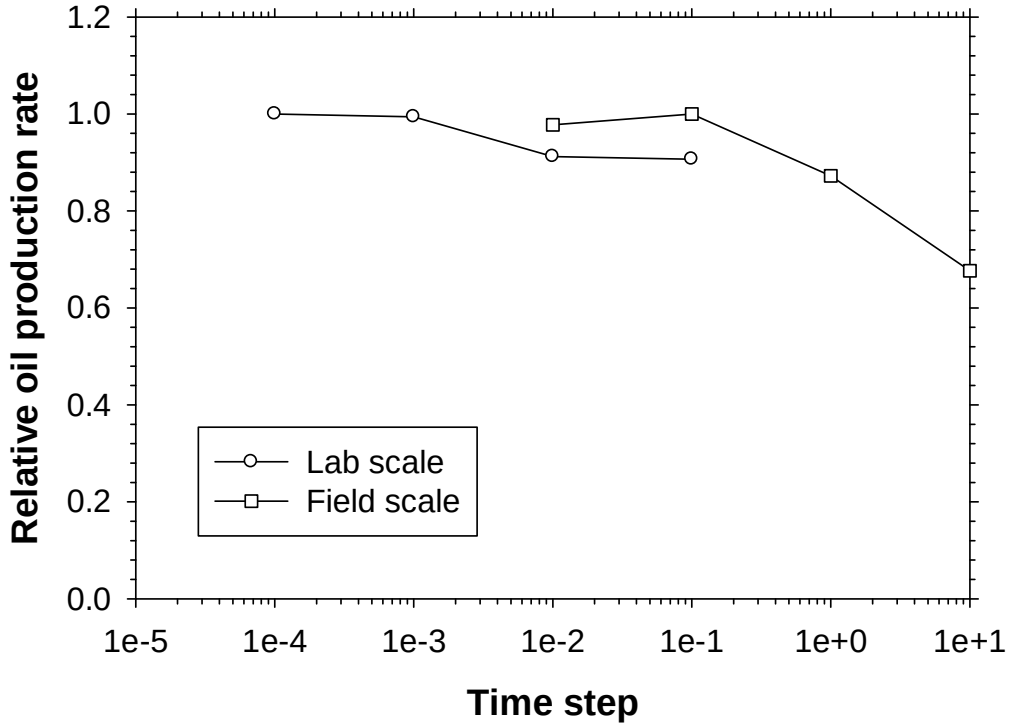

Figure 3.11 Effect of time step size on the relative oil production rate of simulation.

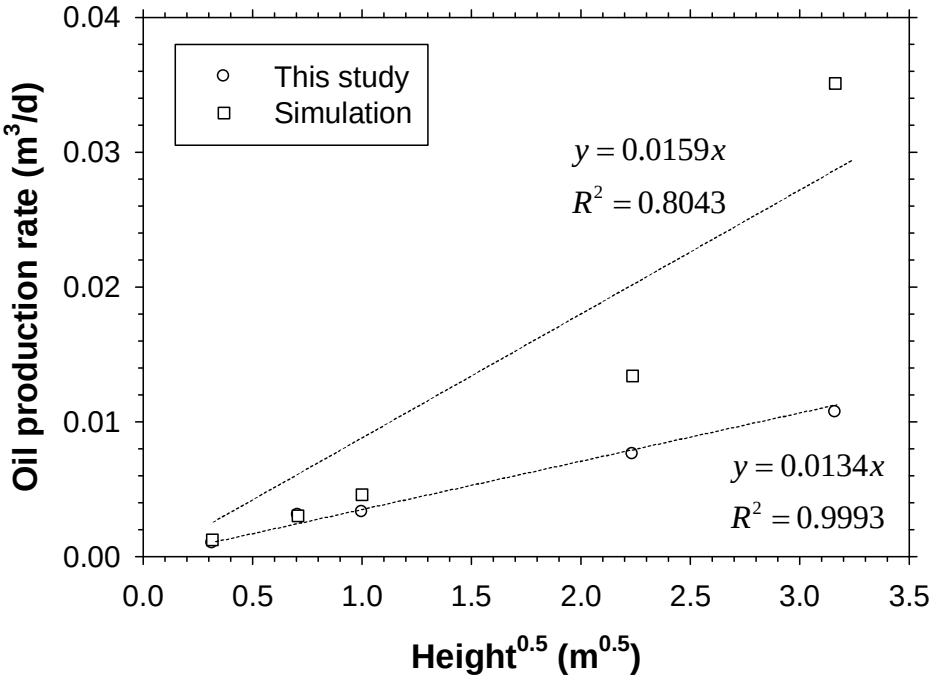

(a)

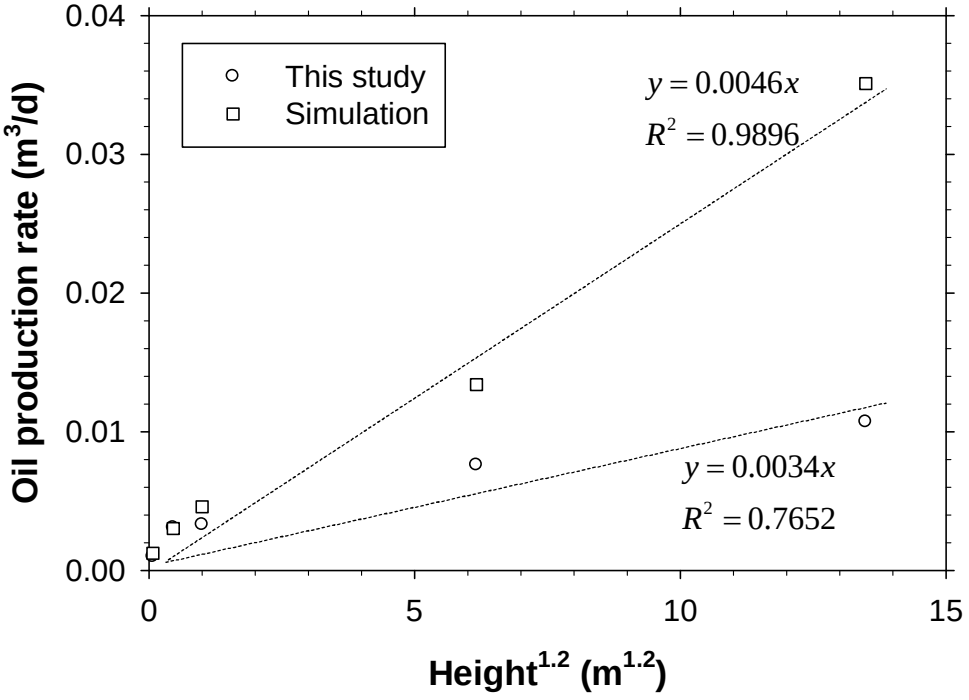

(b)

Figure 3.12 Effect of drainage height on oil production rate: **(a)** q vs $h^{0.5}$ and **(b)** q vs $h^{1.2}$.

Effect of D

One of the principal recovery mechanisms of VAPEX is oil viscosity reduction through solvent dissolution. This process is controlled by a diffusion coefficient between heavy oil and solvent vapor. It is worthwhile to note that the diffusion coefficient in Equation (3.1) is treated as an effective diffusivity that incorporates the effects of molecular diffusion and mechanical or convective dispersion. **Figure 3.13** investigates the interaction between the stabilized oil production rate and the effective diffusion coefficient for both lab- and field-scales. Four different effective diffusion coefficients (D = 1, 10, 50 and 100 $\times 10^{-10}$ m^2/s) are modeled and simulated. It is found that at the lab scale, the square-root of D shows a better linear trend with the calculated oil production rate than with the simulated data (**Figure 3.13a**). At field scale, the oil production rates are still fairly sensitive to the effective diffusion coefficients. But the simulation results show a huge discrepancy with a zero intercept on the ordinate (**Figure 3.13b**), which is because of the larger numerical dispersion in a field-scale simulation thanks to the corresponding bigger gridblocks and time steps. In short, this study can accurately and consistently describe the dependence of oil production rates on the heavy oil–solvent mixing process in various scales.

Numerical dispersion is an inherent property of numerical simulation. Thus, the simulated oil production data contains the effects of both physical diffusion and numerical dispersion. Since the new developed model is free of a truncation error, the calculated oil production data is affected only by the physical diffusion. Subtracting the analytical calculated oil production rate from the numerical simulated data, the effect of numerical dispersion can be estimated. **Table 3.2** lists the calculated and simulated oil production rates for four different diffusivities at both lab- and field-scales. The ratio of the oil rate due to numerical dispersion and the oil rate due to physical dispersion is plotted against diffusivity (Figure 3.14). It is found that the ratios show a power-law trend for either scale. The smaller the physical diffusivity is, the larger the contribution of numerical dispersion in the oil production rate will be. In addition, the simulation results at the field scale are less reliable than those at the lab scale, which is because the numerical dispersion at a large scale involves more numerical dispersion than at a small scale.

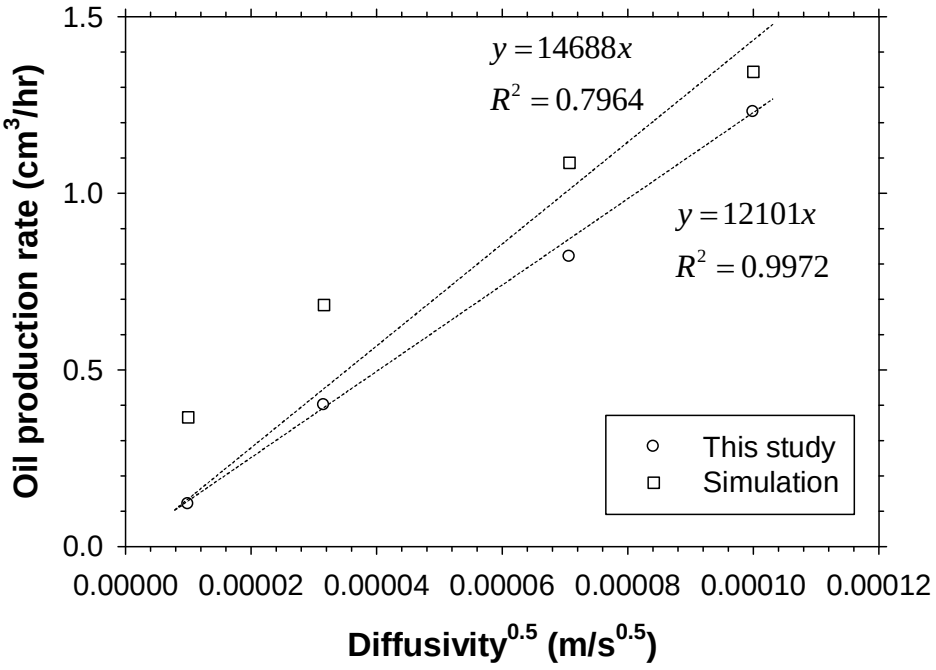

(a)

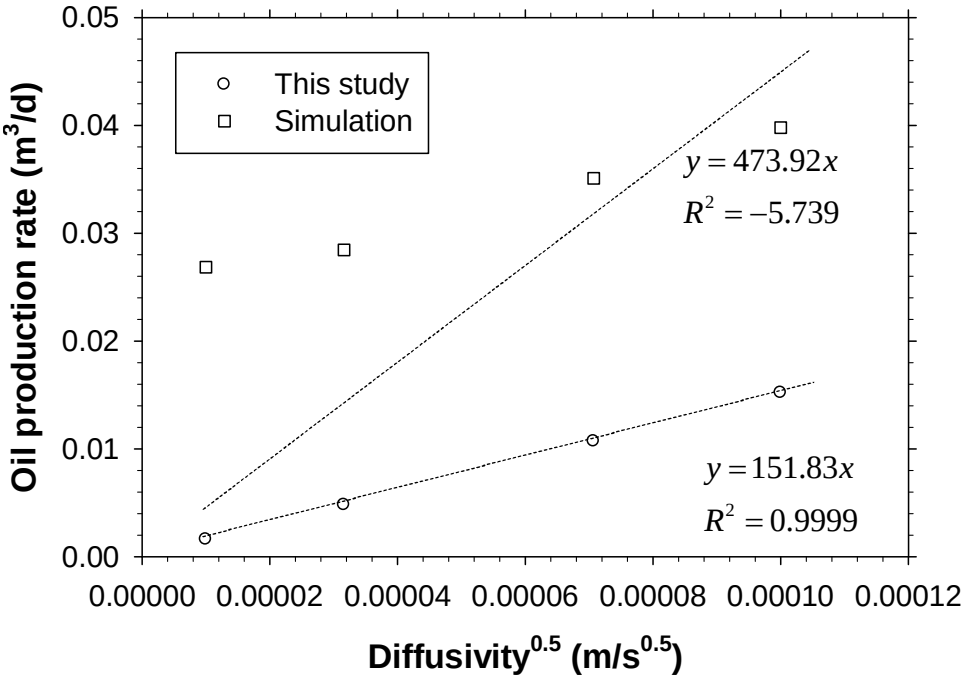

(b)

Figure 3.13 Effect of diffusivity on cumulative oil production at **(a)** lab-scale and **(b)** field-scale.

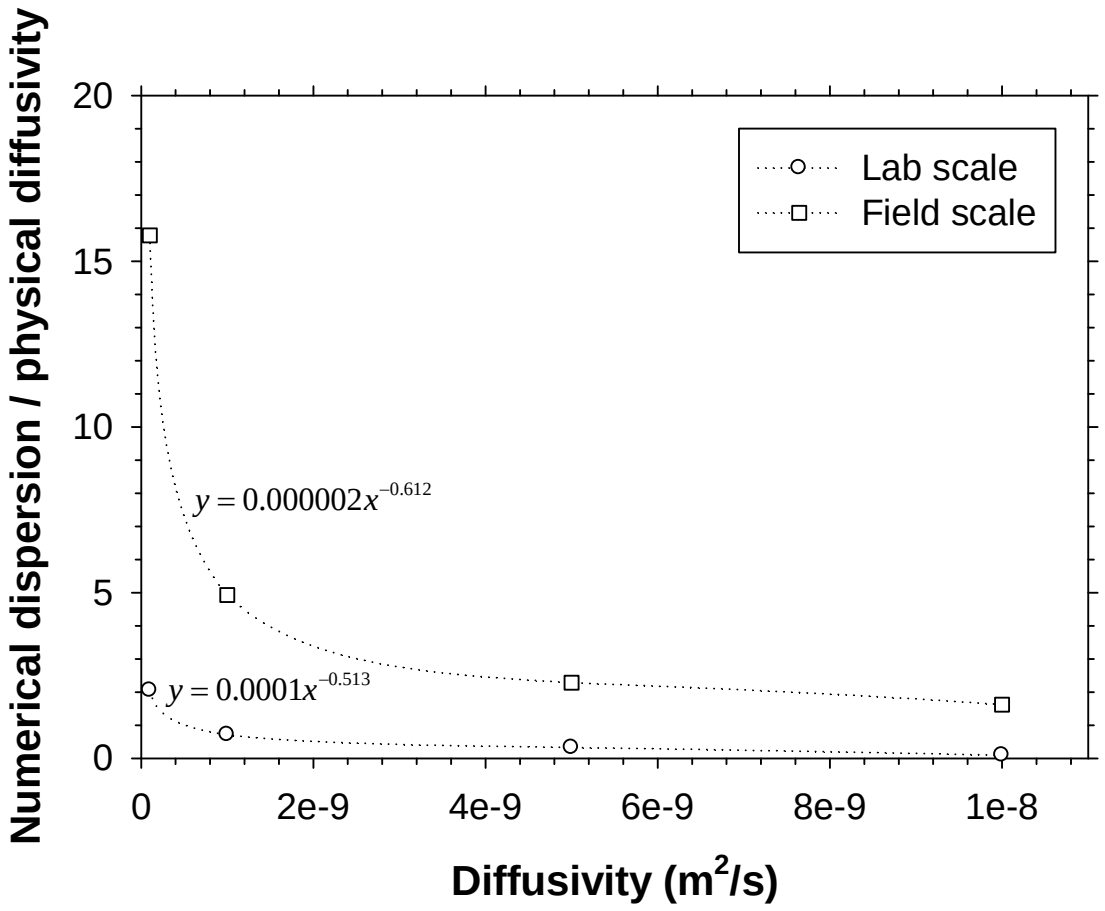

Figure 3.14 Effect of numerical dispersion and physical dispersion

Table 3.2 Estimation of numerical diffusivity.

	Lab scale			Field scale		
D	$q_{simulation}$	$q_{calculation}$	α_{lab}*	$q_{simulation}$	$q_{calculation}$	α_{field}*
1E-10	0.366	0.0269	2.050	0.0269	0.122	15.781
1E-09	0.684	0.0285	0.710	0.0285	0.401	4.927
5E-09	1.086	0.0351	0.324	0.0351	0.821	2.280
1E-08	1.344	0.0398	0.093	0.0398	1.232	1.618

* α_{lab} and α_{field} are used to estimate the relative effect of numerical dispersin to physcial diffusivity on the lab-scale and field-scale oil production rates, respectively. It is defined as: $\alpha = (q_{simulation} - q_{calculation}) / q_{calculation}$.

3.3.5 Model comparison

Table 3.3 compares the stabilized oil production rates predicted by using five analytical, empirical, and simulation models for a lab-scale VAPEX process. It is found that estimation by using the Butler–Mokrys analytical model is much higher than the rest, which is probably due to some over-simplified assumptions such as a steady-state mass transfer process. The simulation and calculation results are close to each other due to the small scale and a weak effect of numerical dispersion at small scale simulation.

3.4 Chapter Summary

This chapter develops a new mathematical model for the solvent chamber evolution in a VAPEX heavy oil recovery process. This model takes into account major oil recovery mechanisms of VAPEX including dynamic mass transfer, gravity drainage, surface renewal, and multiphase flow within a solvent chamber boundary. It is found the solvent concentration in the transition zone grows slower at the top than at the bottom while rather stable at the middle along the drainage surface. The model is then used to compare and analyze the reliability of a numerical simulation model. It is found that regarding the dependence of the stabilized oil rate on drainage height, this study's results agree well with the previous analytical correlations at both lab- and field-scales. In addition, the newly developed VAPEX model can accurately describe the relationship between an oil production rate and a diffusion coefficient in various scales thanks to the absence of numerical dispersion. Moreover, the numerical dispersion is estimated to increase with an increase in gridblock sizes but decrease with an increase in physical diffusivity.

Table 3.3 Predicted lab-scale oil production rates by different VAPEX models.

No.	Oil production rate (cc/hr)	method	Reference
1	2.227	Analytical	Das and Butler, 1995
2	0.585	Empirical, cubic correlation	Yazdani and Maini, 2005
3	0.718	Empirical, quadratic correlation	Yazdani and Maini, 2005
4	1.086	Simulation	with STARS, this study
5	0.823	Analytical	This study

CHAPTER 4 MASS TRANSFER IN VAPEX

Diffusivity is the most important parameter to characterize the mass transfer between heavy oil and solvent in VAPEX. It is considered as either constant or variable in the literature. Based on the VAPEX mathematical model developed in the last chapter, this chapter is going to determine the diffusivity between heavy oil and solvent in VAPEX by history matching theoretically predicted cumulative oil production and experimentally measured data. The best-fitted constant and variable diffusivities are then compared and analyzed.

4.1 Introduction

One of the most important recovery mechanisms of VAPEX is the mixing of heavy oil and solvent, which is actually a transient process dominated by molecular diffusion and affected by convective dispersion [Das 1996]. Mathematically, this process can be described by using Fick's second law whose diffusivity is a key parameter in the calculation of a mutual diffusive flux. Modelers have come to consider diffusivity either as constant or variable, the latter justified in the progressive change of properties such as viscosity in the media within the transition zone. Diffusivity is assumed as a constant value when the solubility of solvent in heavy oil is small under test conditions. Previous experimental studies mostly measure the molecular diffusivity between a heavy oil and a vaporized solvent as a constant [Schmidt, 1985; Upreti and Mehrotra, 2000, 2002; Tharanivasan et al., 2006; Yang and Gu, 2006; Etminan et al., 2010]. **Table 2.4** lists some measured diffusivity through laboratory tests. Meanwhile, Hayduk and Cheng [1971] concluded that the diffusivity of a solvent–oil system (ethane in n-hexane, heptanes, octane, dodecane, and hexadecane, or carbon dioxide in hexadecane) depends on the mixture viscosity, which is commonly expressed in a power law equation:

$$D(\mu) = \alpha \mu^{-\beta}, \tag{4.1}$$

where α and β are constants depending on the crude oil and solvent properties as well as operating conditions; and μ is the viscosity of an oil−solvent mixture, Pa·s. The exponent, β, is usually less than unity. Based on this general form, a number of variable correlations

for diffusivity and viscosity are proposed [Hayduk *et al*, 1971; Hayduck and Cheng, 1973; Hiss and Cussler, 1973; Das and Butler, 1996].

4.2 Mathematical Model

4.2.1 Mass transfer model

The transient heavy oil–solvent mixing process within a transition zone can be described by using Fick's second law:

$$\frac{\partial c}{\partial t} = \frac{\partial}{\partial x}\left(D \frac{\partial c}{\partial x} \right) \tag{4.2}$$

here c is the concentration of solvent, vol%; D is the diffusivity, m^2/s; x is the spatial variable, m; and t is the temporal variable, s. Heavy oil–solvent mixing process in porous media is extremely complex since it is affected by numerous factors including molecular diffusion, convective dispersion, improved interfacial contact, and enhanced surface renewal by capillary imbibition [Upreti et al., 2007]. It is difficult to separate and evaluate their respective effects on the heavy oil–solvent mixing process. Therefore, this study adopts a terminology, effective diffusivity, to account for all physical phenomena that may contribute to oil dilution [Dunn et al., 1989; Boustani et al., 2000].

Diffusivity in Equation (4.2) is found to depend on the viscosity of a heavy oil–solvent mixture. For example, Das and Bulter [1996] regressed a correlation for the diffusion coefficient of Suncor's bitumen and propane:

$$D = 13.06 \times 10^{-10} \mu^{-0.46} \text{ (for propane–bitumen mixture)} \tag{4.3}$$

The viscosity of a heavy oil–solvent system is commonly modeled in terms of the solvent concentration by using the Lederer–Shu correlation [Lederer, 1933; Shu, 1984]. Since viscosity is a function of concentration, the governing equation with the concentration-dependent viscosity becomes:

$$\frac{\partial c}{\partial t} = D \frac{\partial^2 c}{\partial x^2} + \frac{\partial D}{\partial x} \frac{\partial c}{\partial x} \tag{4.4}$$

Initially, the heavy oil is free of solvent. The oil at the left boundary of the transition zone is fully saturated with solvent and the right boundary of the transition zone is impermeable.

$$c\left(x, t=0\right)=0 \tag{4.5}$$

$$c\left(x=s\left(t\right), t\right)=c_{\max} \tag{4.6}$$

$$\frac{\partial c}{\partial x}\left(x=L, t\right)=0 \tag{4.7}$$

4.2.2 Transformation and solution

It is noted that $x = s(t)$ represents the dynamic position of the left boundary, which advances towards the untouched heavy oil zone due to the depletion of solvent-diluted heavy oil from the peripheral transition zone. This makes the mathematical model a moving boundary problem or a Stephen problem. This study applies a front tracking method to solve the moving boundary problem, in which a new coordinate is defined to immobilize the front:

$$\xi = x-\int_0^t U\left(t\right)dt \tag{4.8}$$

where U is the boundary moving velocity normal to the solvent chamber boundary, m/s. Apply the chain rule to obtain the first- and second-order derivatives of c with respect to ξ, respectively:

$$\frac{\partial}{\partial x}=\frac{\partial}{\partial \xi}\frac{\partial \xi}{\partial x}=\frac{\partial}{\partial \xi} \tag{4.9}$$

$$\frac{\partial^2}{\partial x^2}=\frac{\partial}{\partial x}\left(\frac{\partial}{\partial x}\right)=\frac{\partial}{\partial \xi}\left(\frac{\partial}{\partial \xi}\right)\frac{\partial \xi}{\partial x}=\frac{\partial^2}{\partial \xi^2} \tag{4.10}$$

The first-order derivative of c with respect to t:

$$\frac{\partial}{\partial t}=\frac{\partial}{\partial \xi}\frac{\partial \xi}{\partial t}+\frac{\partial}{\partial t}\frac{d\tau}{dt}=\frac{\partial}{\partial \xi}\left(-U\right)+\frac{\partial}{\partial t}=-U\frac{\partial}{\partial \xi}+\frac{\partial}{\partial t} \tag{4.11}$$

Applying the above transformation to the governing equation, IC, and BCs, a transformed mass transfer model in the new coordinates becomes

$$\frac{\partial c}{\partial t}=D\frac{\partial^2 c}{\partial \xi^2}+\frac{\partial D}{\partial \xi}\frac{\partial c}{\partial \xi}+U\frac{\partial c}{\partial \xi} \tag{4.12}$$

$$c\left(\xi, t=0\right)=0 \tag{4.13}$$

$$c\left(\xi=0, t\right)=c_{\max} \tag{4.14}$$

$$\frac{\partial c}{\partial \xi}\left(\xi = L, t\right) = 0 \tag{4.15}$$

Due to the complex relationship between D and c, Equation (4.13) is a second-order nonlinear parabolic partial different equation (PDE) whose analytical solution is not readily available. Therefore, this model is solved numerically by using the Newton–Raphson iterative method.

Except the mass transfer model, the rest of the mathematical model of VAPEX including transformation of the mass transfer model, solvent chamber evolution, and solution procedures are the same as those in Chapter 3.

4.2.3 Diffusivity determination

Based on the VAPEX mathematical model developed in the last chapter, this chapter determines the diffusivity in VAPEX by history match theoretically predicted cumulative oil production and experimentally measured data. A numerical optimization strategy is applied to determine the effective diffusivity. First, the following objective function is defined to represent the discrepancy between the theoretically predicted and experimentally measured cumulative heavy oil production data at different times:

$$Err = \sqrt{\frac{1}{n}\sum_{i=1}^{n}\left|Q_{\text{cal}}\left(t\right) - Q_{\text{exp}}\left(t\right)\right|_{t_i}^{2}} \tag{4.16}$$

Then, with all other properties fixed, the effective diffusivity is used as an adjustable parameter and thus determined when the objective function reaches its minimum value. For the two-parameter viscosity-dependent diffusivity in Equation (4.1), the exponent is first fixed and the coefficient is then determined through history matching. Figure 3 shows the flow chart for the calculation of the VAPEX theoretical model.

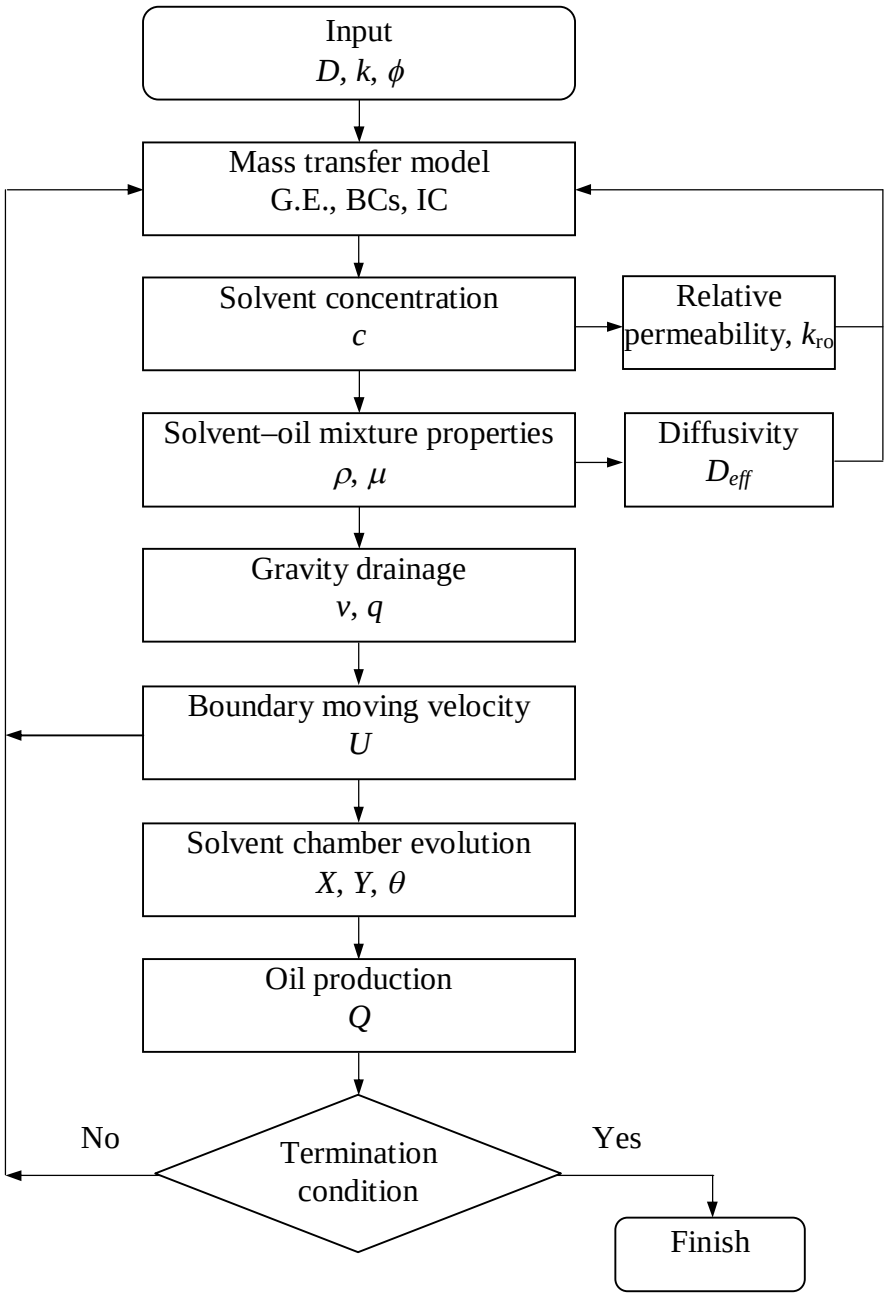

Figure 4.1 Flow chart of the solution to the VAPEX mathematical model.

4.3 Results and Discussion

4.3.1 Constant diffusivity (D_c)

Diffusivity between heavy oil and solvent can be considered as either a concentration-independent constant or a concentration-dependent variable. This chapter first considers it as a constant and determines it by history matching theoretically predicted cumulative oil production and experimentally measured data from a literature. Variations of the objective function $Err(D_c)$ with the diffusivity of propane in the heavy oil are shown in **Figure 4.2a**. The best-matched effective diffusivity is $D_c = 4.3\times10^{-9}$ m^2/s at the minimum objective function of $Err_{min} = 7.2$. **Figure 4.2b** shows the best fit of the experimentally measured and theoretical calculated oil production. It can be seen that for the cumulative oil production, the prediction matches well with the measurement. In addition, regarding the oil production rate, the prediction follows the general trend of the real data except in the first couple of hours. Because during the very early stage of VAPEX, the injector and producer are in communication by applying a large pressure difference in-between, and this displacement results in higher oil production.

4.3.2 Variable Diffusivity (D_v)

The effective diffusivity between heavy oil and solvent is then considered as a power function of viscosity, the same as Equation (3.1). Since this formula has two variables, this study first sets the exponent as a fixed value and adjusts the coefficient α to fit the theoretically predicted and experimentally measured production data. The range of β (β = –0.45, –0.5, –0.55, and –0.6) are consistent with that in the literature. For each β value, the exponent is tuned to obtain the best match. The *Err* versus α profiles (**Figure 4.3a**) shows that minimum objective functions are reached between 7.28 and 7.65 at α = 7.5, 6.0, 4.5, and 3.6×10^{-10} m^2/s for the four β values. **Figure 4.3b** shows the four best-matched cumulative oil productions with variable diffusivities.

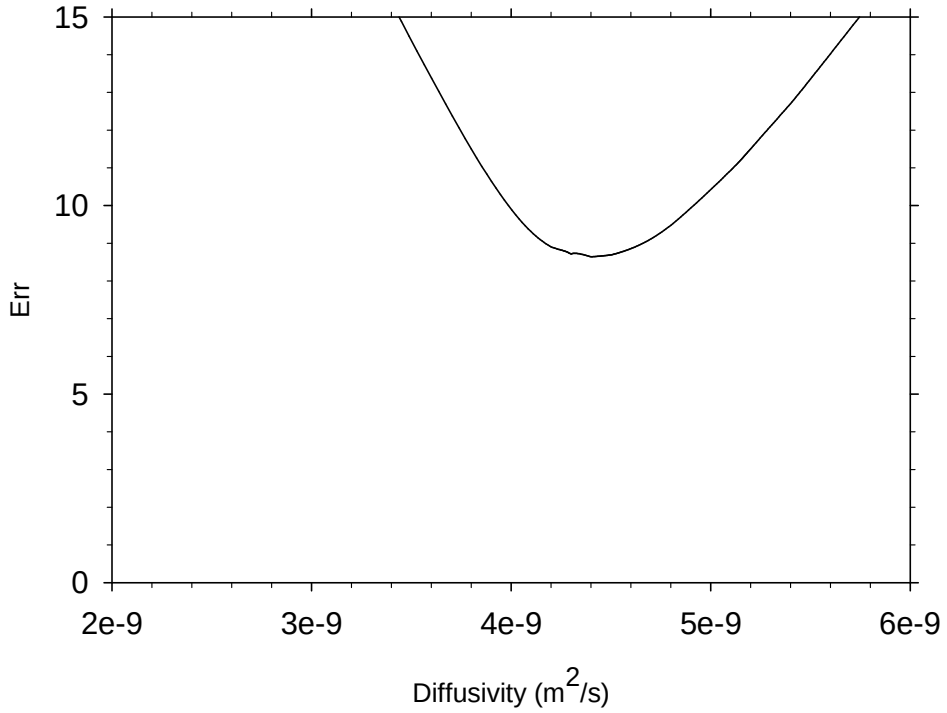

(a)

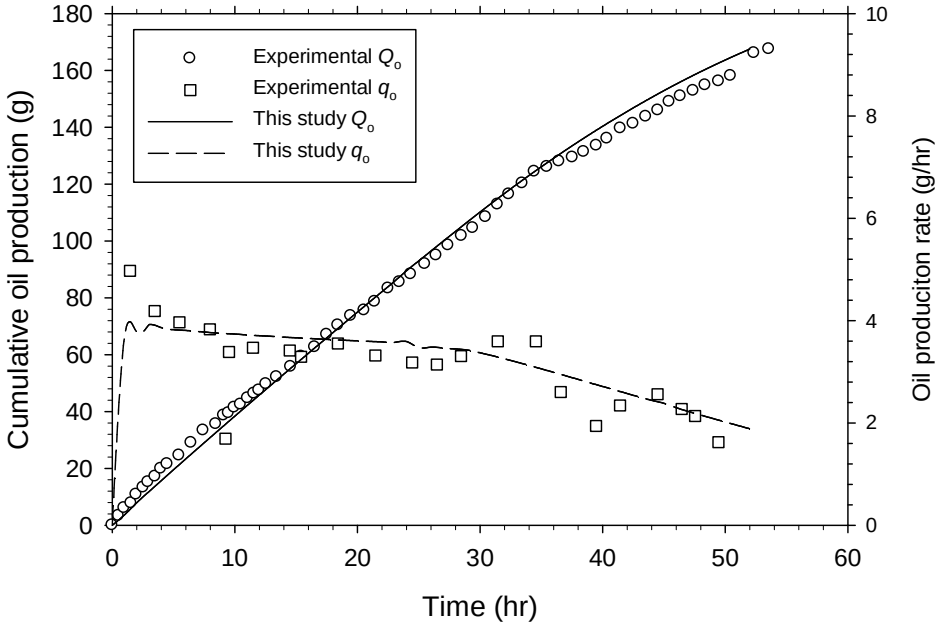

(b)

Figure 4.2 Simulation results with a constant diffusivity: **(a)** *Err* vs. D_c and **(b)** best fit of experimentally measured and theoretically calculated cumulative production data.

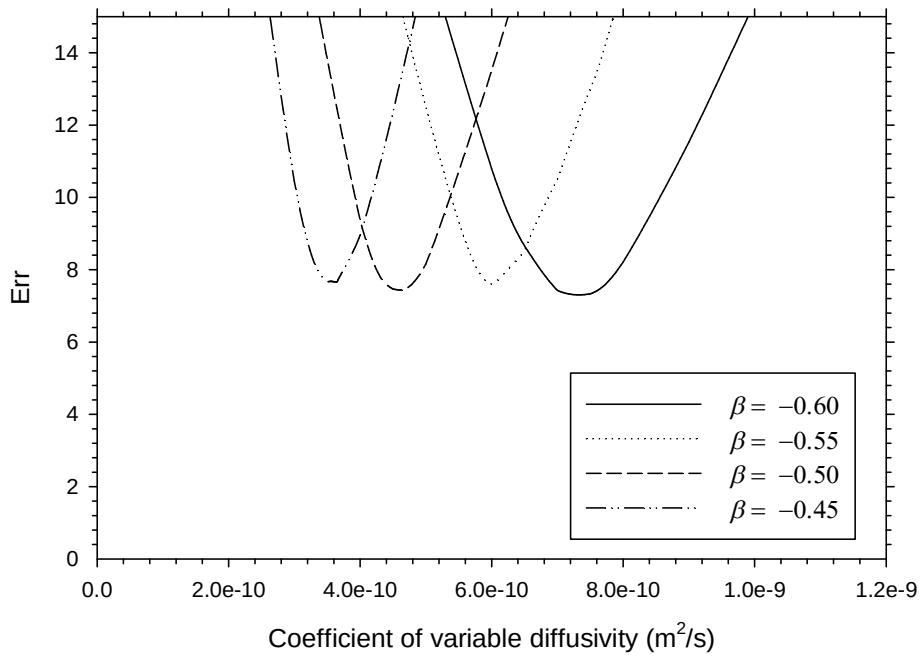

(a)

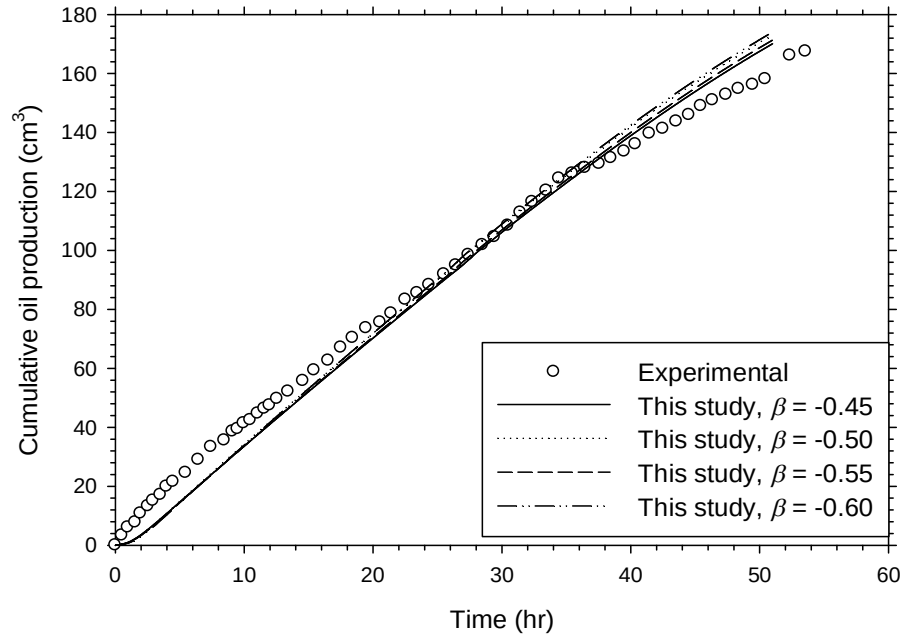

(b)

Figure 4.3 Simulation result with variable diffusivities: **(a)** *Err* vs. D_v and **(b)** best fit of experimentally measured and theoretically calculated cumulative production data.

It can be seen that, first, the best-matched cumulative oil production profiles for the four β values almost overlap each other. It seems that a decent fit can be obtained for a selected β value. Second, for the best-matched points, some smaller exponent leads to a larger coefficient. **Figure 4.4** plots the best-matched coefficients against the four exponents. It is found the variable coefficient of diffusivity rises exponentially with the exponent. A correlation between the two parameters is regressed as:

$$\beta = 9.26\times10^{-9}e^{5.47\alpha} \tag{4.17}$$

This indicates that mathematically the viscosity-dependent diffusivity in Equation (4.1) can be determined given its exponent or coefficient.

The approach in this study also simultaneously adjusts the coefficient and exponent of variable diffusivity function to match the theoretically predicted and experimentally measured cumulative oil production. The coefficient α ranges in [1×10^{-10}, 1.5×10^{-9}] and the exponent β varies between [–0.3, –0.6]. **Figure 4.5** shows the calculated error by using Equation (4.3). The optimized coefficient and exponent of variable diffusivity distribute in a curved, narrow band highlighted in dark blue. These best-fitted coefficients and exponents are plotted and compared with the prediction by using the regressed formula Equation (4.2) in **Figure 4.6**. It shows that the best-matched coefficient of variable diffusivity is exponentially correlated with the corresponding exponent.

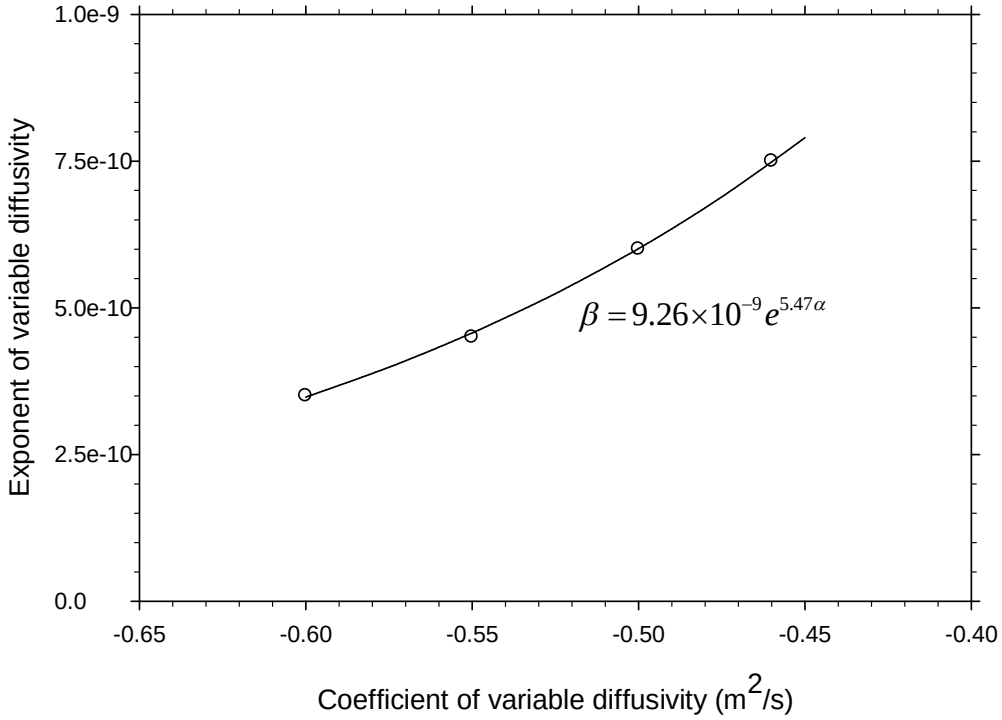

Figure 4.4 Coefficient versus exponent of the variable effective diffusivity.

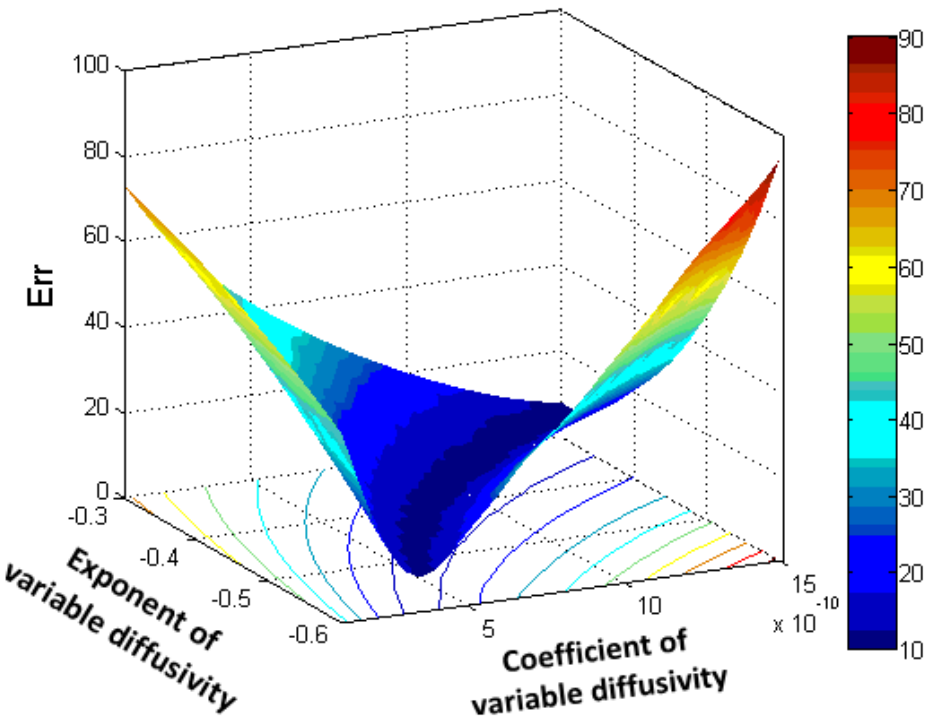

Figure 4.5 *Err* vs. α and β for simultaneous adjustment of the coefficient and exponent of variable diffusivity.

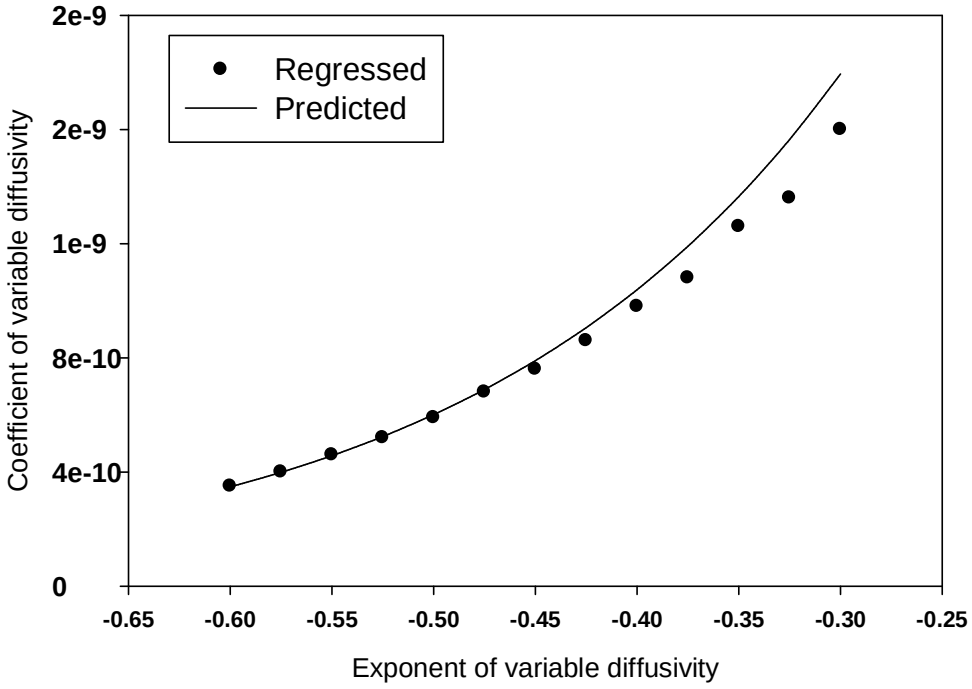

Figure 4.6 Coefficient vs. exponent of variable diffusivity through optimization (this figure) and prediction (formula in Figure 4.4).

4.3.3 Constant Diffusivity vs. Variable Diffusivity (D_c vs. D_v)

Figure 4.7 compares the dimensionless concentration and gravity drainage velocity profiles across the transition zone for the five best-matched diffusivities including a constant diffusivity ($D_c = 5.7e^{-10}$ m^2/s) and four variable diffusivities ($D_v = 7.5e^{-10}\mu^{-0.45}$, $6.0e^{-10}\mu^{-0.50}$, $4.5e^{-10}\mu^{-0.55}$, and $3.6e^{-10}\mu^{-0.60}$). Constant diffusivity gives a convex concentration profile while variable diffusivities yield concave ones. Also, the former has a much deeper solvent invasion than the latter at the same moment (t = 20 hrs). Physically, oil in the latter case is better diluted and thus flows faster near the interface. Whereas it is less diluted but has a wider mobile band in the constant diffusivity case. In particular, it is found that both concentration and velocity profiles with the four variable diffusivities are rather close to each other, which somewhat agrees well with the corresponding cumulative oil production profiles (**Figure 4.3**). Although both the constant and variable diffusivities can achieve a fairly good history match in production data, their respective characterizations of the fluid properties in the transition zone are rather different. The thicknesses of the mobile zone are found to be about 2.0 cm and 0.7 cm at the middle part by using constant and variable diffusivities, respectively. In addition, the gravity drainage velocity peaks at about 0.2 cm ahead of the solvent chamber boundary for both scenarios. The calculated transition zone thickness by using variable diffusivity agrees better with the experimental data in the literature, whereas the calculated transition zone thickness by using constant diffusivity predicts an unrealistically wide transition zone.

From the above investigation, it is found variable diffusivity can get nearly the same cumulative oil production as constant diffusivity does as long as their values are properly selected. The relationship between constant and variable diffusivities is further analyzed in the following procedures: First, we select four constant diffusivities for a VAPEX process, D_c = 1, 3, 5, 8×10^{-10} m^2/s. Second, for each constant diffusivity, we calculate the cumulative oil production, Q_c, by using the newly developed VAPEX model and the base-case data. Third, we assume $\beta = -0.45$ and run the VAPEX model to determine the optimum α by matching Q_v with Q_c for each D_v. Fourth, we repeat the previous step for

β = –0.50, –0.55, and –0.60, respectively. Finally, we plot the best-matched α for each D_c and β (**Figure 4.8**). It is found that for each one of the four βvalues, the best matched α can be fairly linearly regressed with constant diffusivity:

$$\alpha = 0.0993 D_c, \ for \ \beta = -0.45 \tag{4.18}$$

$$\alpha = 0.0881 D_c, \ for \ \beta = -0.50 \tag{4.19}$$

$$\alpha = 0.0647 D_c, \ for \ \beta = -0.55 \tag{4.20}$$

$$\alpha = 0.0494 D_c, \ for \ \beta = -0.60 \tag{4.21}$$

Therefore, a constant diffusivity can be converted to an equivalent variable diffusivity by using Equations (4.18)–(4.21) for the VAPEX process.

4.3.4 Back-calculated constant D_{eff}

Heavy oil-solvent diffusivity is back-calculated for four VAPEX experimental data sets in the literature by using the theoretical model developed in this chapter. For the constant diffusivity between propane and heavy oil, the searching range starts from $D_c = 0.8\times10^{-9}$ m^2/s and ends at $D_c = 8.0\times10^{-9}$ m^2/s. For variable diffusivity, this study assumes the exponent β = –0.5 and determines the coefficient α through history matching the theoretically calculated and experimentally measured cumulative oil production data. **Table 4.1** lists the major fluid and model properties, and best-matched constant and variable diffusivities. Comparing **Tables 2.4** and **4.1**, it is found that for propane, the back-calculated constant effective diffusivity is about 10–30 times the molecular diffusivity measured in the laboratory. It is noted that the large difference between the model-calculated effective diffusivity and lab-measured molecular diffusivity implies that dispersive mixing should play a major role in the heavy oil-solvent mass transfer. **Figure 4.9** shows the experimental observation and theoretical prediction of solvent chamber evolution. Obviously, this study's description is closer to experimental data over the entire VAPEX process

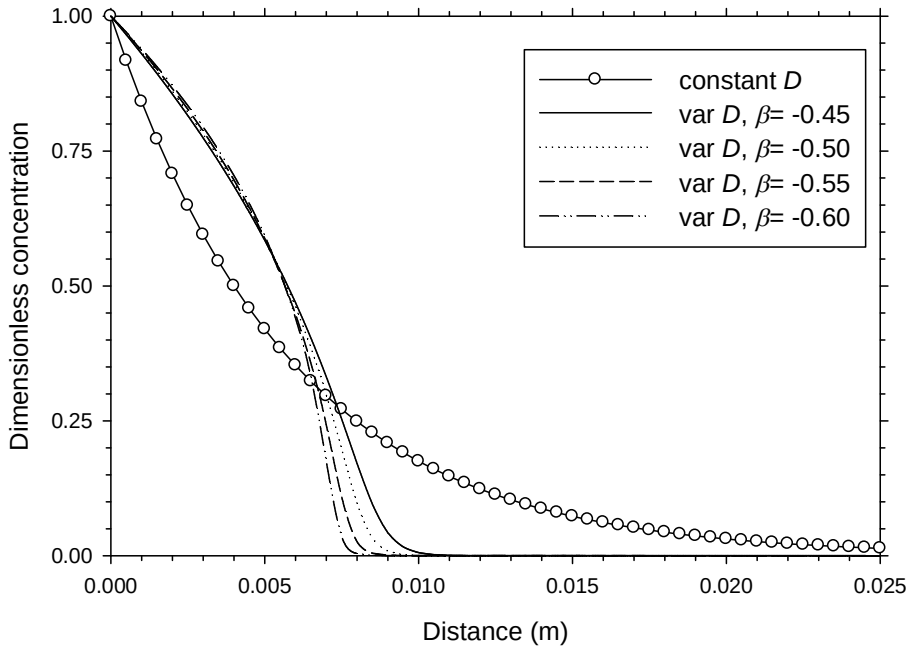

(a)

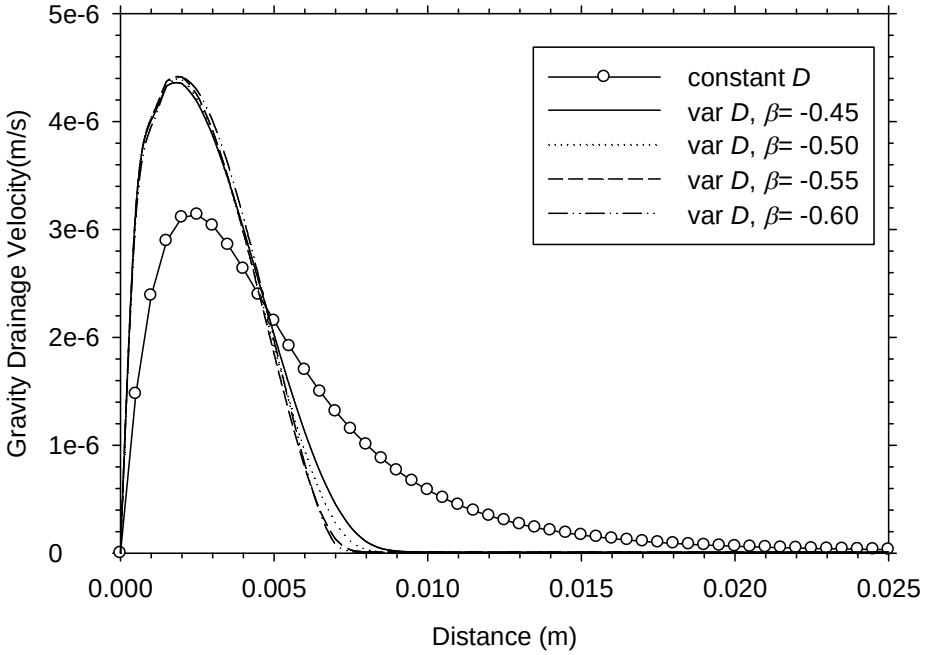

(b)

Figure 4.7 Effects of constant and variable diffusivity on **(a)** dimensionless concentration and **(b)** gravity drainage velocity profiles.

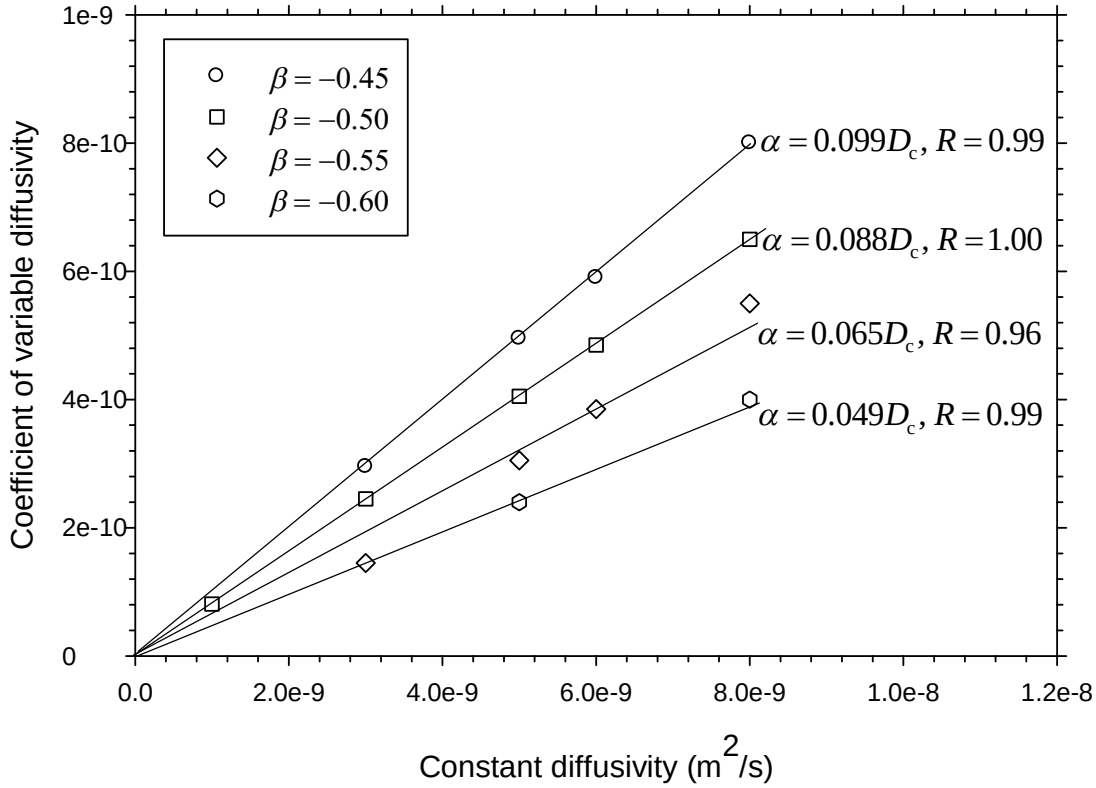

Figure 4.8 Coefficient of variable diffusivity versus constant diffusivity.

Table 4.1 Back-calculated constant and variable diffusivity*.							
Test No.	ϕ	k	S_{oi}	S_{or}	S_{or}–S_{oi}	**Constant D (D_c)**	**Variable D (D_v)**
1	32.9	52	97.7	7.1	90.6	5.2×10^{-9}	$7.5\times10^{-10}\mu^{-0.5}$
2	36.1	36	97.2	7.7	89.5	4.3×10^{-9}	$6.2\times10^{-10}\mu^{-0.5}$
3	35.4	25	97.1	7	90.1	6.3×10^{-9}	$4.1\times10^{-10}\mu^{-0.5}$
4	35.7	18	96.2	10.9	85.3	7.6×10^{-9}	$2.3\times10^{-10}\mu^{-0.5}$

* Experimental data is referred to [Lin et al., 2014].

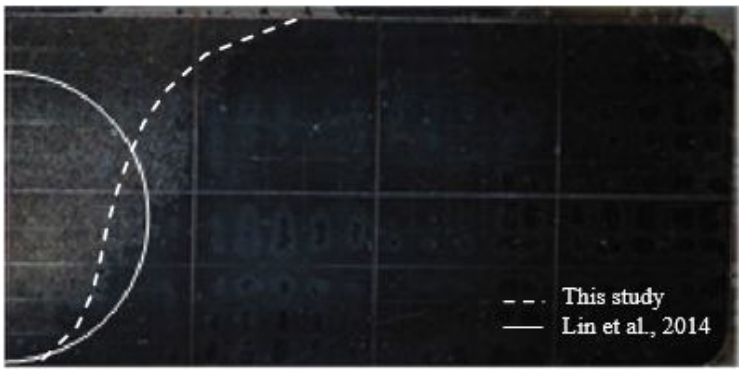

(a)

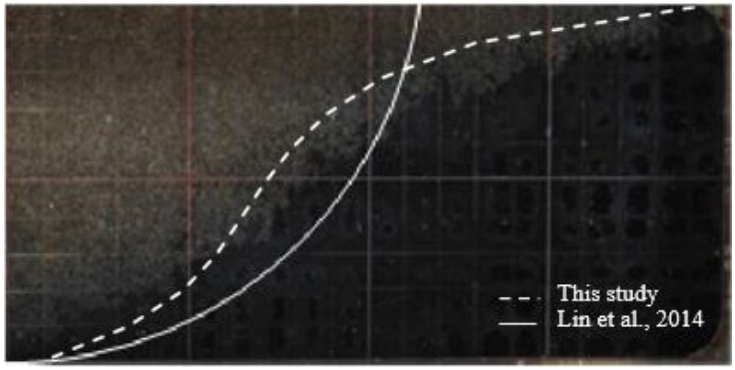

(b)

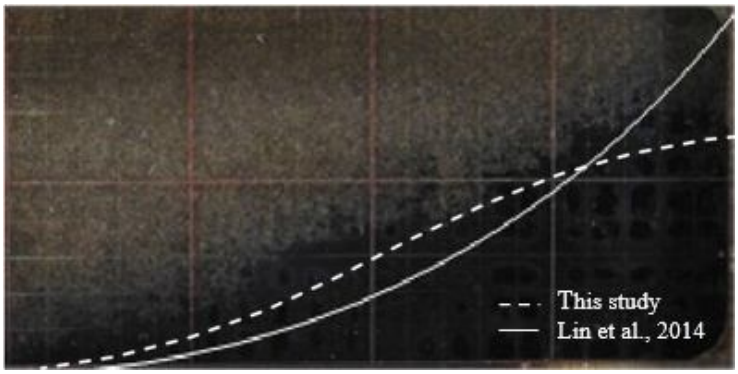

(c)

Figure 4.9 Match of theoretical estimation of this study and experimental observation at **(a)** early spreading, **(b)** late spreading, and **(c)** falling periods.

4.4 Chapter Summary

This chapter determines the heavy oil–solvent diffusivity in VAPEX through history matching theoretical prediction and experimental measurement. The following conclusions can be made through this study:

1. The solvent chamber development during the spreading and falling phases of VAPEX can be reasonably described by the newly developed theoretical model.
2. Although both the constant and variable diffusivities can achieve a fairly good history match in cumulative production data, their respective characterizations of the fluid properties in the transition zone are rather different. Variable diffusivity estimates the mobile zone as about 0.7 cm thick in the middle part of solvent chamber, whereas constant diffusivity predicts it as unrealistically 2.0 cm wide.
3. Constant diffusivity can be converted to equivalent variable diffusivity by using some correlations regressed in this study.
4. The back-calculated effective diffusivity can be about 10–30 times the molecular diffusivity measured in the laboratory, which the latter plays a minor role in the mixing of a heavy oil and a solvent vapor, and other mass transfer mechanisms such as convection and dispersion should be more important.

CHAPTER 5 MATHEMATICAL MODELING OF WARM VAPEX

This chapter presents a mathematical model for a hot solvent-based gravity drainage process, or warm VAPEX (W-VAPEX). A W-VAPEX takes advantage of both thermal recovery processes (heating) and solvent-based processes (dilution). The model starts from the characterization of the transient mass transfer between hot solvent and cold oil and is featured with the distribution of the injected solvent elaborated. Solvent recovery and a solvent-oil ratio are calculated, which help a comprehensive evaluation of a hot solvent injection process performance.

5.1 Introduction

As mentioned in Chapter 1, heavy oils are characterized by high viscosity, small (American petroleum institute) API gravity, and negligible mobility under initial reservoir conditions. Primary cold production can achieve about 5% of OOIP by using natural energy without sand control. Secondary recovery processes such as water or chemical flooding are employed because of their low cost and easy implementation [Mai and Kantzas, 2009]. However, because of an unfavorable mobility ratio and the resultant water channeling (so-called “viscous fingering”), the oil recovery factors for such unstable displacement processes are usually low.

Thermal recovery processes including steam-assisted gravity drainage (SAGD) are used to enhance heavy oil recovery [Moore et al., 1999; Vittoratos, 1990; Butler et al., 1981; Farouq Ali, 1994]. These techniques either inject a hot fluid from the surface or generate heat in situ by burning a portion of the resident oil, to heat the reservoir and reduce oil viscosity. As shown in **Figure 5.1a**, heavy oil viscosity can be effectively reduced by an increase in temperature. Although having achieved great successes in some field applications, these methods, particularly SAGD, are seriously challenged by such reservoir conditions as thin pay zones, bottom aquifers, gas caps, thief zones, and low rock thermal conductivity. Under these circumstances, thermal processes can be

economically unviable due to excessive heat losses, large energy consumption, and expensive water treatments [Pooladi–Darvish and Matter, 2001; Karmaker and Maini, 2003; Deng, 2005].

As an alternative of thermal techniques, solvent-based recovery processes have been considered promising to enhance heavy oil production. In particular, vapor extraction (VAPEX), a solvent-analogue of SAGD, injects a vaporized solvent (e.g., light alkanes, carbon dioxide, etc.) to dissolve and dilute crude heavy oils [Butler and Mokrys, 1993; Talbi and Maini, 2004]. **Figure 5.1b** shows an oil viscosity reduction with an increase in solvent content, which clearly demonstrates its great potential in oil dilution [Butler and Mokrys, 1989]. Besides, solvent-based recovery methods have some distinct advantages over their thermal counterparts in oil upgrading and environmental benefits [James et al., 2008]. For example, VAPEX consumes only 3% of energy needed for a thermal recovery process [Singhal, 199], and it requires much less surface facilities, and respectively saves about 25% and 50% of capital investment and operation cost in comparison with SAGD [National Energy Board, 2006].

As a variant of VAPEX, W-VAPEX injects a heated solvent to take advantage of both thermal recovery processes (quick thermal conduction and viscosity reduction) and solvent-based processes (lower energy consumption and less greenhouse-gas emission) [Rezaei and Chatzis, 2007; Pathak et al., 2011]. In W-VAPEX, hot solvent condenses at a chamber boundary, not only releasing latent heat to oil but also dissolving into heavy oil to further reduce its viscosity [Haghighat and Maini, 2013]. In comparison with conventional or cold VAPEX, W-VAPEX achieves a higher oil production rate and a lower solvent-oil ratio (SOR) [Rezaei and Chatzis, 2007]. For example, a so-called Nsolv process produces oil over 15 times faster than VAPEX [Nenniger and Nenniger, 2005; Nenniger and Gunnewiek, 2013]. Similar to VAPEX, the optimum operating pressure and temperature for hot solvent injection were found to be slightly below the corresponding saturation point [Pathak et al., 2011].

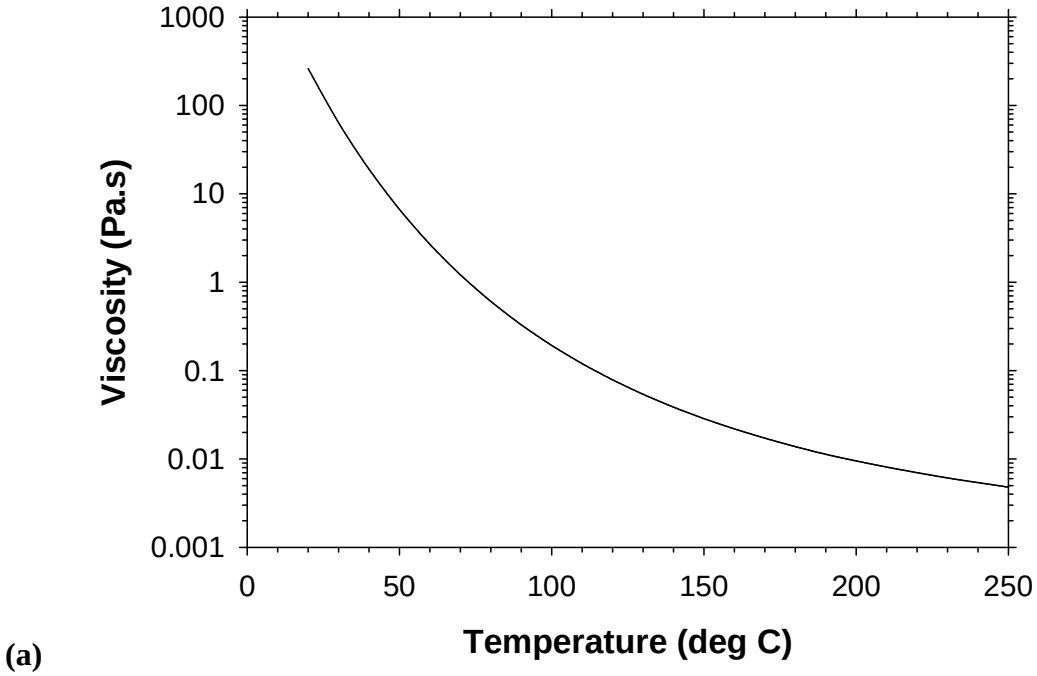

(a)

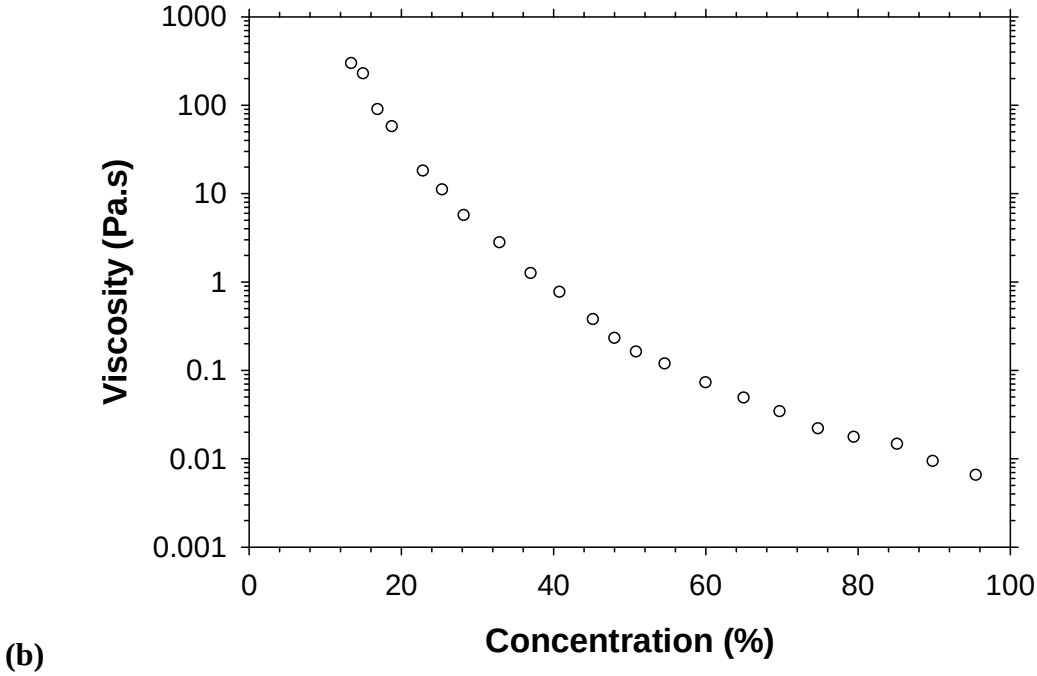

(b)

Figure 5.1 Respective effects of **(a)** temperature and **(b)** solvent concentration on the viscosity of Athabasca bitumen [Mehrotra and Svrcek, 1986; Butler and Mokrys, 1989].

Previous studies on W-VAPEX were mostly conducted by physical experiments and numerical simulation [James et al., 2008; Haghighat and Maini, 2013], and both have some inherent limitations [Chen et al., 2006]. Physical modeling would be limited by physical model properties, a wall effect, and operating conditions. Numerical simulation results can be affected by not only numerical dispersion but also mechanistic inaccuracy. For instance, some software may not properly consider the dependence of diffusivity on viscosity, which weakens the reliability of simulated results. On the other hand, analytical modeling can overcome such constraints and provide an accurate analysis on the performance of W-VAPEX.

This chapter develops a mathematical model for a W-VAPEX process. Transient mass transfer between a heated heavy oil and a hot solvent vapor and dynamic fluid properties in a transition zone are characterized. The mass transfer model is then incorporated into a VAPEX theoretical model to describe solvent chamber evolution and evaluate oil and solvent production. Sensitivity of an oil production rate to solvent temperature, crude heavy oil viscosity, and model height are respectively investigated.

5.2 Theoretical Models

5.2.1 Assumptions

VAPEX employs a pair of parallel horizontal wells with one placed at the bottom of a reservoir and the other one right above it (**Figure 5.2**). The upper horizontal well is used as a solvent injector and the lower one as an oil producer. Throughout a VAPEX process, first, the two horizontal wells are communicated by implementing a big pressure difference in-between. Then, a vaporized solvent with or without a carrier gas is injected into the reservoir. Finally, heavy oil is diluted through solvent dissolution, drained downward by gravity, and pumped out from the producer.

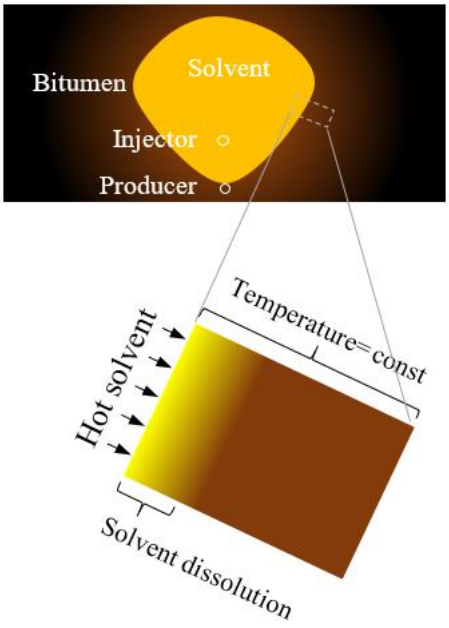

Figure 5.2 Schematics of a warm VAPEX recovery process.

W-VAPEX is a similar process to conventional VAPEX except that the solvent injected is hot instead of cold [Rezaei et al., 2010]. A solvent chamber is assumed to be fully filled with solvent vapor, residual oil, and connate water. Beyond the chamber boundary, heavy oil is heated and diluted, and drains downward by gravity. Farther away, the reservoir remains untouched. It is worthy of noting that a heated zone (about 10 m thick) is much wider than a diluted zone (less than 0.5 m thick) because the thermal diffusivity is usually 2–3 orders higher than the mass transfer diffusivity [Butler, 1991]. The temperature drops slightly in the front of the chamber boundary, as shown in the pseudo-steady temperature distribution [Sharma and Gates, 2010] (**Figure 5.3**). Quantitatively, it falls off by 4.6% within 0.5 m ahead of the chamber edge. Within this range, the concentration profiles for declining temperatures remain nearly the same as that for constant temperature (**Figure 5.4**). Thereby, it is reasonable to assume the temperature as constant in the front.

Since fluid properties in the solvent chamber and the untouched oil zone remain relatively stable, this study only focuses on the transition zone, and simplifies it as a series of rectangular segments with a piecewise linear boundary. More details can be found in **Chapter 3**. Assumptions for the reservoir model, operating conditions, and recovery mechanisms are made: uniform porosity and permeability, linear-source solvent injection at a constant pressure and a constant temperature, and pure gravity drainage of fluids along the chamber boundary. Moreover, due to complexity in recovery mechanisms and a minor contribution to oil production, the solvent-chamber rising phase is ignored in this chapter. In the following sections, a mass transfer model is first developed to characterize dynamic fluid properties in the transition zone, and then integrated into a VAPEX model to describe the chamber evolution, and estimate oil production, solvent consumption, and a solvent–oil ratio (SOR).

5.2.2 Mass transfer model

In each transition-zone segment, the diffusion process between a heavy oil and a hot solvent can be described by using Fick's Second Law:

$$\frac{\partial c}{\partial t} = \frac{\partial}{\partial x}\left(D\frac{\partial c}{\partial x} \right) \tag{5.1}$$

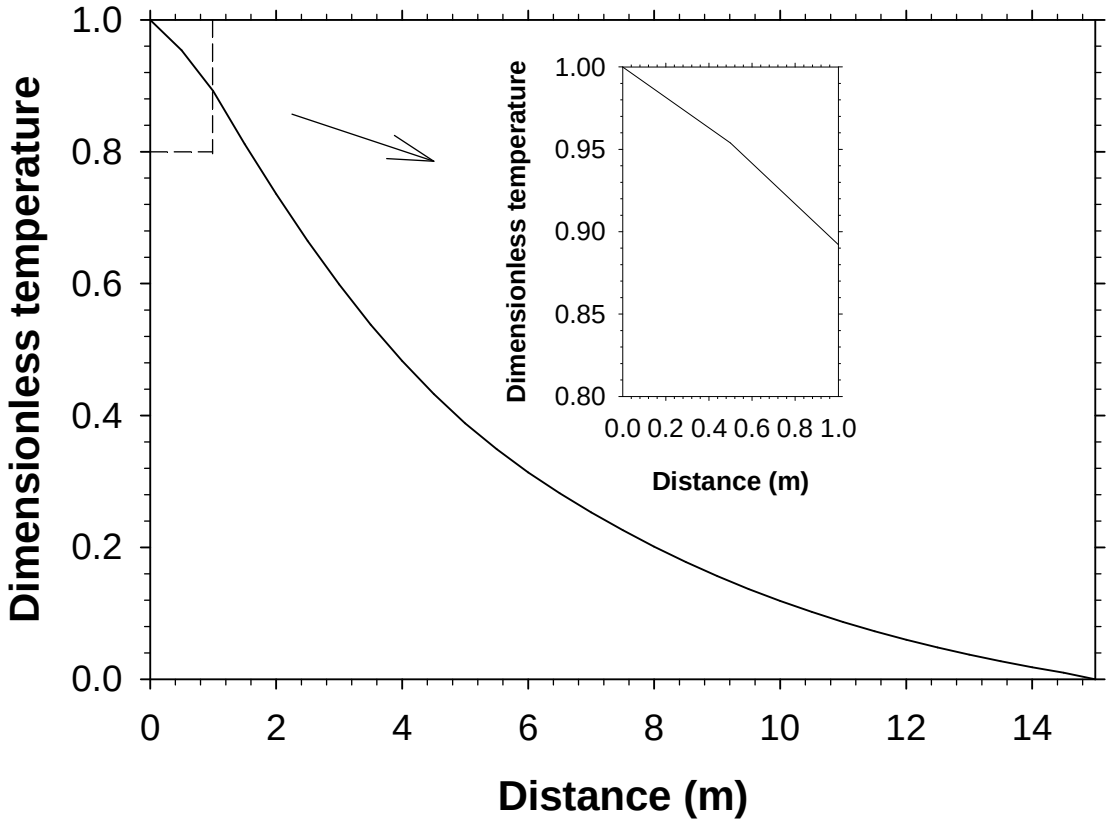

Figure 5.3 Temperature distribution beyond chamber front [Sharma and Gates, 2010].

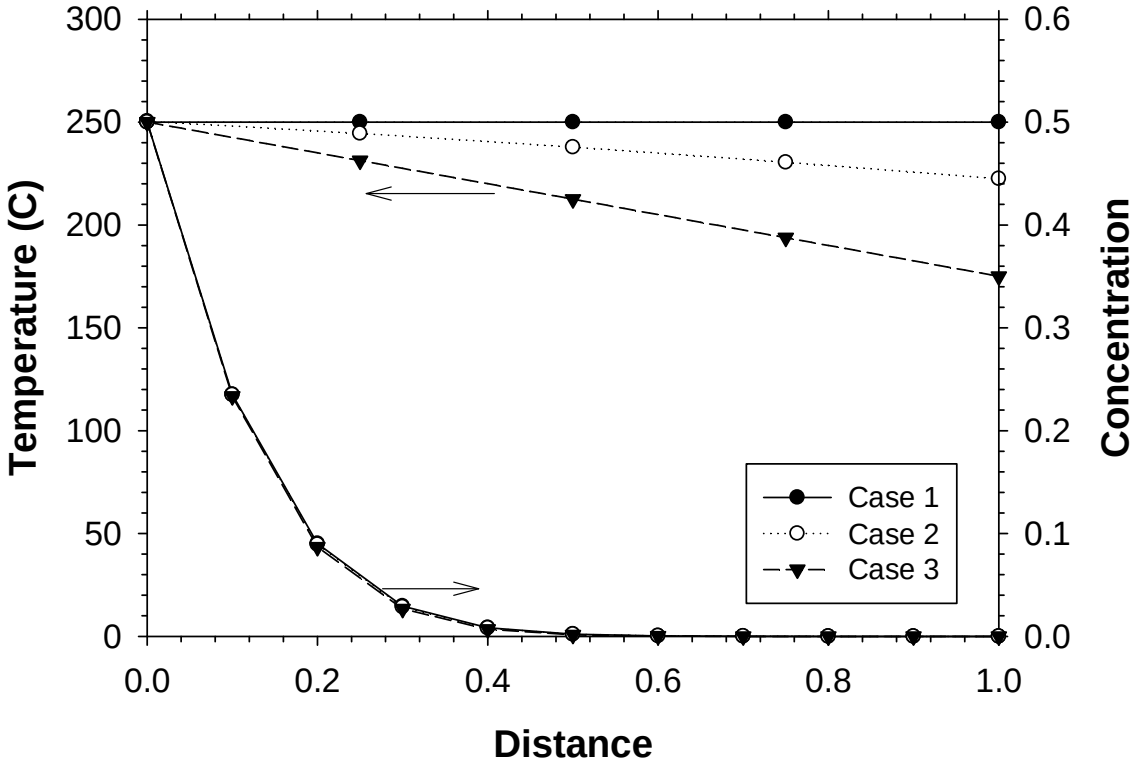

Note: Case 2 in this figure is the same pseudo steady-state temperature profile in Figure 5.3.

Figure 5.4 Concentration distributions for three different temperature profiles.

where c is the solvent concentration, vol.%; D is the effective diffusivity, m^2/s; t is the time, s; and x is the space, m. This study considers the diffusivity as a variable of concentration rather than a constant since the former is found to be able to give a more reasonable characterization of the transition zone than the latter (**Chapter 3**). The solvent chamber expands with time thanks to continuous depletion of solvent-diluted and heated heavy oil from a reservoir. In other words, the chamber boundary is moving toward the oil zone throughout a W-VAPEX process. To solve such a Stefan problem (a moving or free boundary problem), this study adopts a coordinate transform scheme that defines a new spatial variable to replace the reference axis:

$$\xi = x - Ut \tag{5.2}$$

Taking the first- and second-order derivatives of concentration with respect to the new space variable, and the first-order derivative of concentration with respect to time, respectively, we have:

$$\frac{\partial c}{\partial x} = \frac{\partial c}{\partial \xi}\frac{\partial \xi}{\partial x} = \frac{\partial c}{\partial \xi} \tag{5.3}$$

$$\frac{\partial}{\partial x}\left(D\frac{\partial c}{\partial x}\right) = \frac{\partial D}{\partial x}\frac{\partial c}{\partial x} + D\frac{\partial^2 c}{\partial x^2} = \frac{\partial D}{\partial \xi}\frac{\partial c}{\partial \xi} + D\frac{\partial^2 c}{\partial \xi^2} \tag{5.4}$$

$$\frac{\partial c}{\partial t} = \frac{\partial c}{\partial \xi}\frac{\partial \xi}{\partial t} + \frac{\partial c}{\partial t}\frac{d\tau}{dt} = \frac{\partial c}{\partial \xi}(-U) + \frac{\partial c}{\partial t} = -U\frac{\partial c}{\partial \xi} + \frac{\partial c}{\partial t} \tag{5.5}$$

We substituting Equations (5.4) and (5.5) into Equation (5.1) and rearrange the new equation to get the governing equation in a moving frame:

$$\frac{\partial c}{\partial t} = D\frac{\partial^2 c}{\partial \xi^2} + \left(U + \frac{\partial D}{\partial \xi}\right)\frac{\partial c}{\partial \xi} \tag{5.6}$$

The boundary and initial conditions in the moving domain are, respectively, set as

$$c(\xi = 0, t) = c^* \tag{5.7}$$

$$\frac{\partial c}{\partial \xi}(\xi = Z, t) = 0 \tag{5.8}$$

$$c(\xi, t = 0) = 0 \tag{5.9}$$

where c^* is the saturation concentration, vol.%; and Z is the length that extends beyond and is normal to the solvent chamber boundary, m.

5.2.3 Diffusivity under elevated temperature

The diffusivity between a heavy oil and a light alkane can be estimated by using a power-law empirical correlation [Hayduk and Cheng, 1971]:

$$D = \alpha \mu^{-\beta} \tag{5.10}$$

where α and β are constants depending on the properties of specific diffusive materials. The viscosity of solvent-diluted and heated heavy oil relies on not only temperature but also solvent concentration. It is computed by two steps: First, the viscosity of a crude oil due to heating only is represented by a logarithm function of temperature with accuracy by the following equation [Mehrotra and Svrcek, 1986]:

$$\ln\ln\left(\mu_o\right) = A_o \ln\left(T + 273.15\right) + B_o \tag{5.11}$$

where μ_o is the viscosity of heavy oil, Pa.s; T is the temperature, °C; A_o and B_o are the constant coefficients. Likewise, the viscosity of a hot condensed solvent in a liquid state is calculated by using a logarithm function [Reid et al., 1977]:

$$\log \mu_s = A_s \left(\frac{1}{T} - \frac{1}{B_s} \right) \tag{5.12}$$

where μ_s is the viscosity of a condensed solvent, Pa.s; A_s and B_s are the constant coefficients. The viscosity of the mixture of a heated heavy oil and a hot condensed solvent is calculated by using the Lederer–Shu correlation [Lederer, 1933; Shu, 1984]:

$$\mu = \mu_s^{f_s} \mu_o^{f_o} \tag{5.13}$$

$$f_s = \frac{c}{\lambda(1-c)+c}, \quad f_o = 1 - f_s \tag{5.14}$$

$$\lambda = \frac{17.04\left(\gamma_o - \gamma_s\right)^{0.5237} \gamma_o^{3.2745} \gamma_s^{1.6316}}{\ln\left(\mu_o / \mu_s\right)} \tag{5.15}$$

where μ is the mixture viscosity, Pa.s; f_o and f_s are the respective weighted volume fractions for heavy oil and solvent; γ_o and γ_s are the respective specific gravities of a heated heavy oil and a hot condensed solvent, dimensionless. The viscosity coefficients

of a typical Lloydminster heavy oil and liquid propane are respectively specified as follows:

$$A_o = -3.6261,\ B_o = 22.8339 \tag{5.16}$$

$$A_s = -222.67,\ B_s = 133.41 \tag{5.17}$$

5.2.4 Gravity drainage

Under the effect of gravity, the diluted heavy oil slips downward along the solvent chamber boundary. The gravity drainage velocity can be calculated by using Darcy's law:

$$u = -\frac{kk_{ro}}{\mu}(\rho - \rho_s) g \sin\theta \tag{5.18}$$

where k is the absolute permeability, m^2; k_{ro} is the oil-phase relative permeability, dimensionless; ρ is the density of the mixture, kg/m^3; ρ_s is the density of vaporized solvent, kg/m^3; g is the gravitational acceleration, m/s^2; and θ is the slip angle, degree. The relative permeability of the oil phase is determined by using Corey's correlation:

$$k_{ro} = k_{ro,rw}\left(\frac{S_o - S_{or}}{1 - S_{wc} - S_{or}}\right)^m \tag{5.19}$$

where $k_{ro,rw}$ is the oil relative permeability at minimum water saturation, dimensionless; S_{or} and S_{wc} are the residual oil and the connate water saturations, respectively, dimensionless; and m is a Corey coefficient, dimensionless. Oil saturation in the transition zone in this study adopts a linear correlation [Sharma and Gates, 2010]:

$$S_o = S_{or} + (S_{oi} - S_{or})\left(1 - \frac{c}{c^*}\right) \tag{5.20}$$

where S_{io} is the initial oil saturation, dimensionless. Given the solvent concentration, the heavy oil–solvent mixture density is calculated by using the ideal solution principle [McCain, 1990]:

$$\rho = \rho_o(1 - c) + \rho_s c \tag{5.21}$$

where ρ_o and ρ_s are the densities of a heavy oil and a condensed solvent, kg/m^3, respectively. The densities of a Lloydminster heavy oil and liquid propane are respectively specified as:

$$\rho_o = \rho_{15}\left[1 - 0.0603\left(\frac{T-20}{100}\right)\right] \tag{5.22}$$

$$\rho_s = -0.02T^2 - 0.13T + 507.81 \tag{5.23}$$

5.2.5 Chamber development

The oil gravity drainage rate from a transition-zone segment can be determined by integrating the drainage velocity over the cross-section of a transition-zone segment:

$$q_o = \phi W \int_{\xi_{\min}}^{\xi_{\max}} u\,(1-c)\,\mathrm{d}\xi \tag{5.24}$$

As mentioned above, the depletion of oil results in the spreading of a solvent chamber boundary. Thus, the advancement of a transition-zone segment boundary can be calculated by using a mass balance equation:

$$(q_{in} - q_{out})\delta t = \phi(S_{oi} - S_{or})Wl\delta\xi \tag{5.25}$$

where q_{in} and q_{out} are the rate of fluids flowing into and draining out of a transition-zone segment, respectively, m^3/s; δt is the time interval, s; l is the length of a transition-zone boundary, m; $\delta\xi$ is the distance moved by the boundary during δt, m. If the time snippet is small enough, the flow rates and transition-zone boundary length in the above equation can be treated as constant, and the boundary moving velocity, U, can be reasonably approximated as

$$U \approx \frac{\delta\xi}{\delta\tau} = \frac{(q_{in} - q_{out})}{\phi(S_{oi} - S_{or})wl} \tag{5.26}$$

Thus, the movement of a boundary during a time snippet can be easily calculated by

$$\Delta\xi_{mv} = U\Delta t \tag{5.27}$$

where $\Delta\xi_{\text{mv}}$ is the movement of a transition-zone boundary, m. The respective advancements of a transition-zone segment in the horizontal and vertical directions can be determined by using trigonometric correlations:

$$\Delta X = \frac{\Delta\xi_{mv}}{\sin\theta},\ \Delta Y = \frac{\Delta\xi_{mv}}{\cos\theta} \tag{5.28}$$

5.2.6 Performance Evaluation

The cumulative heavy oil production can be obtained by integrating the area of a solvent chamber from which the oil has been completely depleted:

$$Q_o = \phi\left(S_{oi} - S_{or}\right)W\int_0^L \left(H - Y\right)\mathrm{dX} \tag{5.29}$$

where Q_o is the cumulative oil production, m^3. The instantaneous oil production or oil production rate can be calculated by taking the derivative of Q_o with respect to *t*.

The solvent consumption is more complicated than the oil production. Once injected, some hot solvent remains as a gaseous phase in the solvent chamber, and some condenses as a liquid in the transition zone. In addition, part of the condensed solvent stays mixed with oil (segments above the producer) and the rest (near the producer) is produced with oil. In short, the solvent consumption is made up of three parts: filling in the chamber, mixed with oil, and produced with oil. The mole number of solvent vapor in the chamber can be calculated by using a real gas state equation:

$$n_{s,chamber} = \frac{PQ_o}{\rho_o zR\left(273.15 + T\right)} \tag{5.30}$$

where *P* is the pressure, Pa; *z* is the real gas compressibility factor, dimensionless; *R* is the real gas constant, m^3·Pa/(K·mol); and *T* is the temperature, °C. Thus, the volume of solvent in the chamber can be computed by

$$Q_{s,chamber} = n_{s,chamber} \cdot MW \tag{5.31}$$

The MW is the molecular weight of the solvent. The condensed solvent that remains mixed with oil is calculated by integrating the solvent concentration in each segment:

$$Q_{s,dissolved} = \sum_{j=1}^{N}\left[\rho_s\phi W l_j\int_{\xi_{\min}}^{\xi_{\max}}\left(S_{o,j} - S_{or}\right)c_j d\xi\right] \tag{5.32}$$

The produced solvent can be computed by the oil production rate and the transient average solvent concentration in the bottom transition-zone segment:

$$Q_{s,produced} = \int_0^t \rho_s\phi W\int_{\xi_{\min}}^{\xi_{\max}} u_N c_N \mathrm{d}\xi\mathrm{d}t \tag{5.33}$$

The total solvent consumption can be obtained by summing up the above three quantities:

$$Q_s = Q_{s,chamber} + Q_{s,dissolved} + Q_{s,produced} \tag{5.34}$$

The cumulative produced solvent-oil ratio (cSOR) is defined to calculate the quantity of solvent required to produce a unit mass of heavy oil, as well as to evaluate the performance of a W-VAPEX process:

$$cSOR = \frac{Q_s}{Q_o} \tag{5.35}$$

5.2.7 Solution

Thanks to the complex relationship between diffusivity and concentration, the diffusion–convection equation is a nonlinear second-order partial differential equation and its exact solution is hardly available. Thus, the mass transfer model is discretized by using implicit finite difference method and solved by using the Gauss-Seidel iterative method. The solution is briefly described in the appendix. After the concentration is obtained, other dependent fluid properties such as viscosity, diffusivity, and gravity drainage velocity can be calculated. **Figure 5.5** shows the flowchart of the calculation procedures of the solution to the above-developed mass transfer model.

5.3 Results and Discussion

5.3.1 Base case

This study investigates the performance of a W-VAPEX process, in which a heated propane vapor is injected to recover a typical Western Canadian heavy oil. The physicochemical properties of a reservoir model and the fluids of a base case are listed in **Table 5.1**. The solvent solubility at a chamber edge can be determined by using a K-value correlation that is a function of a solvent type, temperature, and pressure [McCain, 1990]. It is then converted to the solvent saturation concentration at the chamber boundary with the following formula:

$$c^* = \frac{KV_{m,s}}{KV_{m,s} + (1-K)V_{m,o}} \tag{5.36}$$

where $V_{m,o}$ and $V_{m,s}$ are the molar volume of heavy oil and solvent, respectively, m^3/mol. In the base case, the saturation concentration is set as $c^* = 0.8$. After mixed with solvent, the heavy oil will become lighter in terms of viscosity and density, as shown in **Figure 5.6**. The mass transfer rate between a heavy oil and a solvent is usually calculated by

using diffusivity, which adopts a two-parameter power-law correlation as generated in **Chapter 4**, also see equation (5.10).

5.3.2 Base case results

Chamber evolution

Figure 5.7 shows the evolution of the solvent chamber boundary for the W-VAPEX base case over four years' time period. It is found that the top grows faster than the bottom, and the solvent chamber boundary takes an 'S' shape throughout the process.

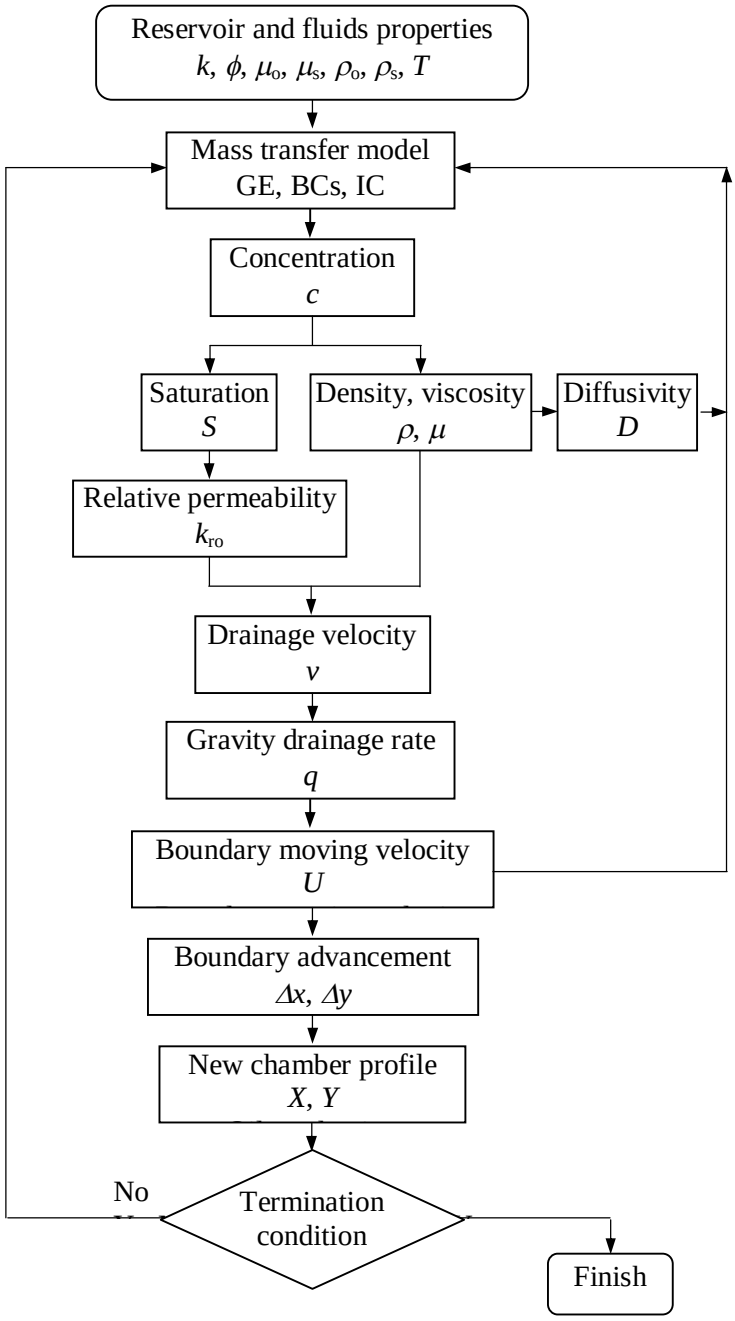

Figure 5.5 Flowchart for calculating the solution to the heat transfer and pressure diffusion models.

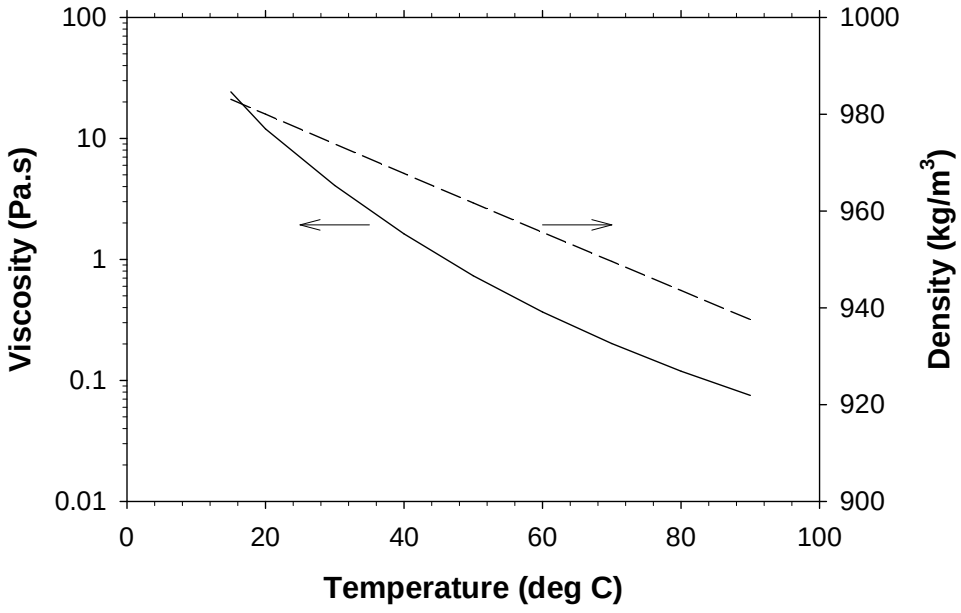

(a)

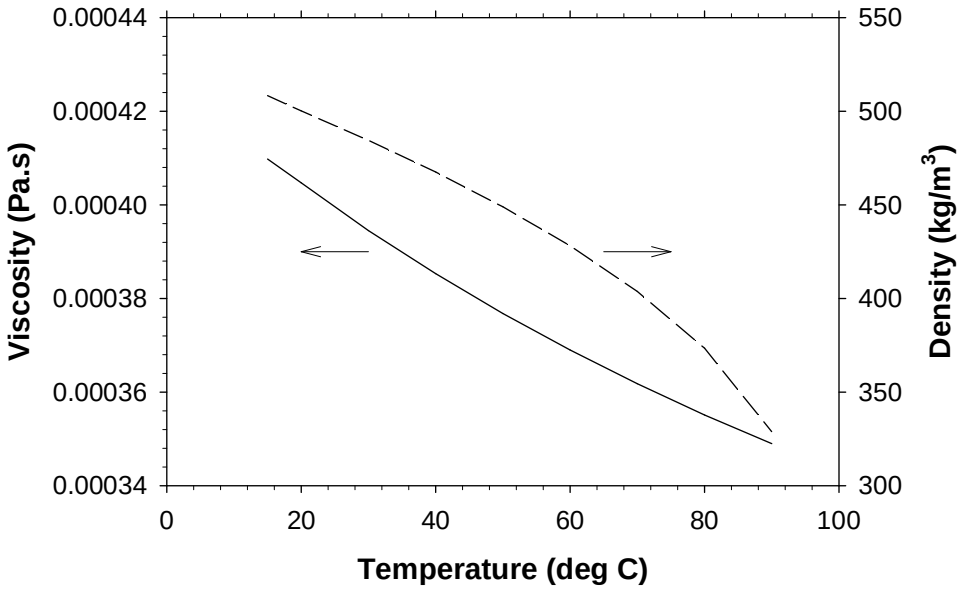

(b)

Figure 5.6 Viscosity and density versus temperature profiles for **(a)** heavy oil and **(b)** condensed propane (liquid).

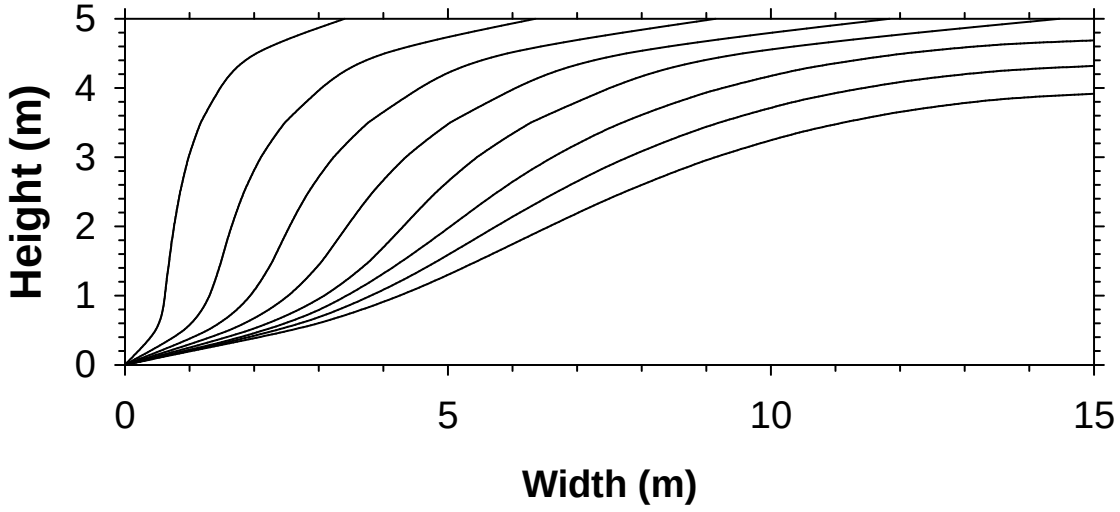

Figure 5.7 Solvent chamber evolution.

Table 5.1 Reservoir and fluid properties of a base case.

Property	Symbol	Value	Unit
Reservoir model			
Model dimension	$H \times L \times W$	5×15×1	m×m×m
Permeability	k	5×10^{-12}	m^2
Porosity	ϕ	30	vol.%
Cross-sectional area	A	0.02	m^2
Relative permeability at residual water saturation	$k_{ro,rw}$	0.8	unity
Bitumen			
Viscosity @ 20°C	μ_o	12000	mPa.s
Density @ 20°C	ρ_o	1000	kg/m^3
Initial oil saturation	S_{io}	80	vol.%
Residual oil saturation	S_{or}	10	vol.%
Connate water saturation	S_{wc}	20	vol.%
Solvent			
Viscosity @ 20°C	μ_s	0.17	mPa.s
Density @ 20°C	ρ_s	578	kg/m^3
Injection temperature	T	50	°C
Diffusivity	D	$D = 7\times10^{-10}\mu^{-0.46}$	m^2/s
K-value	K	$K = \frac{K_{v1}}{P} e^{\frac{K_{v4}}{T-K_{v5}}}$ K_{v1} = 90085 K_{v4} = -1872.46 K_{v5} = -247.99	dimensionless, P in kPa, T in °C

Oil production

Correspondingly, the cumulative oil production increases linearly with time. It can be identified into three stages on the oil production rate profile (**Figure 5.8a**). The first stage (<4 months) accounts for the linear-injection boundary condition and can be seen as the rising phase of the solvent chamber, in which the oil production rate increases from zero to the peak level. In the second stage (4–24 months), the oil production rate nearly stabilizes and the solvent chamber spreads to the edge. This validates the constant oil production rate observed from physical tests [Butler and Mokrys, 1993; Zhang et al., 2006] and assumed in analytical models [Butler and Mokrys, 1989]. Afterwards (>24 months), the chamber gradually falls to the reservoir bottom, and the oil production rate gradually declines to the end due to the declining slip angle.

Solvent recovery

Cumulative solvent injection or solvent consumption also increases linearly with an approximately constant rate (**Figure 5.8b**). The solvent–oil ratio (SOR) is a key factor to evaluate the economic viability of a solvent-based recovery process. Corresponding to the oil production profile, three stages can also be identified on the SOR profile. The high level of SOR in the first month is because the injected solvent is mostly used to dilute heavy oil, initially the crude oil is solvent free and little is produced. It then remains nearly constant (6-24 months) because of the stable oil and solvent production rates. Finally, it inclines slightly upwards due to the declining oil production rate in the solvent chamber falling phase (**Figure 5.7c**).

Solent recovery is another factor that decides the cost efficiency of a solvent-based recovery process. **Figure 5.9a** presents the solvent distribution and its recovery for the base case. It is found that in the first twenty days, a majority of the injected solvent is dissolved into oil rather than being produced. Later on, more of the solvent is produced with oil. The solvent retaining in the chamber always accounts for a smaller proportion. At t = 24 month, 90% of the injected solvent is produced out, 6% of solvent remains condensed and mixed with oil, and only 4% of the injected solvent retians in the solvent

chamber as a gaseous phase (**Figure 5.9ba**). This is the first-time analytical estimation of the

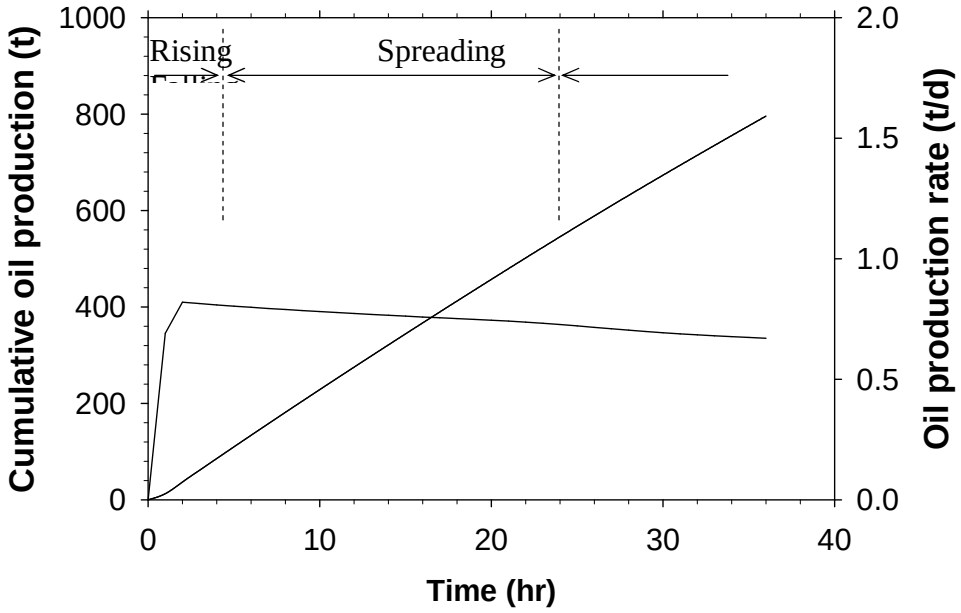

(a)

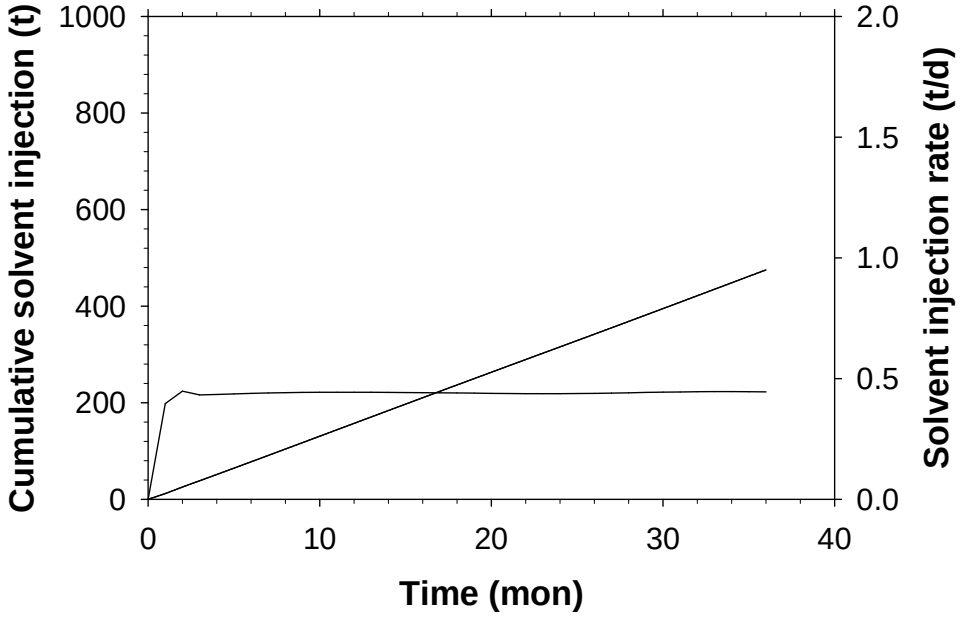

(b)

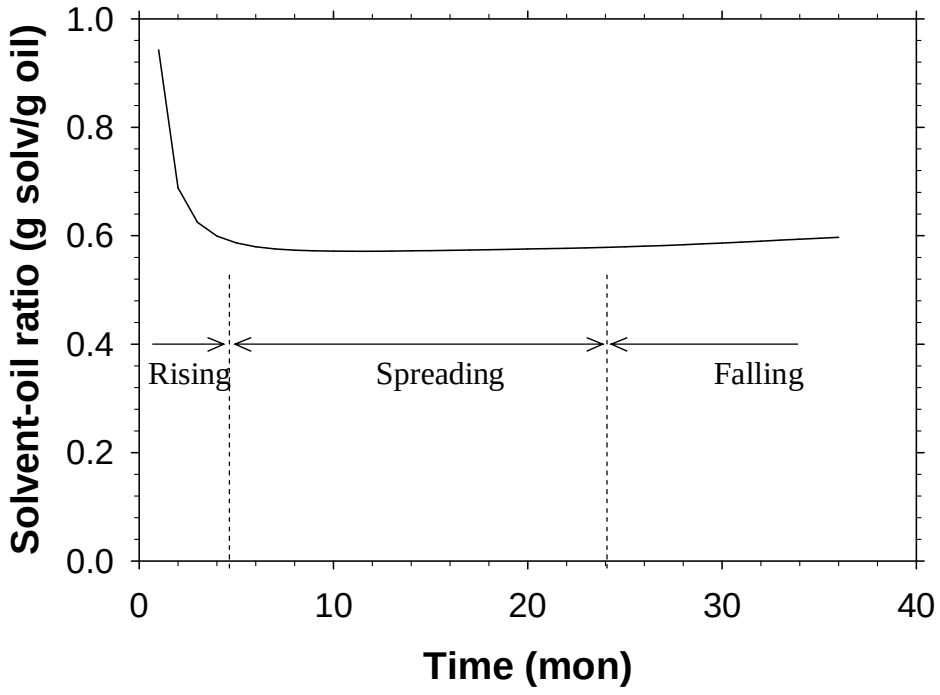

(c)

Figure 5.8 (a) cumulative oil production and oil production rate, **(b)** cumulative solvent injection and solvent injection rate, and **(c)** solvent-oil ratio.

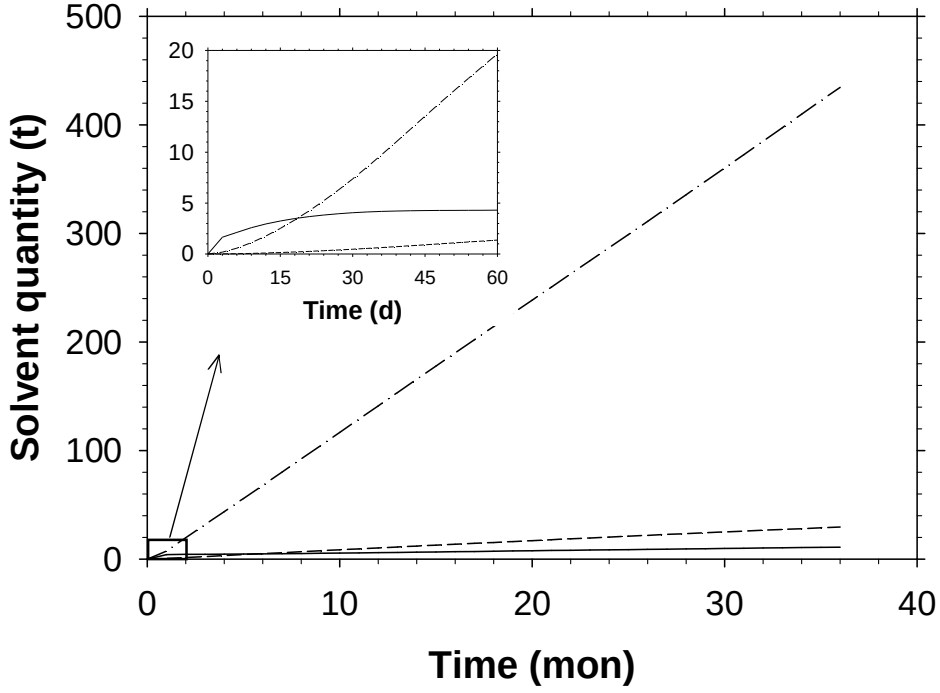

(a)

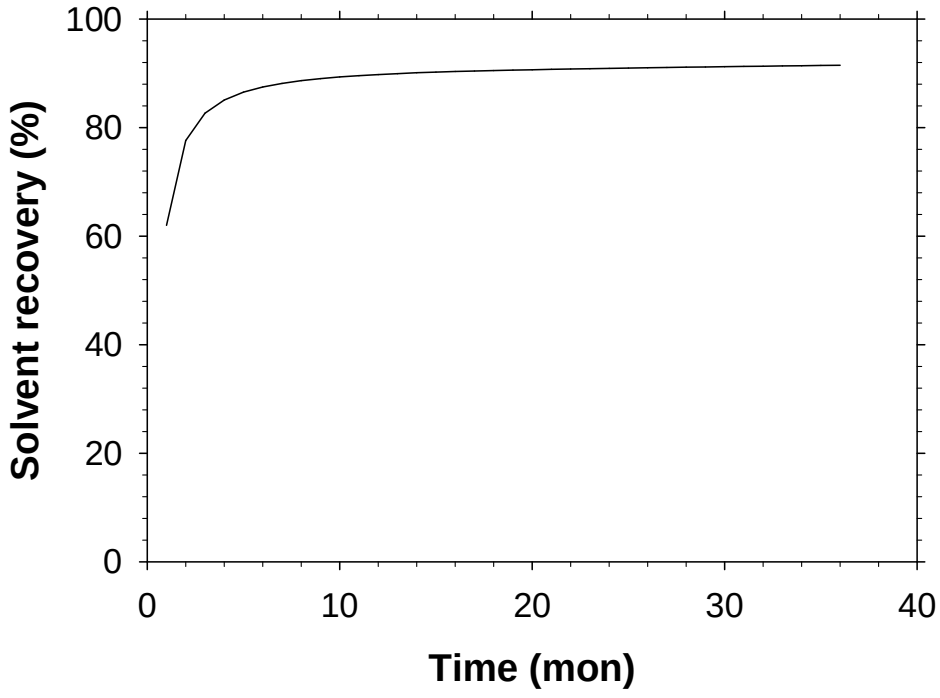

(b)

Figure 5.9 (a) solvent distribution and **(b)** cumulative solvent recovery.

distribution of injected solvent. The solvent recovery profile (the ratio of the solvent production to the solvent injection) can be identified into two stages. Initially (t < 2 months), as aforementioned, a good portion of injected solvent is used to dissolve oil, which leads to a relatively lower solvent recovery. Afterwards (t > 2 months), as more solvent is produced with oil to the surface, the solvent recovery increases fast and gradually levels off at about 90%.

Fluid properties

Figure 5.10 shows the fluid properties in the middle part of a solvent chamber boundary for the base case, including solvent concentration, viscosity, density, and gravity drainage velocity at three moments (t = 1, 2, and 3 yrs). It is found that the propane penetrates into heavy oil as deeply as 0.3 m at t = 2 yrs (**Figure 5.10a**). The gravity drainage velocity starts from zero at the chamber edge because of zero mobile oil saturation, peaks at about 0.1 m away from the edge at t = 2 yrs and declines further away to zero in the transition zone (**Figure 5.10d**).

Transition zone thickness

Transition zone properties change with position along the solvent chamber boundary, as shown in **Chapter 3**. **Figure 5.11** shows the concentration distribution at the top, middle, and bottom. First, the concentration profile at the top (Figure 5.11a) is wider than that in the middle but narrower than that at the bottom. This is because the slipping angle at the top is rather small throughout the late spreading and the entire falling phases [Butler and Mokrys, 1989; Zhang et al., 2006], so that solvent takes longer time to mix with oil. Second, the solvent concentration seems stabilized in the middle (**Figure 5.11b**), which reflects a balance between the dissolution and drainage of solvent and validates the assumption of steady-state mass transfer and a constant boundary moving velocity in previous analytical models [Butler and Mokrys, 1989; Das and Butler, 1998]. Finally, the concentration at the bottom is the widest, which is related to the small boundary expansion at the bottom.

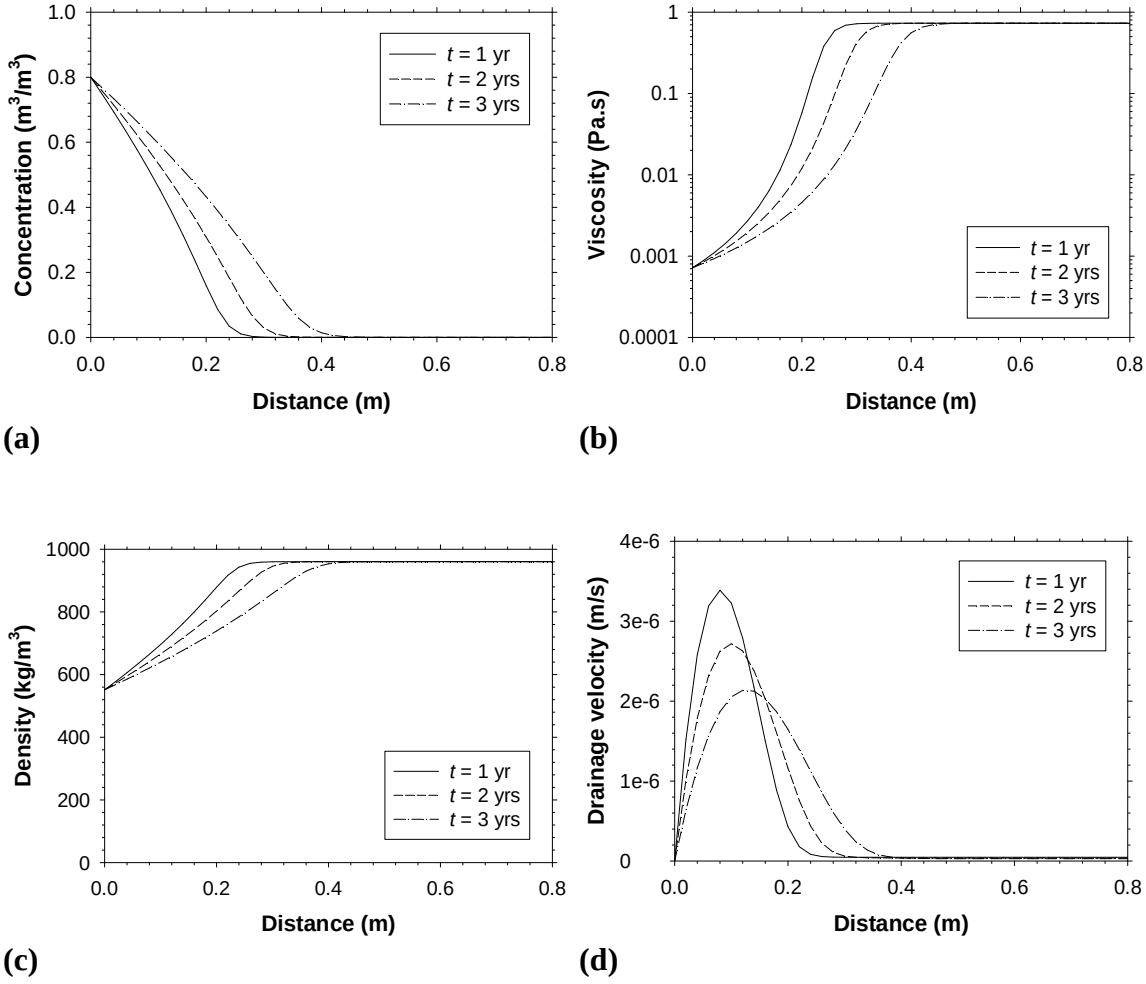

Figure 5.10 Calculation results of the base case: **(a)** solvent concentration, **(b)** viscosity of solvent-diluted heavy oil, **(c)** density of solvent-diluted heavy oil, and **(d)** gravity drainage velocity.

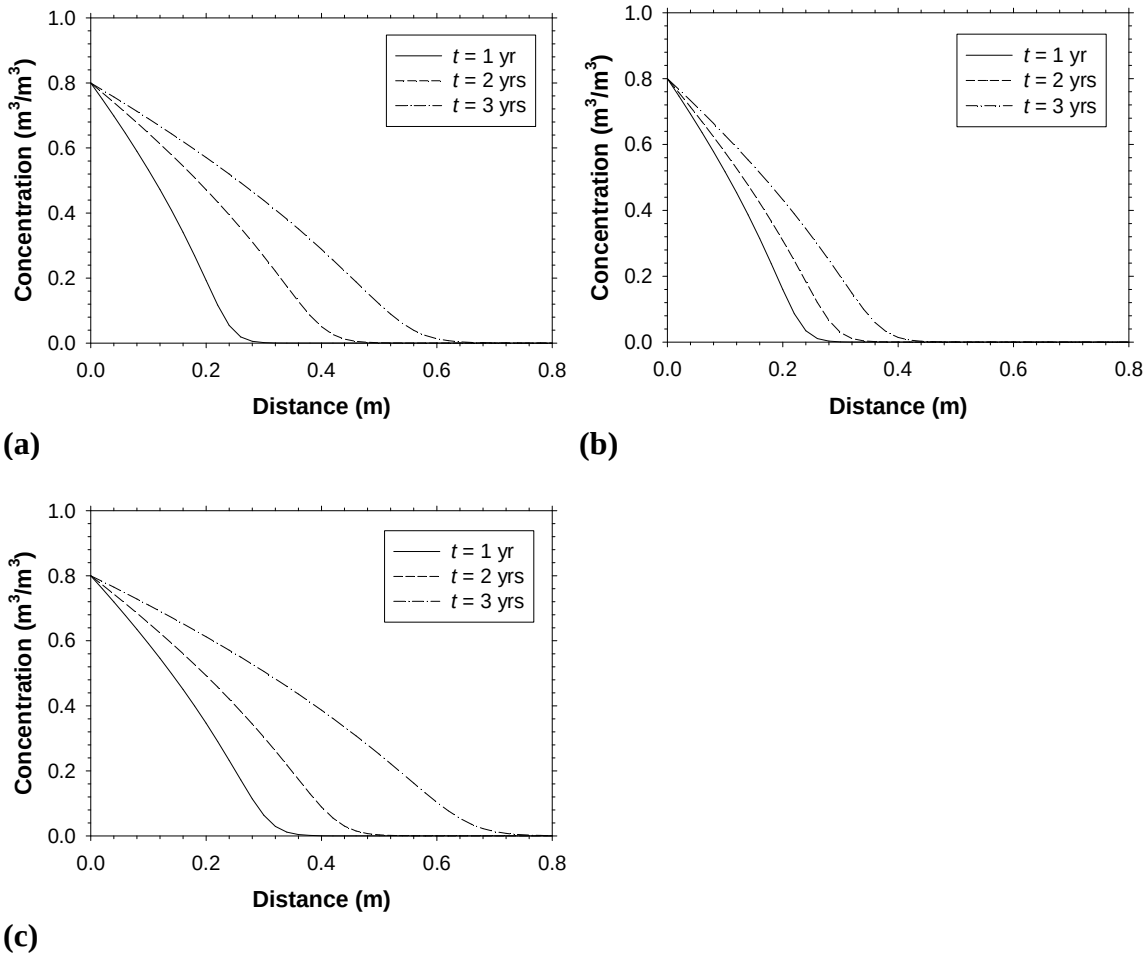

Figure 5.11 Concentration at the **(a)** top, **(b)** middle, and **(c)** bottom of a chamber boundary at three moments.

The transition zone thickness stands for the solvent invasion zone, extending from $c = c^*$ to $c = 0.01$. **Figure 5.12** shows the transition zone thickness at the top, middle, and bottom of the chamber boundary over three years'-period. It can be seen that in the first several months the transition at the top is thinnest, because the chamber expands fastest at the top so that solvent does not have much time to invade deeply. As time goes by, the slip angle at the top gradually decreases and gravity drainage weakens, so the solvent takes longer time to diffuse and reach a deeper invasion depth. As a result, the transition zone thickness grows steadily with time. In contrast, the transition zone thickness seems to be constant in the spreading phase ($t < 24$ months), which is consistent with the near-steady state concentration profiles in **Figure 5.11**. It widens at later times because of declining slip angle. As expected, the transition zone is always the widest at the bottom and its thickness becomes constant when solvent has reached to the non-penetration boundary at the reservoir bottom. It is worthy of noting that the transition zone seems closely related to the slip angle. Except in the first few months, transition zone thickness is always narrower in the middle than at the top and bottom (**Figure 5.12a**), because the slip angle is mostly larger in the middle. To illustrate this point, **Figure 5.12b** shows the front and back boundaries of the transition zone at $t = 1$ yr.

5.3.3 Saturation concentration/injection pressure

Previous studies concluded that a solvent should be injected slightly below its dew point in the gaseous phase [Nenniger, 1979; Dunn et al, 1989]. The purpose is first to dilute oil effectively by making a high solvent concentration in oil, and second to induce fast gravity drainage by maintaining a vapor phase in a solvent chamber. However, no conclusion has been made regarding on how much in this pressure difference would be reasonable. To address this issue, this study attempts a range of the saturation concentration from $c^* = 0.4$ to 1.0.

The diffusivity versus concentration is plotted in **Figure 5.13**, which shows that diffusivity at $c^* = 1.0$ is 3.5 times that at $c^* = 0.4$ and this means solvent dissolves into oil much faster at a high saturation concentration than at a low level. **Figure 5.14** presents the effect of saturation concentration on the oil production rate, solvent injection rate, SOR, and

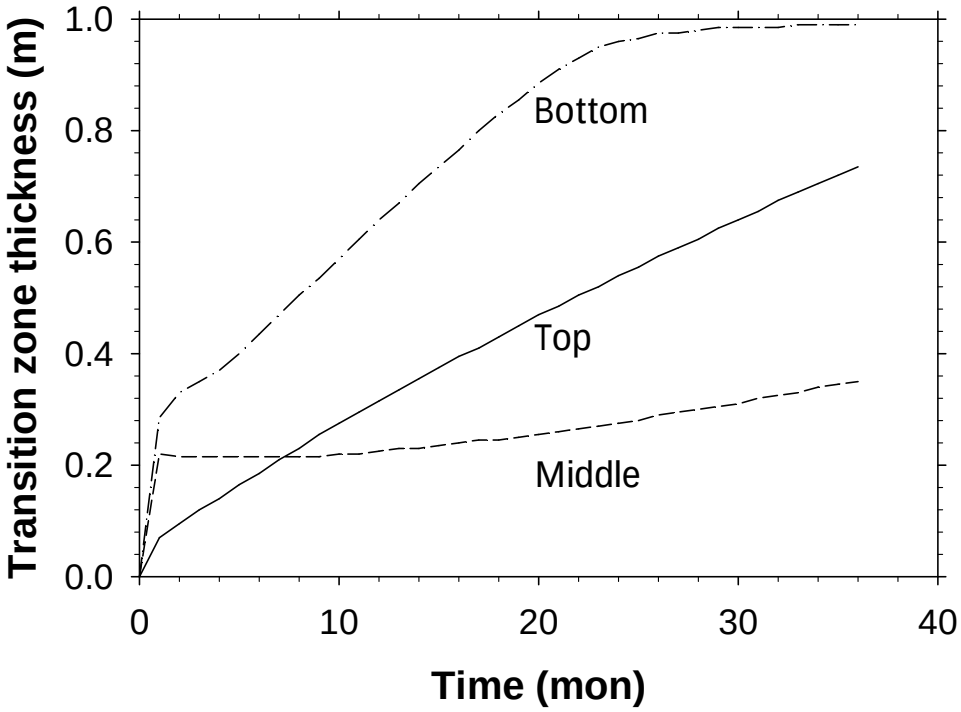

(a)

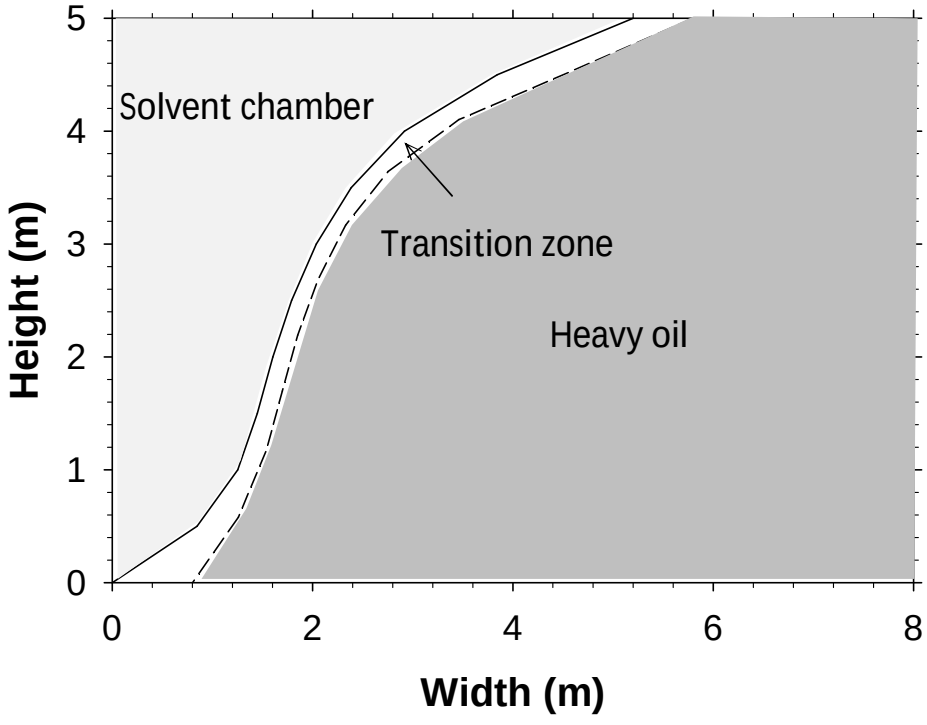

(b)

Figure 5.12 (a) Transition zone thickness at the top, middle and bottom and **(b)** the inner and outer boundaries of transition zone at t = 1 yr.

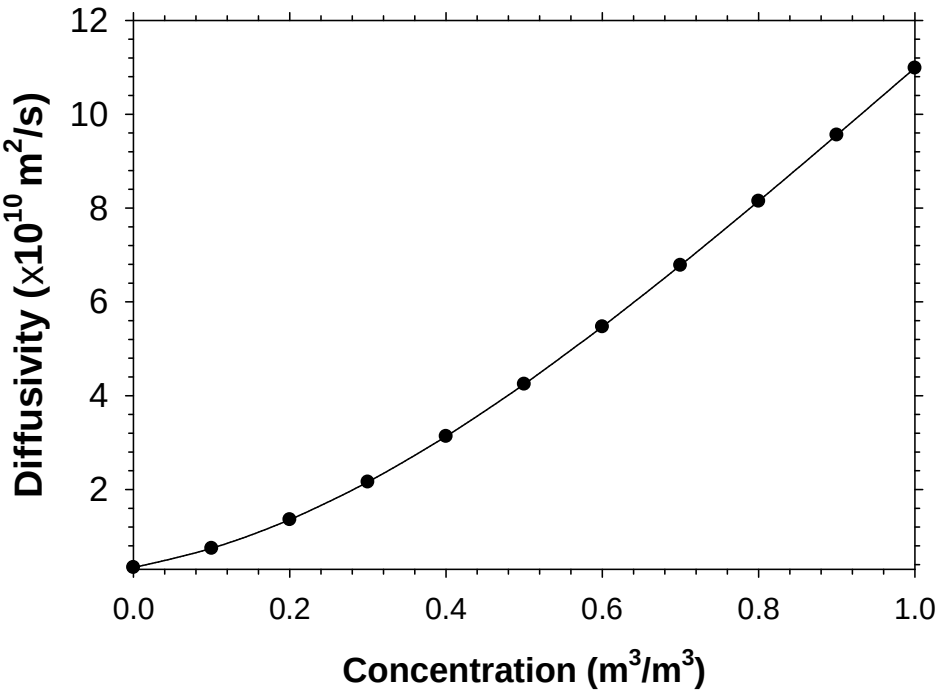

Figure 5.13 Diffusivity versus concentration profile.

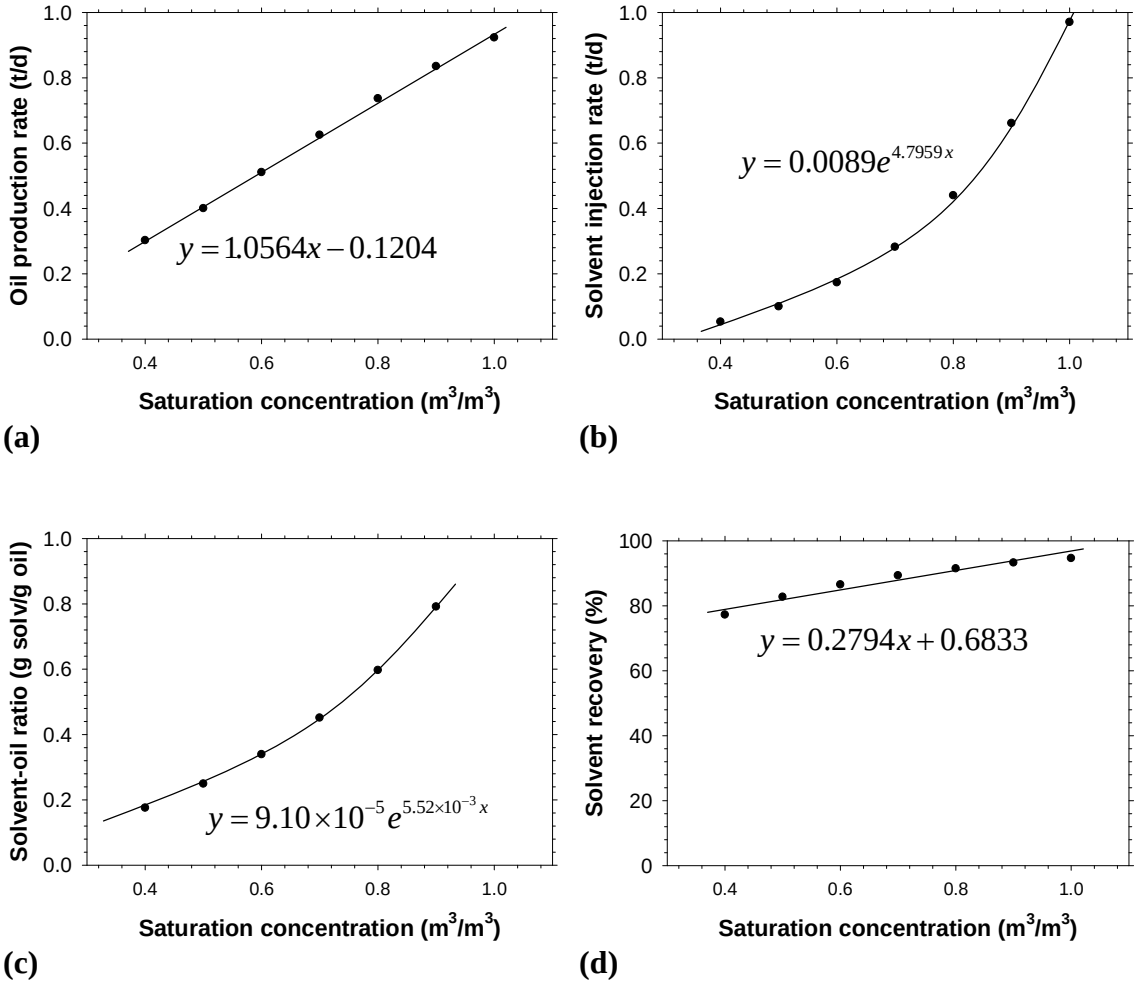

Figure 5.14 Effect of saturation concentration on **(a)** oil production rate, **(b)** solvent injection rate, **(c)** SOR, and **(d)** solvent recovery.

solvent recovery. It can be seen that oil production rate increases linearly while the solvent consumption rate grows exponentially with solvent saturation concentration (**Figure 5.14a-b**). Meanwhile, the SOR grows exponentially from SOR = 0.18 at c^* = 0.4 to SOR = 0.82 at c^* = 1.0 (**Figure 5.14c**). In addition, the solvent recovery increases from 77.2% at c^* = 0.4 to 94.6% at c^* = 1.0 (**Figure 5.14d**).

In practice, the pressure is more concerned since it is more directly-related to field operation. **Figure 5.15** converts pressure to saturation at three temperatures (T = 20, 50, and 80°C). It shows saturation concentration is more sensitive to pressure at lower temperature than at a higher one. For instance, at T = 20°C, reducing pressure from P_c = 834 kPa to 734 kPa results in a decrease in saturation concentration from c^* = 1.00 to c^* = 0.64. However, at T = 80°C, a reduction of 100 kPa from the critical pressure (Pc = 2984 kPa) just leads to a decrease of Δc^* = 0.12 in saturation concentration.

Figure 5.16 converts the coordinate in Figure 5.14 to pressure at T = 50°C. It is found that solvent injection rate is the most sensitive to pressure among the four factors. From P = 1500 kPa to P = 1700 kPa, the respective increases in the oil production rate, solvent injection rate, SOR, and solvent recovery are 77%, 373%, 222%, and 10%. It is worthy of noting that although more solvent is needed at higher pressure, a larger percentage of the injected solvent can be retrieved in the meantime. For instance, solvent recovery increase from 86% at P = 1500 kPa to 95% at P = 1700 kPa.

5.3.4 Temperature

Heavy oil viscosity is highly sensitive to temperature. For instance, elevating temperature from T = 20 to 80°C reduces the oil viscosity from 11.98 to about 0.07 Pa.s (**Figure 5.a**). This viscosity reduction can boost diffusivity by over one order according to the diffusivity–viscosity correlation (**Table 5.1**). As shown in **Figure 5.17**, diffusivity is improved from $D = 9.3\times10^{-12}$ m^2/s at T = 20°C to $D = 9.6\times10^{-11}$ m^2/s at T = 80°C in the absence of any solvent. This will definitely improve the oil production of a VAPEX process. **Figure 5.18** shows the effects of three temperatures (T = 20, 50, and 80°C) on the solvent concentration and gravity drainage velocity profiles of the base case.

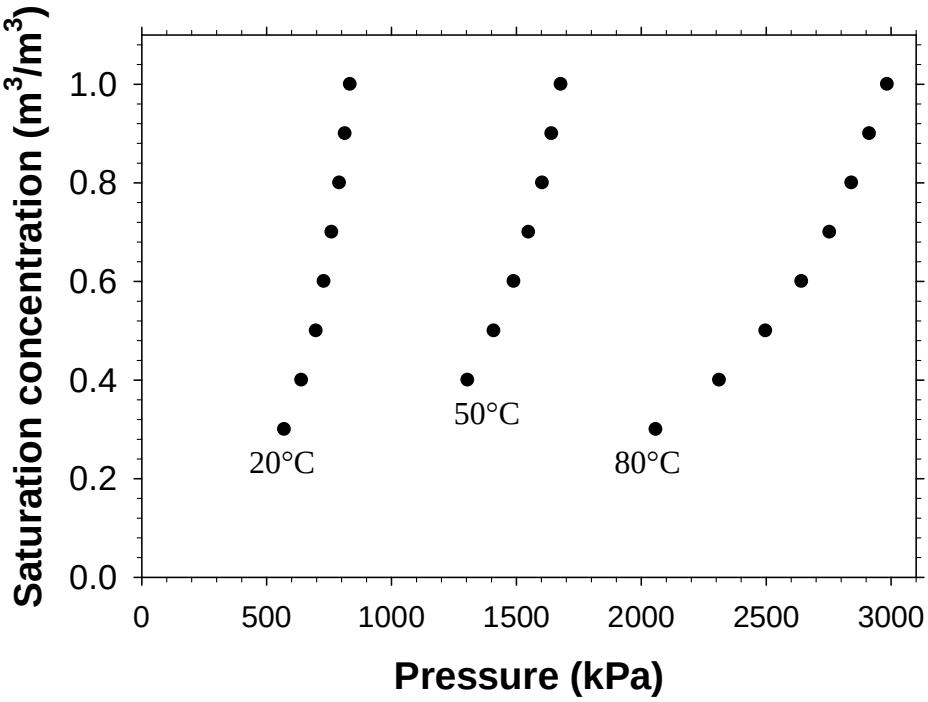

Figure 5.15 Saturation concentration versus pressure profile.

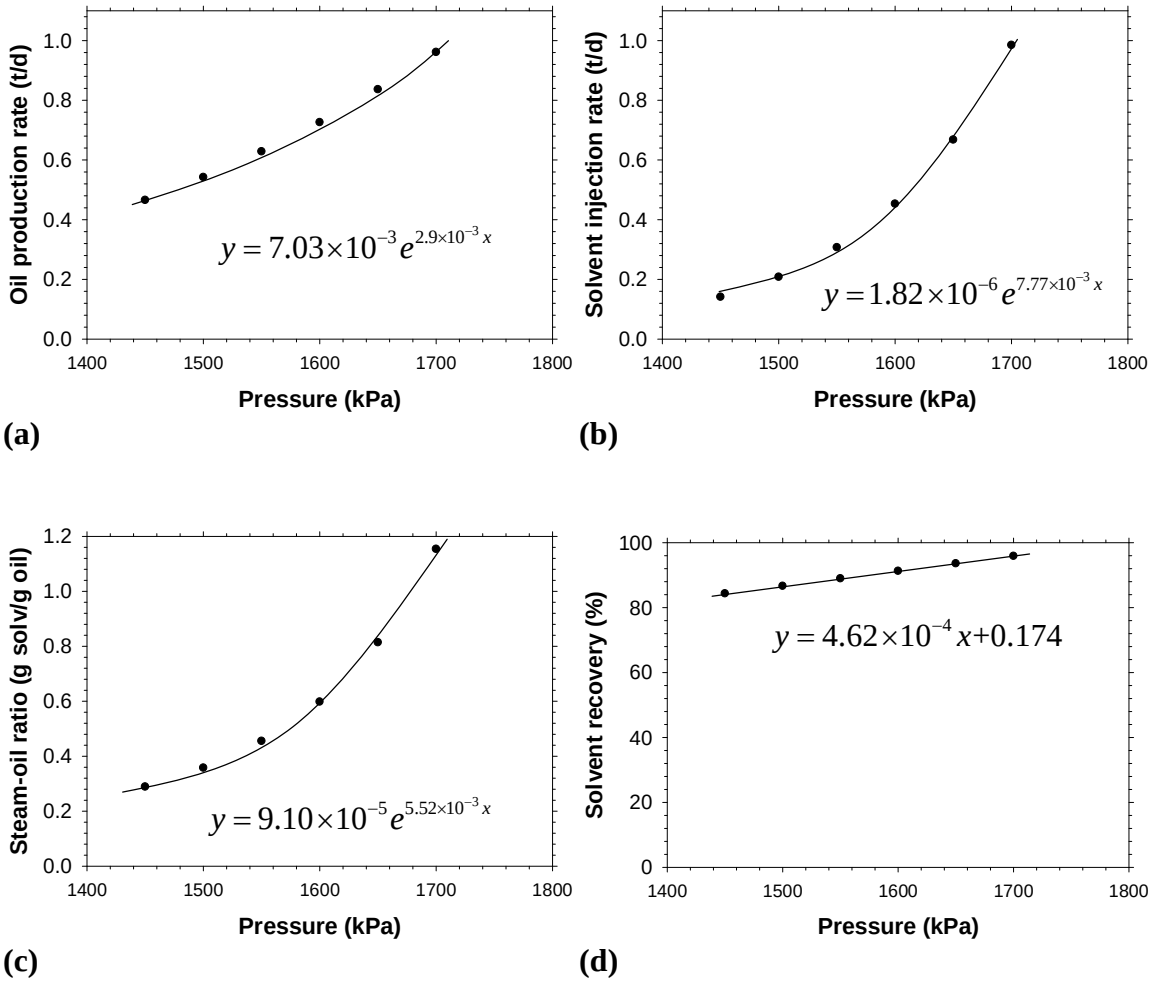

Figure 5.16 Effects of solvent injection pressure on **(a)** oil production rate, **(b)** solvent injection rate, **(c)** SOR, and **(d)** solvent recovery all at T = 50°C.

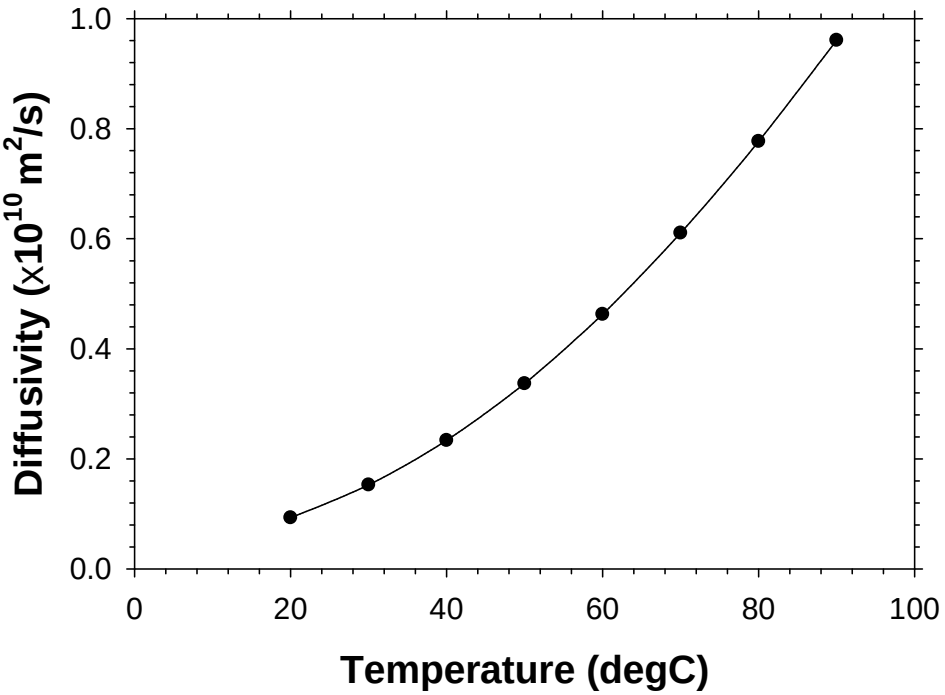

Figure 5.17 Diffusivity versus Temperature profile ($c^* = 0$).

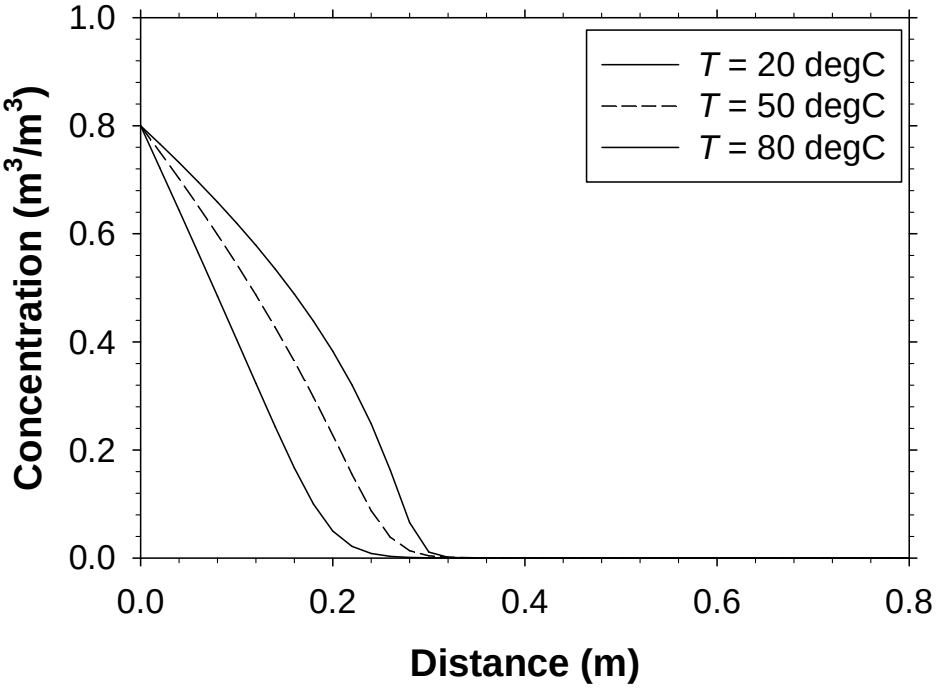

(a)

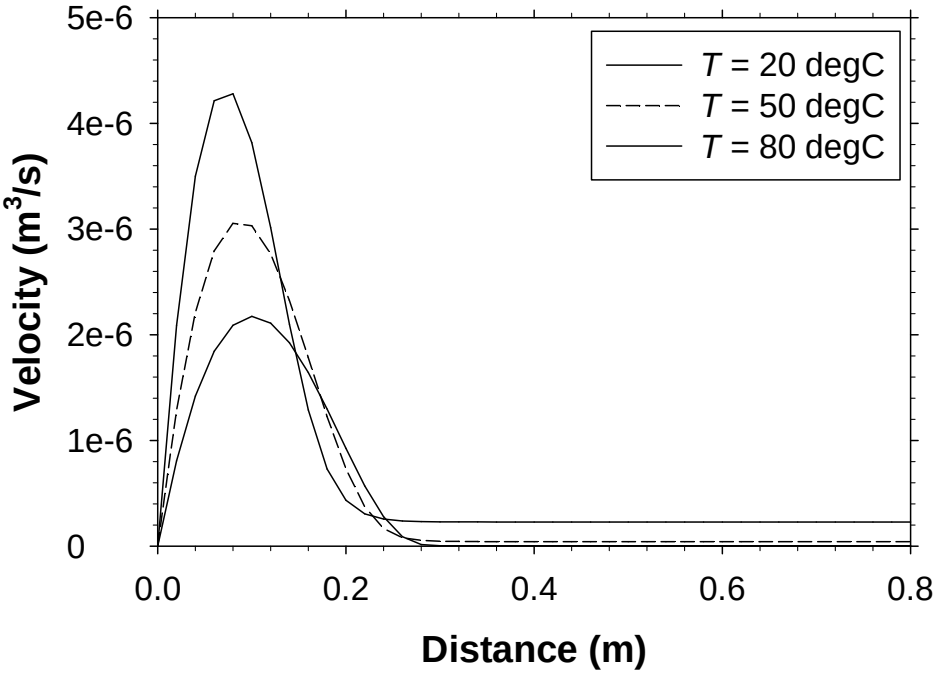

(b)

Figure 5.18 Effects of temperature on **(a)** solvent concentration and **(b)** gravity drainage velocity (Segment no. is 5) at t = 1 yr.

It can be seen that the concentration profile for T = 80°C is narrower than that at T = 20°C (**Figure 5.18a**). This implies less solvent retention at higher temperatures, which is caused by a greater gravity drainage velocity (**Figure 5.18b**). More practically, **Figure 5.19** shows the effects of temperature on the oil production rate, solvent consumption rate, SOR, and solvent recovery from T = 20°C to 90°C. Obviously, W-VAPEX recovers oil much faster than cold-VAPEX: the oil production rate is almost tripled by elevating temperature from T = 20 and 90°C. Meanwhile, the solvent consumption is just increased by 74%, SOR declined by 53%, but solvent recovery falls by 24%. **Table 5.2** shows the quantitative information after two years' operation at four temperatures. It can be seen that at T = 80°C, 384 tons of solvent are injected to recover 909 tons of oil over two-year production, and 74 tons of solvent are left underground when the well reaches an economical cut off.

5.3.5 Permeability

Permeability is one of the most important reservoir physical properties. Typical oil sands or heavy oil reservoir permeability ranges from 1 to 10 Darcy. **Figure 5.20** compares the oil production rate, solvent consumption rate, SOR, and solvent recovery with respect to the square root of four permeabilities (k = 1, 5 10, and 15 Darcy) at T = 50°C. It is found that THE oil production rate and solvent consumption rate both increase linearly with $k^{0.5}$. The oil production rate at k = 10 Darcy is 3.72 times that at k = 1 Darcy. SOR is smaller and solvent recovery is slightly higher in more permeable reservoirs. Meanwhile, SOR and solvent recovery keep almost constant at high permeabilities.

5.3.6 Oil viscosity

High viscosity is the most prominent characteristic of a heavy oil, which results in not only trivial mobility but also small diffusivity (**Figure 5.21**). This study analyzes five typical heavy oil viscosities (μ_o = 1.2, 5.0 12.0, 120.0, and 306.0 Pa.s) at T = 20°C, and **Figure 5.22** shows their respective effects on the oil production rate, solvent injection rate, SOR, and solvent recovery. From μ_o = 1.2 to 120 Pa.s, the oil production rate drops by 47% whereas the solvent injection rate declines just by 19% (**Figure 5.22a-b**). This shows that heavier oil needs more solvent to reach an equivalent oil production rate compared to lighter ones, as reflected by the SOR profile (**Figure 5.22c**). In the meantime,

the solvent recovery increases by just 3% for a 3-order increase of in the oil viscosity (**Figure 5.22d**).

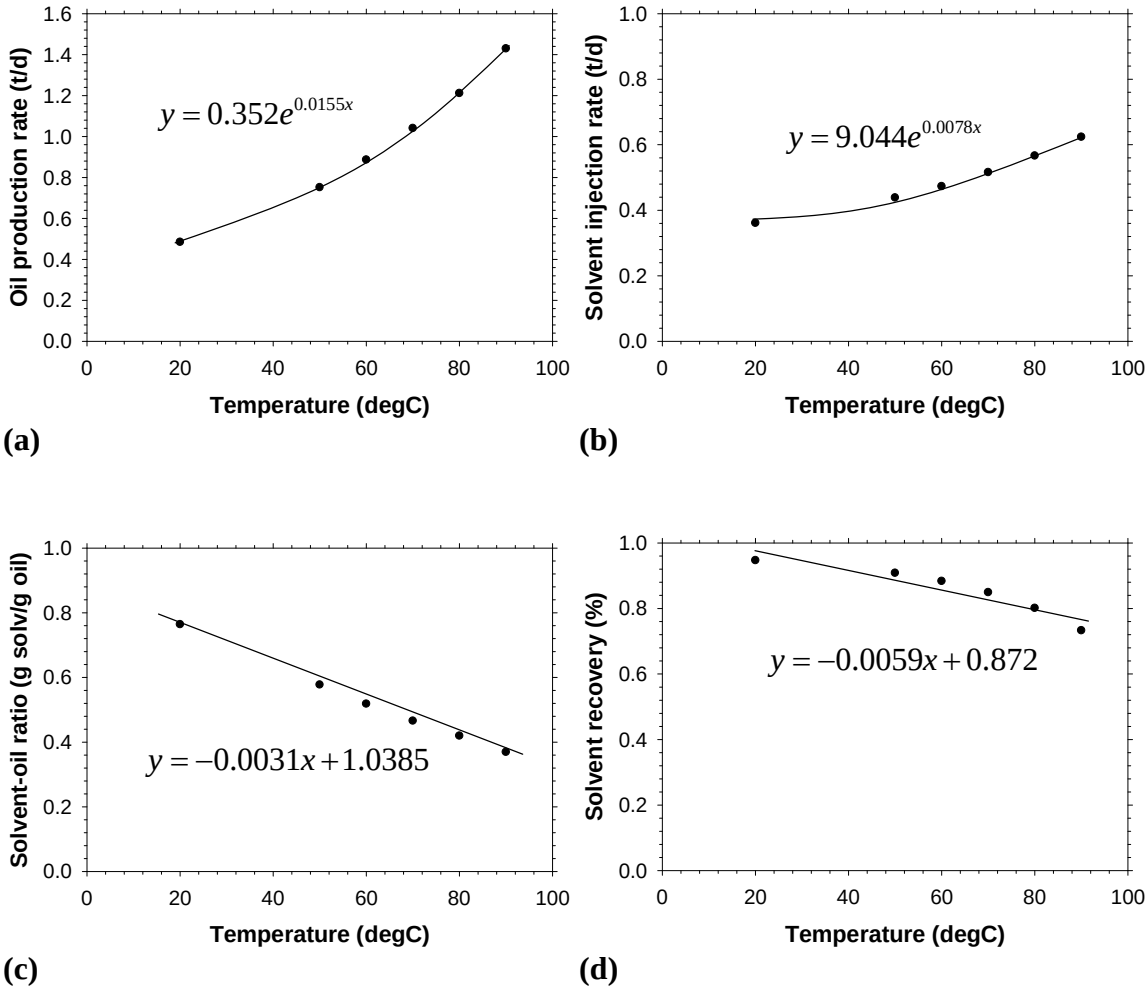

Figure 5.19 Effects of temperature on **(a)** oil production rate, **(b)** solvent injection rate, **(c)** SOR, and **(d)** solvent recovery at t = 2 yrs.

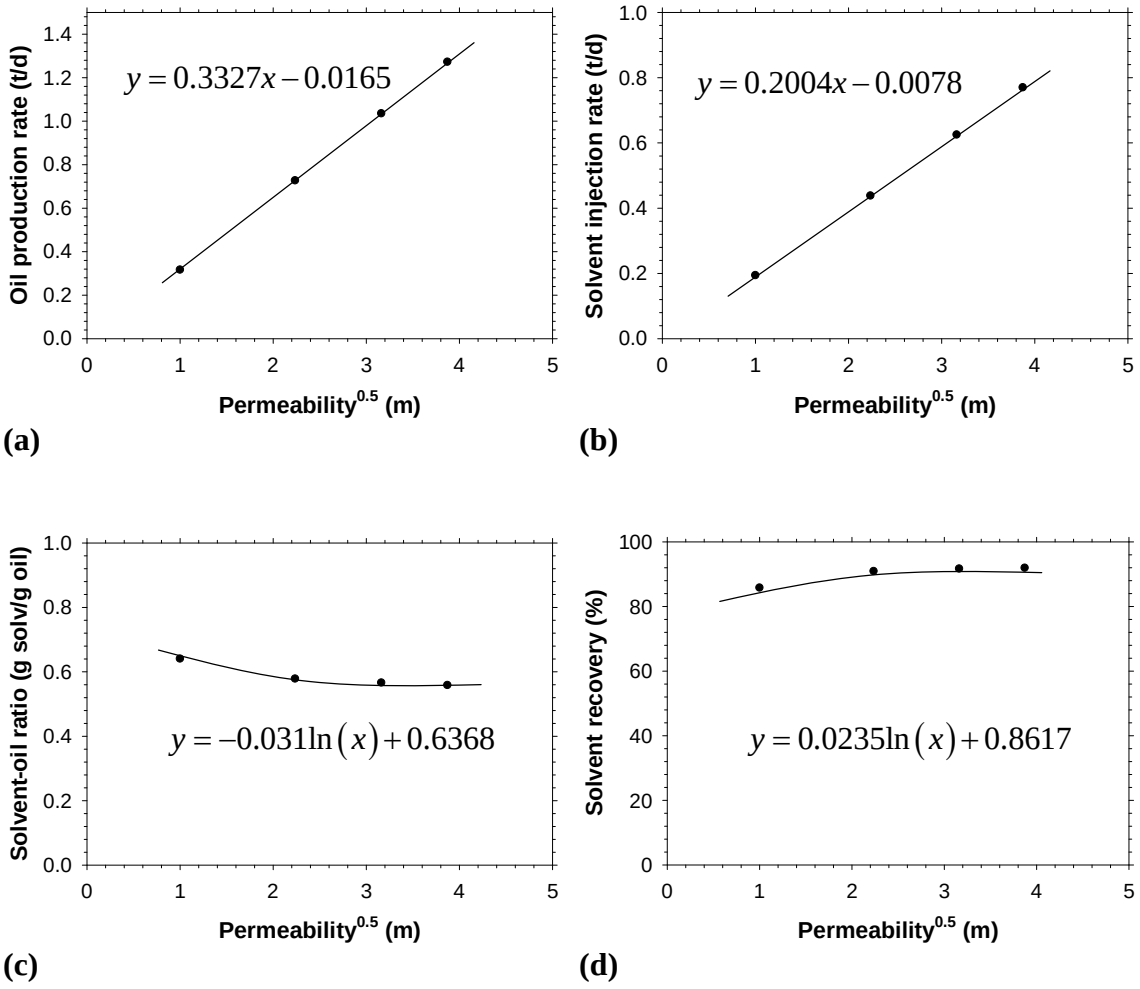

Figure 5.20 Effects of permeability on **(a)** oil production rate, **(b)** solvent injection rate, **(c)** SOR, and **(d)** solvent recovery at t = 2 yrs.

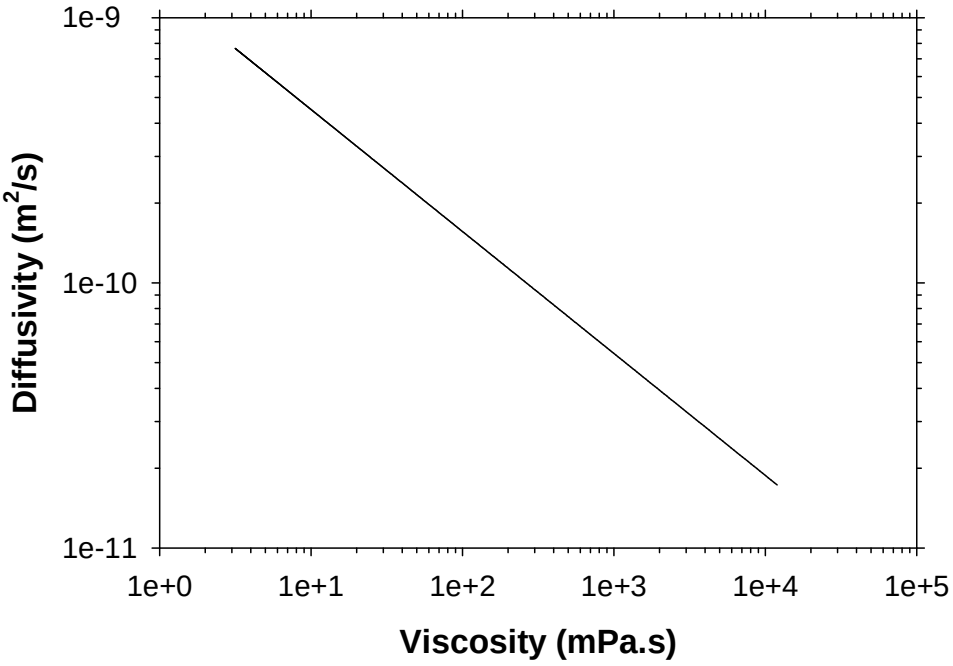

Figure 5.21 Diffusivity versus viscosity profile.

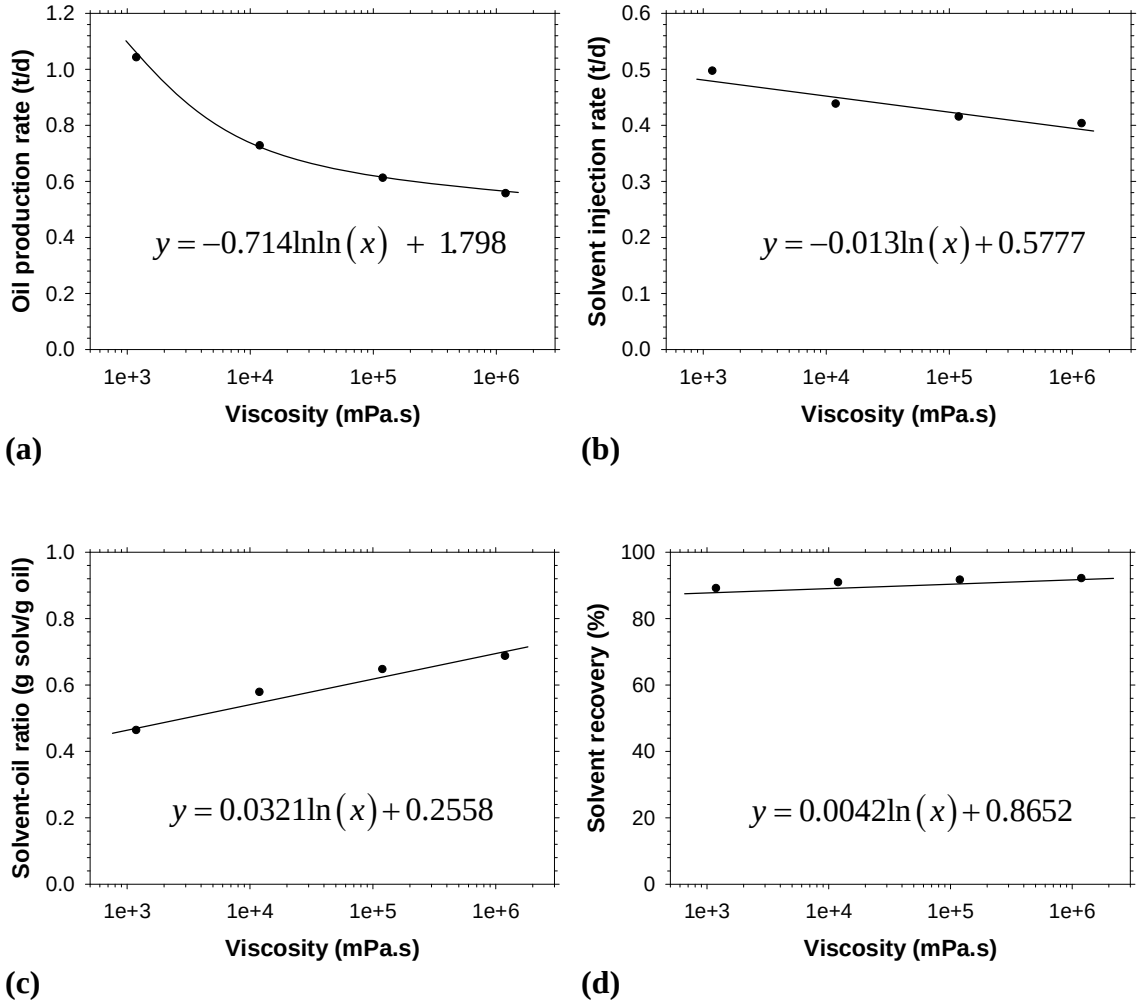

Figure 5.22 Effects of original oil viscosity on **(a)** oil production rate, **(b)** solvent injection rate, **(c)** SOR, and **(d)** solvent recovery at t = 2 yrs.

Table 5.2 Injection and production data for warm VAPEX at t = 2 yrs.

Temperature (°C)	Cum. oil production (t/d)	Oil production rate (t/d)	Cum. solvent injection (t/d)	Solvent injection rate (t/d)	Solvent recovery (%)	Solvent retention (t)	SOR (g solv./ g oil)
20	340.37	0.47	249.09	0.35	0.95	13.18	0.76
50	545.48	0.76	314.43	0.44	0.91	29.27	0.58
80	909.15	1.26	384.58	0.53	0.81	74.92	0.42
90	1043.00	1.45	393.48	0.55	0.73	104.35	0.38

5.3.7 Model height

Four model heights (that stand for a pay-zone thickness): h = 3, 5, 10, and 15 m, are analyzed and their effects are shown in **Figure 5.23**. All the results show a decent linear relationship with the square root of the pay-zone thickness. Larger heights lead to a greater gravity drainage. The linear trend between the oil production rate and $h^{0.5}$ is consistent with the experimental observation [Butler and Mokry, 1989]. From h = 3 to 10 m, it can be seen that the oil production rate and solvent injection rate rise by 133% and 116%, respectively (**Figure 5.23a-b**). The similar increases in the oil and solvent rates lead to a relatively unchanged SOR (**Figure 5.23c**). In addition, the solvent recovery appears insensitive to the model height: It increases by merely 2.7% from h = 3 to 15 m (**Figure 5.23d**).

5.4 Chapter Summary

This study develops a theoretical model for a W-VAPEX process. The following conclusions can be made through the above analyses:

1. SOR shows three stages throughout a W-VAPEX process: it is initially high, remains nearly constant in the middle stage, and increases slightly in the late stage.
2. A transition zone is mostly thinner in the middle than at the top and the bottom.
3. Solvent distribution is analytically modelled: About 90% of the injected solvent is produced with oil, only about 4% is retains in the solvent chamber, and the rest is mixed with oil in the transition zone for the case study in this chapter.
4. At a certain temperature, higher injection pressure can enlarge an oil production rate, and leads to a larger SOR. At T = 80°C and P = 1600 kPa, 384 tons of solvent are injected to recover 909 tons of oil over two-year production, and 74 tons of solvent are left underground when the well reaches the economical cut off.
5. The oil production rate is almost tripled by elevating temperature from T = 20 to 90°C. Meanwhile, the SOR is reduced by 53%.
6. The oil production rate increases linearly with the square root of permeability and the square root of a pay-zone thickness, respectively.
7. With an increase in the crude oil viscosity, the oil production rate decreases logarithmically and the SOR increases linearly.

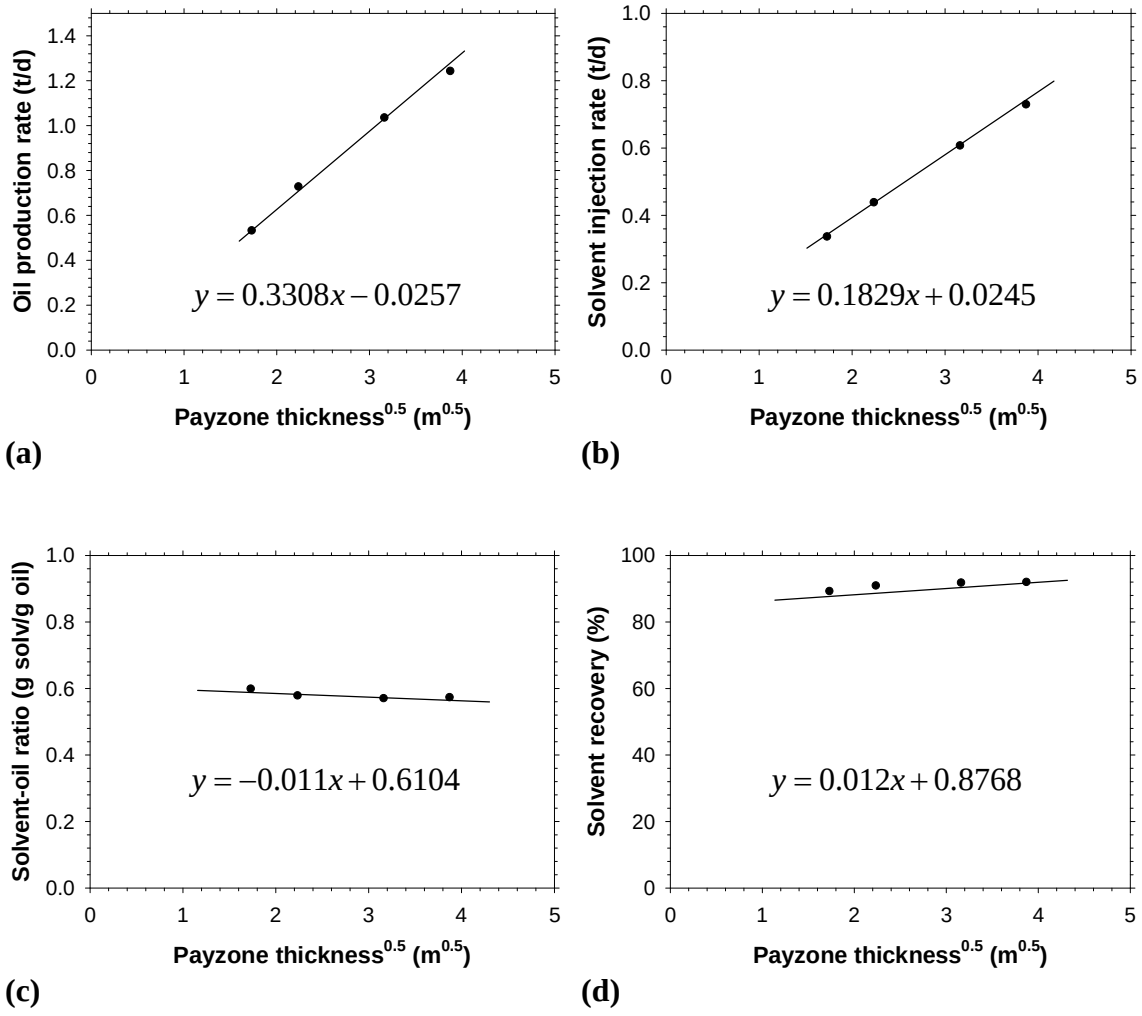

Figure 5.23 Effects of pay-zone thickness on **(a)** oil production rate, **(b)** solvent injection rate, **(c)** SOR, and **(d)** solvent recovery at t = 2 yrs.

CHAPTER 6 STEAM-ASSISTED VAPOR EXTRACTION

The last chapter investigates a pure hot solvent injection process through mathematical modeling. This chapter proposes and assesses a new hybrid process through numerical simulation. This new process, steam-assisted vapor extraction (SAVE), produces heavy oil in a cyclic manner. Each cycle contains a very short steam-injection period and a relatively long solvent-injection period. The steam is first injected at a certain pressure and temperature, which is intended to heat the heavy oil not far away from a chamber boundary. Solvent is then injected to dissolve into the heated and less viscous heavy oil around the chamber. Field-scale simulations are employed to assess the new process. Operating parameters such as steam temperature, soaking period, and solvent injection pressure are systematically evaluated.

6.1 Introduction

The first and most important step to recover heavy oil is to reduce oil viscosity and improve mobility. As afore-mentioned, there are two categories of methods to make heavy oil lighter. The first is to increase crude oil temperature, known as thermal recovery processes, such as steam-assisted gravity drainage (SAGD). These methods perform excellently for resources with thick and clean sands, high bitumen saturation, and large permeability because of relatively large thermal diffusivity. In contrast, they become inefficient in low-quality reservoirs with thin pay-zones or water interlayers. Meanwhile, these energy-intensive and cost-sensitive processes can be uneconomical when the oil prices fall below certain levels. Another type of methods to make heavy oil less viscous is through the usage of diluent, named as solvent-based recovery techniques, such as vapor extraction (VAPEX). These recovery techniques inject a vaporized solvent (light alkanes, CO_2, toluene, *etc*) to dilute heavy oil and reduce its viscosity. In comparison with thermal recovery processes, these techniques require less investment on surface facility and site operation. Ideally, the operation cost for per unit oil production of VAPEX is only 3% of that of SAGD. However, their field application is constrained due to the fairly low oil production rate.

To take advantage of both thermal processes (quick thermal conduction) and solvent-based processes (lower energy consumption), a number of steam-solvent hybrid processes has been proposed to minimize energy input per unit of oil production in the past three decades. **Table 6.1** lists some of the recent advances in hybrid processes in the literature. These hybrid processes can be generally classified into three types. These first class is to inject a heated solvent instead of heated water or steam. Palmgren and Edmunds [1995] proposed a naphtha-assisted gravity drainage (NAGD) process. Naptha is a diluent at the site for pumping and pipeline transport of the produced heavy oil. It is injected as a substitute of steam to combine an effective thermal process with its diluent mechanism. However, their calculation shows that naptha can produce oil faster at the expense of a high cumulative naptha–oil ratio (about 14). Nsolv injects moderately heated (30–50°C) and pure solvent (propane, butane) to produce heavy oil. Last chapter models the warm VAPEX and shows that moderate increase of solvent injection temperature can lead to a significant improvement in oil production rate.

Another class is the simultaneous co-injection of steam and a solvent or a non-condensable gas (NCG). Gupta et al. [2002] proposed a solvent-aided process (SAP), in which butane, as an additive, is co-injected with steam in a SAGD process. Field pilot tests reported encouraging results with accelerated oil production rate and improved economics. Nasr et al. [2002] suggested the addition of C_7-C_{12} into steam and an injection pressure of P = 1400 kPa, so that the solvent content is reduced from 10 to 5 vol.%. Léauté [2002] proposed Liquid Addition to Steam for Enhancing Recovery (LASER) to uplift oil-steam ratio and evaluate the diluent recovery. In this process, a small amount of liquid hydrocarbon (C_{5+}) (3–10 vol.%) is injected with steam at certain stages of a CSS process. The solvent used is a light-hydrocarbon condensate or diluent, which is the same solvent used for mixing with the bitumen to produce a sales blend to meet pipeline specifications. The solvent-co-injected ranges from a low concentration of a heavy solvent (e.g., hexane and pentane) to a high concentration of light solvent (e.g., propane and butane).

Table 6.1 Variants of solvent-steam hybrid processes.

Name	Scheme	Reference
NAGD	High-temperature naphtha is injected to replace steam in a SAGD process.	Palmgren and Edmunds, 1995
SAP	A mixture of 15 wt.% of butane and 85 wt.% of steam is injected instead of steam alone at 218°C.	Gupta et al., 2002 Gupta and Gittins, 2006
LASER	6 vol.% of C_{5+} condensate is added into steam at the late stages of a CSS process.	Leaute et al., 2002 Leaute and Carey, 2005
ETS	A hydrocarbon solvent (propane, butane) is injected into a heated horizontal well to extract heavy oil.	Suncor report to AER in 2002
ES-SAGD	C_7-C_{12} is co-injected with steam at 1400 kPa. Solvent content is reduced from 10 to 5 vol.%	Nasr et al., 2002
SAS	Steam and heated solvent (98 mol.% of propane and 2 mol.% of methane) are alternately injected.	Zhao et al., 2004
N-Solv	Moderately heated (30–50°C) and pure solvent (propane, butane) is injected to produce heavy oil.	Nenniger, 2008
CSSS	Hexane is alternately or simultaneous injected with steam	Chang, et al., 2009
STRIP	Oxygen, fuel, and water are co-injected to generate steam in situ through a combustor placed at the bottom of a wellbore.	Schneider, et al., 2011

The last method is to cyclically inject steam and solvent. Zhao et al. [2005] proposed and studied a steam alternate solvent process by using a SAGD well configuration. Steam and a same-temperature solvent are injected alternately into a reservoir. Chang et al. [2012] extended this scheme to cyclic steam-solvent stimulation and intensively analyzed a variety combination of steam and hexane as well as the sequence of steam and hexane injection.

From the above-described strategies, it is found the reservoir temperature is usually maintained at a high level, which is beneficial to bitumen and oil sands reservoirs with a thick pay-zones. However, for those with thin pay-zones or water-interlayers, it would be detrimental because maintaining a high temperature would lead to serious heat losses and low economy.

This chapter proposes a new steam-solvent hybrid process for heavy oil reservoirs in thin pay-zones, steam-assisted vapor extraction (SAVE). This strategy is essentially a solvent-based process in which a short slug of steam or heated solvent is intermittently injected to raise the reservoir temperature beyond a solvent chamber. Numerical simulation is resorted to analyze the performance of this new strategy. Sensitivity of the oil production and SOR to reservoir and fluid properties and operating parameters are analyzed, and corresponding conclusions are made.

6.2 Simulation Study

6.2.1 Numerical model

A rectangular field-scale numerical simulation model is developed by using a commercial simulator, STARS [Version 2014, Computer Modeling Group Limited, Canada] (**Figure 6.1a**). As one of the most important properties, heavy oil viscosity is plotted versus temperature in **Figure 6.1b.** Relative permeability curves for water and oil phases are presented in **Figure 6.1c**. **Table 6.2** lists the detailed reservoir and fluid properties in the numerical model. In particular, the model is set as 10 m thick, which is designed for a thin heavy oil reservoir. VAPEX and SAGD are also simulated with the same reservoir model for the purpose of comparison with the newly developed SAVE process.

6.2.2 Operation procedure

In conventional VAPEX or SAGD processes, the steam/solvent pressure in a depleted chamber is maintained relatively constant (**Figure 6.2a**). Whereas SAVE is operated in a cyclic process, and each cycle has four periods, as shown in **Figure 6.2b**:

1. *Steam injection*. Shut in the producer and inject steam continuously into a reservoir at a constant rate, until the reservoir pressure is raised to a preset value. This period lasts typically two to five days.
2. *Soaking*. Shut in the injector for two days, so that the heat in the hot steam can be released to the reservoir and heavy oil.
3. *Pressure falloff*. Open the producer to pump out the heated heavy oil and steam, also to let the pressure in a steam chamber drops to certain low level. The length of this period depends on the stages of operating constraints as well as the size of steam/solvent chamber.
4. *Solvent injection*. Inject vaporized solvent at a certain pressure, and produce the heated and diluted heavy oil in a VAPEX manner. This steady production will last one to four months.

6.3 Results and Discussion

Figure 6.3 shows the pressure and oil production within a cycle of a SAVE process with the base-case parameters. The typical lengths of the four periods in this simulation are about 4, 2, 30, and 70 days, respectively. It can be seen that there is no oil production during steam injection and soaking periods, during which the heavy oil is heated by steam, drains downward by gravity, and accumulates above the producer. This heated oil is first produced during the early stage of the pressure drop period. Afterwards, the oil production rate gradually declines with the decrease of pressure and temperature in the chamber. Once the solvent injection starts, the oil production rate stopped falling but almost stabilizes throughout the last period. Quantitatively, it decreases from $q_o = 0.033$ m^3/d at the beginning to $q_o = 0.025$ m^3/d at the end of this period.

Table 6.1 Reservoir and Fluid Properties in Numerical model

Property	Symbol	Value	Unit
Model			
Dimension (field-scale)	L×H×W	25×10×1	m×m
Porosity	ϕ	35	vol.%
Absolute permeability	k	5×10^{-12}	m^2
Initial oil saturation	S_{oi}	90	vol.%
Residual oil saturation	S_{or}	10	vol.%
Heavy oil			
Viscosity @ 20.8°C and 800 kPa	μ_o	126,500	mPa.s
Density @ 20.8°C and 800 kPa	ρ_o	930.5	kg/m^3
Solvent			
Solvent name		Propane	
Viscosity (liquid) @ 20.8°C and 800 kPa	μ_s	0.165	mPa.s
Density (liquid) @ 20.8°C and 800 kPa	ρ_s	547.6	kg/m^3
Diffusivity	D	5×10^{-9}	m^2/s
Others			
Injection Temperature	T	21	°C
Injection pressure	P	800	Pa
Gravity acceleration	g	9.8	m/s^2

(a)

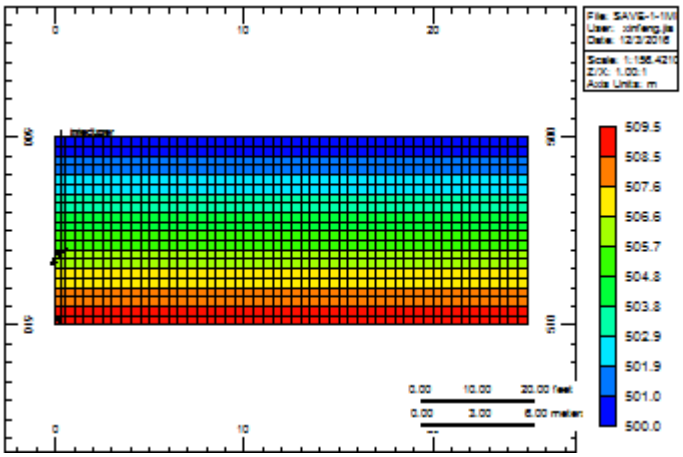

(b)

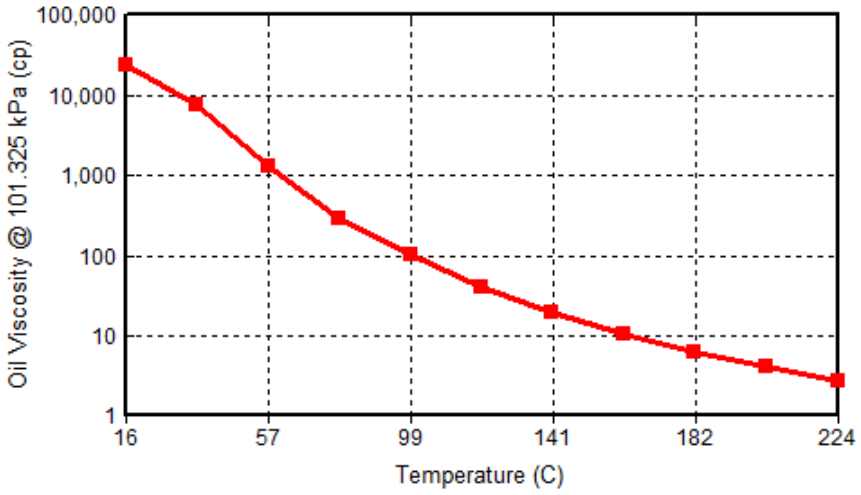

(c)

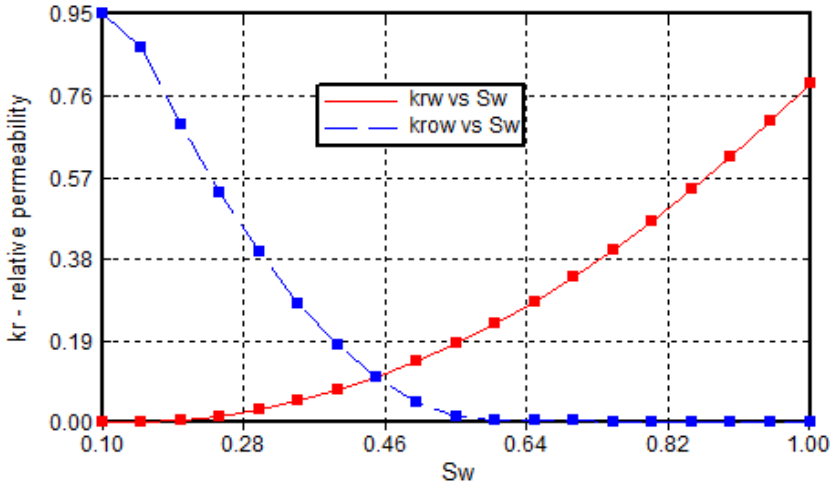

Figure 6.1 (a) A reservoir simulation model, **(b)** oil viscosity vs. temperature profile, and **(c)** oil-water phase relative permeability profiles.

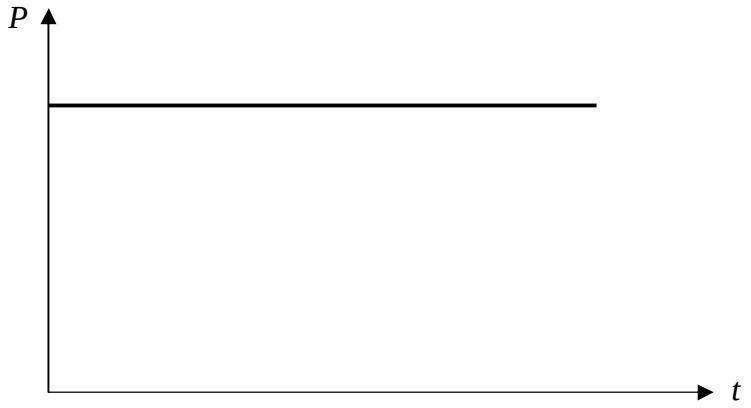

(a)

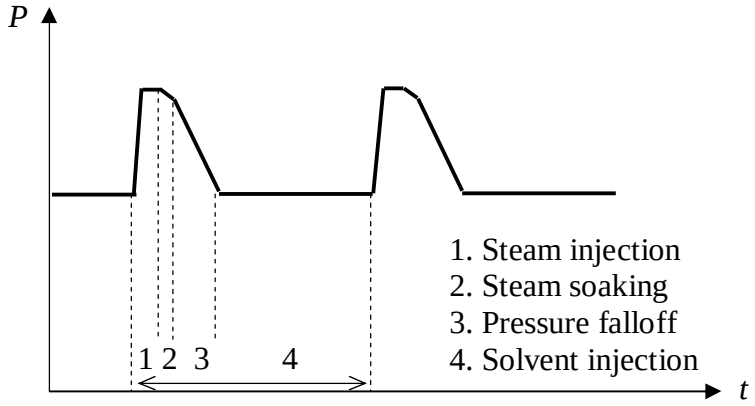

(b)

Figure 6.2 Schematics of pressure control of **(a)** SAGD/VAPEX and **(b)** SAVE processes.

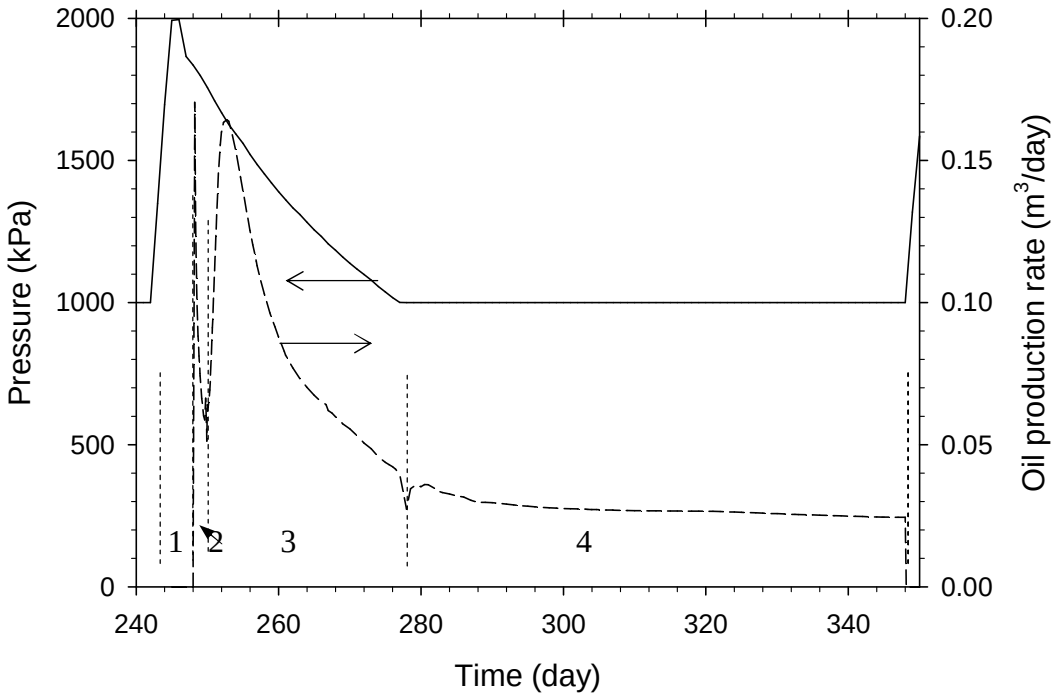

Figure 6.3 Pressure at the injector and oil production rate of a SAVE process.

Figure 6.4 shows the cumulative oil production, oil production rate, cumulative steam injection, steam-oil ratio, and solvent injection and production, solvent recovery of seven cycles (two years) of the SAVE base case. One important characteristic of the SAVE process is that the non-production period is very short: just 42 days out of 728 days in the base case. This means that the oil production is rather continuous (**Figure 6.4a**). Besides, the overcall cost on water heating/treatment/disposal is a main economic and environmental concern for thermal recovery processes. But in SAVE, the steam-oil ration can be as low as 0.6–0.8 m^3/m^3 (**Figure 6.4b**), which saves a considerable amount of water and can significantly improve the economics of heavy oil recovery processes. Moreover, another factor that needs serious attention is the solvent retention. **Figure 6.4c** shows that approximately 60% of the injected solvent are produced after two years of production in the SAVE manner. This means that over 30% of the injected solvent remains mixed with oil during the SAVE process, which indicates the strong capacity of SAVE in solvent dissolution and heavy oil dilution. In the end, most of the injected solvent should be recovered.

6.3.1 Effect of numerical dispersion

Numerical dispersion is always a big concern for the numerical simulation, since it is inherent in the finite difference method and comes from the spatial and temporal discretization or the truncation error because of gridding. **Figure 6.5** shows that the effect of three gridblock sizes (Δx = 0.25, 0.50, 1.00 m) on the cumulative heavy oil production and steam-oil ratio. It can be seen that different gridblock sizes result in a slight difference in the cumulative oil production profiles and somewhat deviation in the cumulative steam-oil ration profiles. **Figure 6.6** shows the effect of three time-steps (Δt = 0.0001, 0.001, 0.01 day) on the cumulative heavy oil production and steam-oil ratio. It is found that the correspondent cumulative heavy oil production profiles almost overlap each other and the differences are nearly insensible. This clearly shows that the effect of time step is negligible in this study. In the following section, a gridblock size of $\Delta x = \Delta y = \Delta z$ = 0.5 m and a time step of Δt = 0.0001 day are adopted in the simulation.

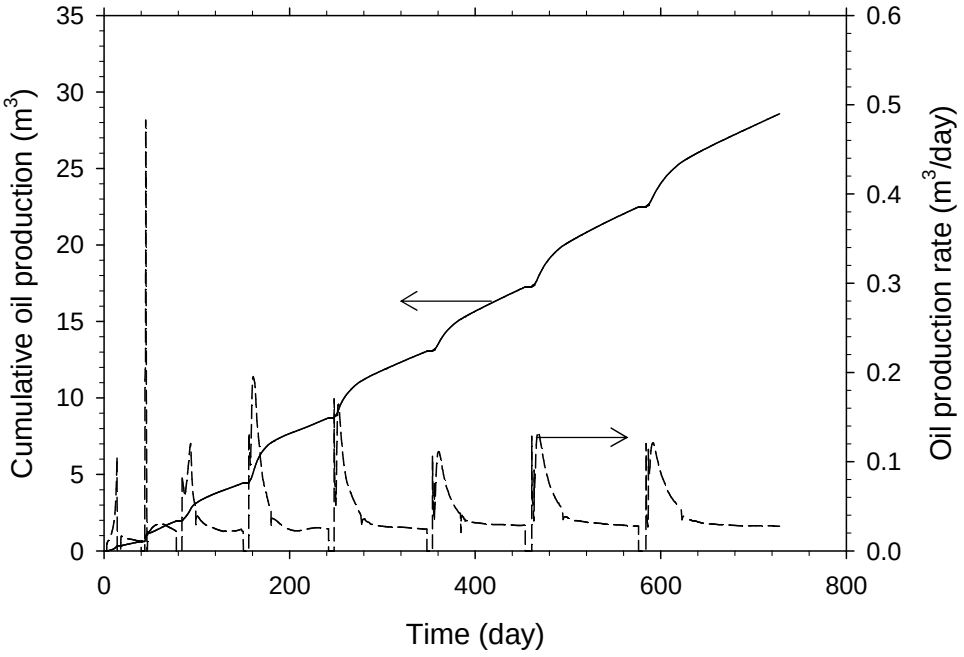
Cumulative oil production (m3)
Oil production rate (m3/day)
Time (day)
0
5
10
15
20
25
30
35
0.0
0.1
0.2
0.3
0.4
0.5
0.6
0
200
400
600
800

(a)

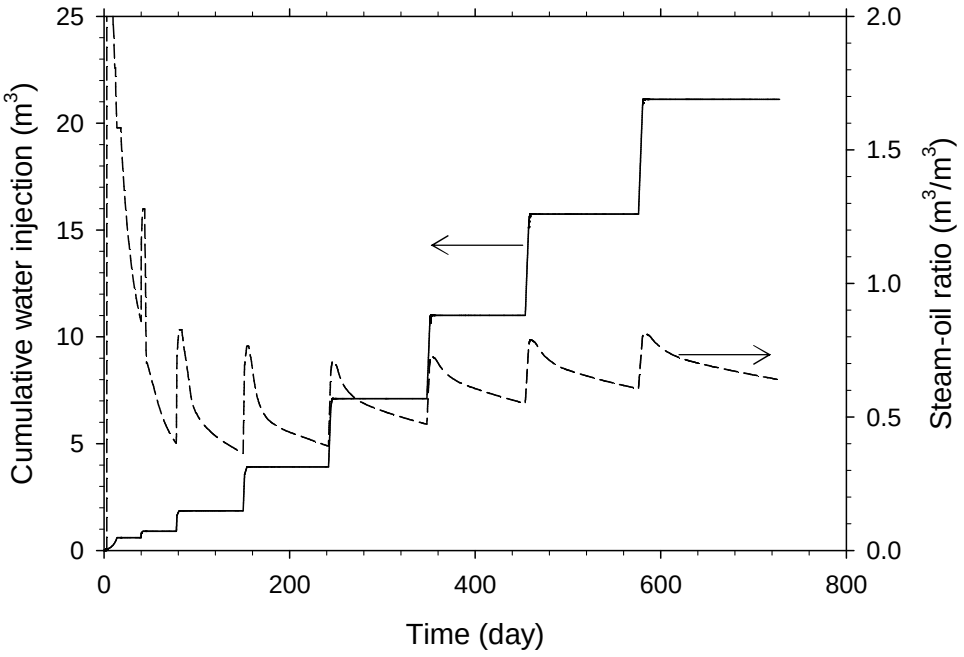
Cumulative water injection (m3)
Steam-oil ratio (m3/m3)
Time (day)
0
5
10
15
20
25
0.0
0.5
1.0
1.5
2.0
0
200
400
600
800

(b)

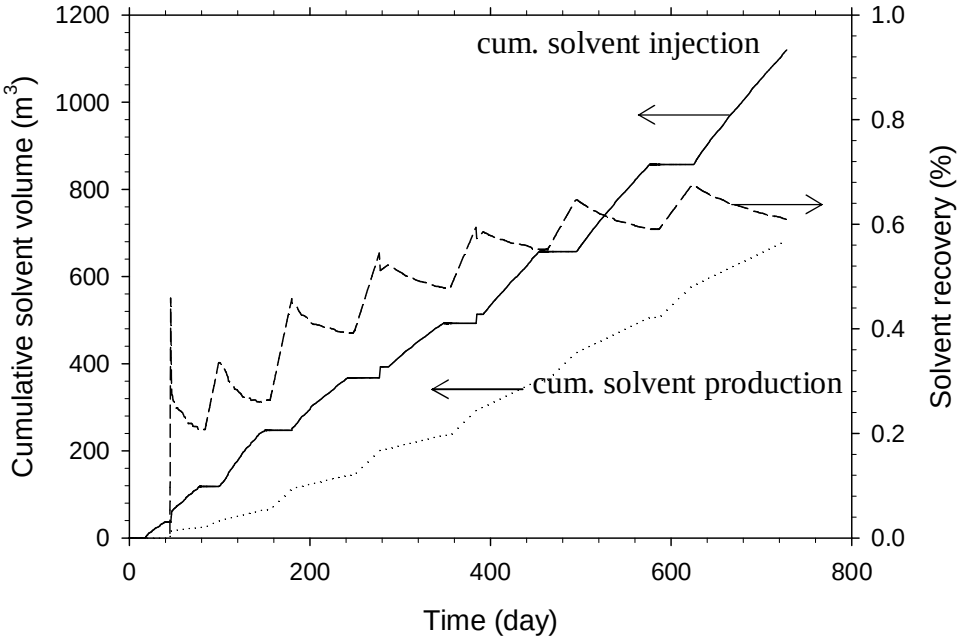

(c)

Figure 6.4 Simulation results of SAVE: **(a)** oil production, **(b)** water injection and steam-oil ratio, and **(c)** gas injection, gas production and cumulative solvent retention.

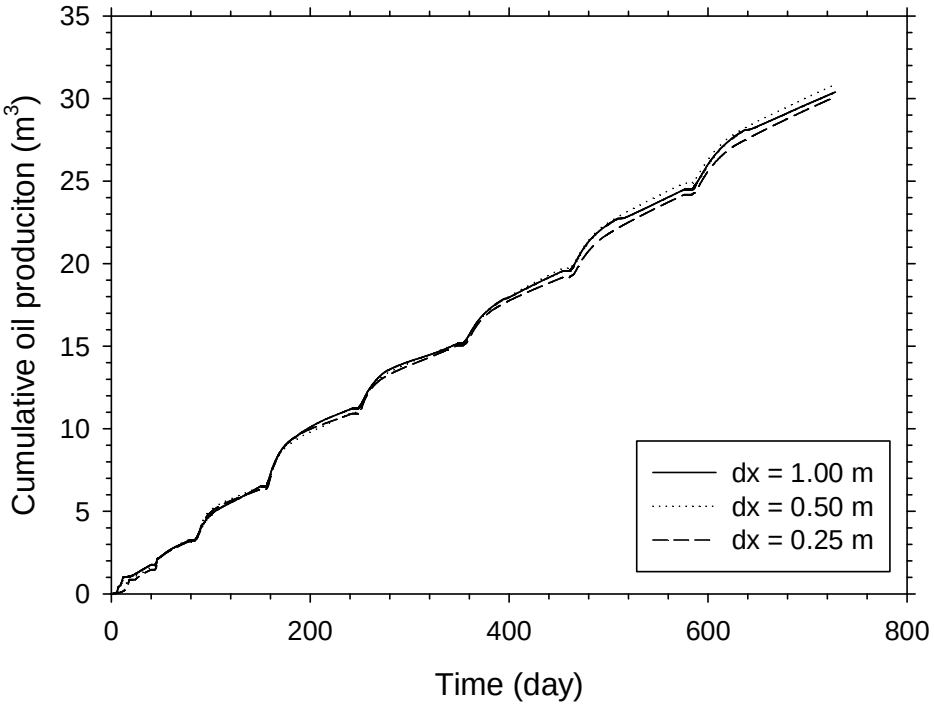

(a)

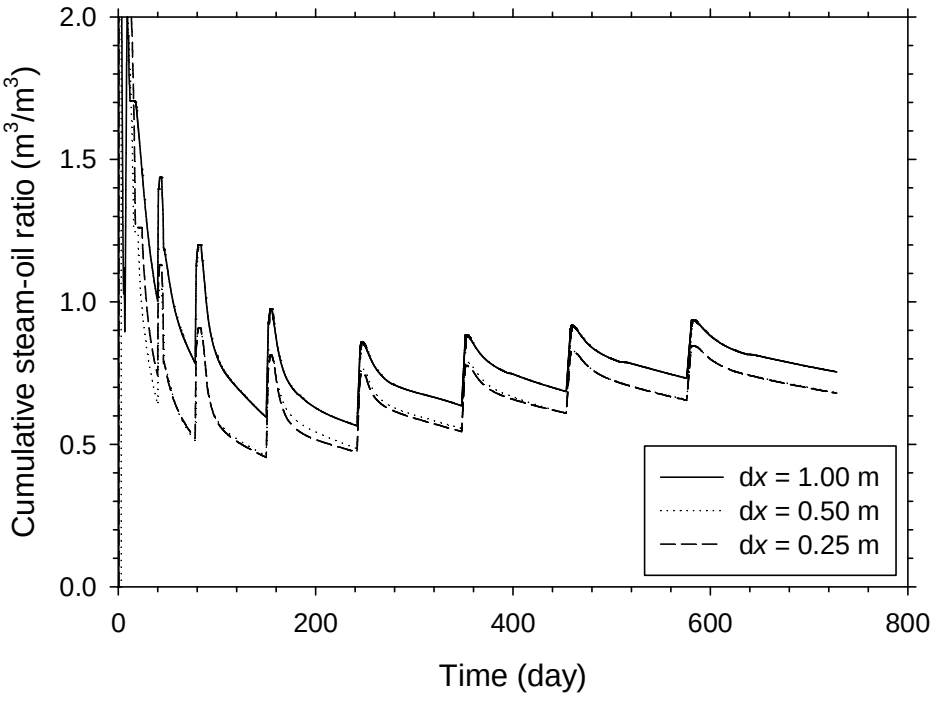

(b)

Figure 6.5 Effect of three gridblock sizes on the **(a)** cumulative oil production and **(b)** cumulative steam-oil ratio of a SAVE process

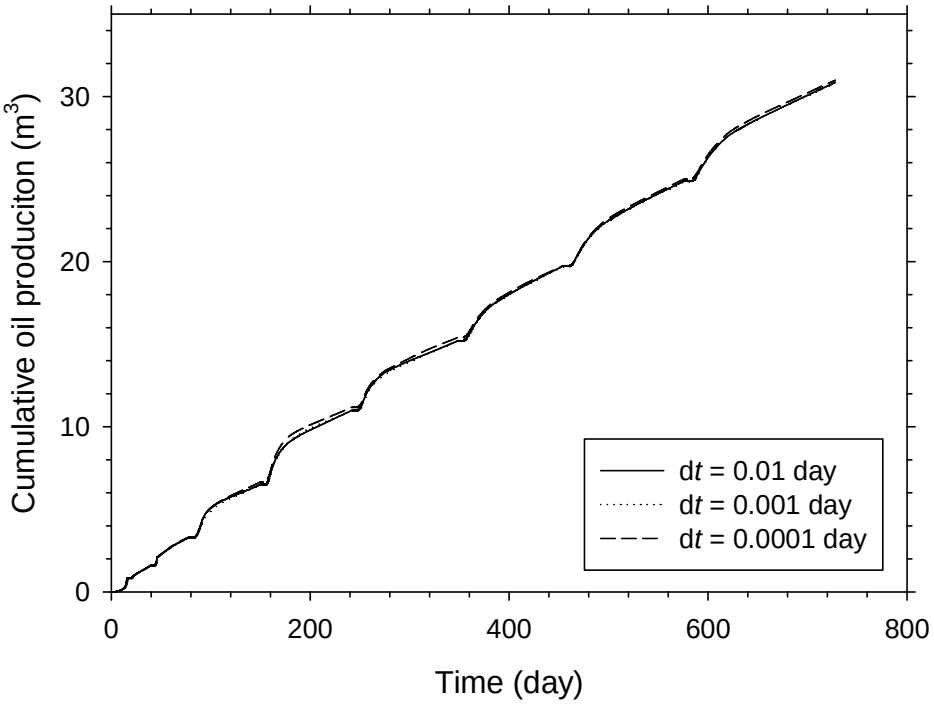

(a)

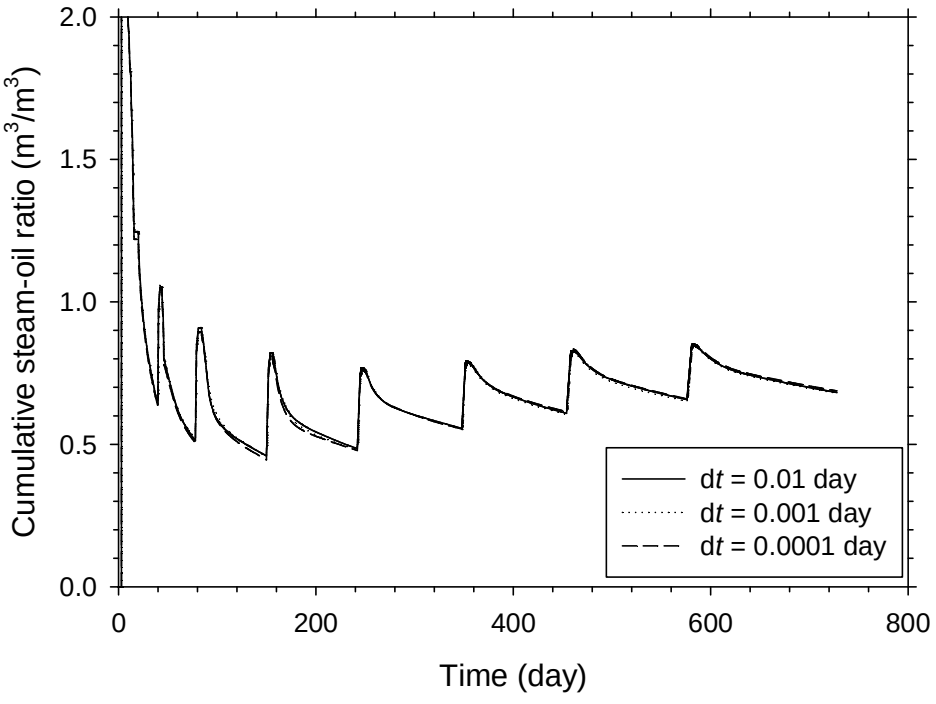

(b)

Figure 6.6 Effect of three time-steps on the **(a)** cumulative oil production and **(b)** cumulative steam-oil ratio of a SAVE process

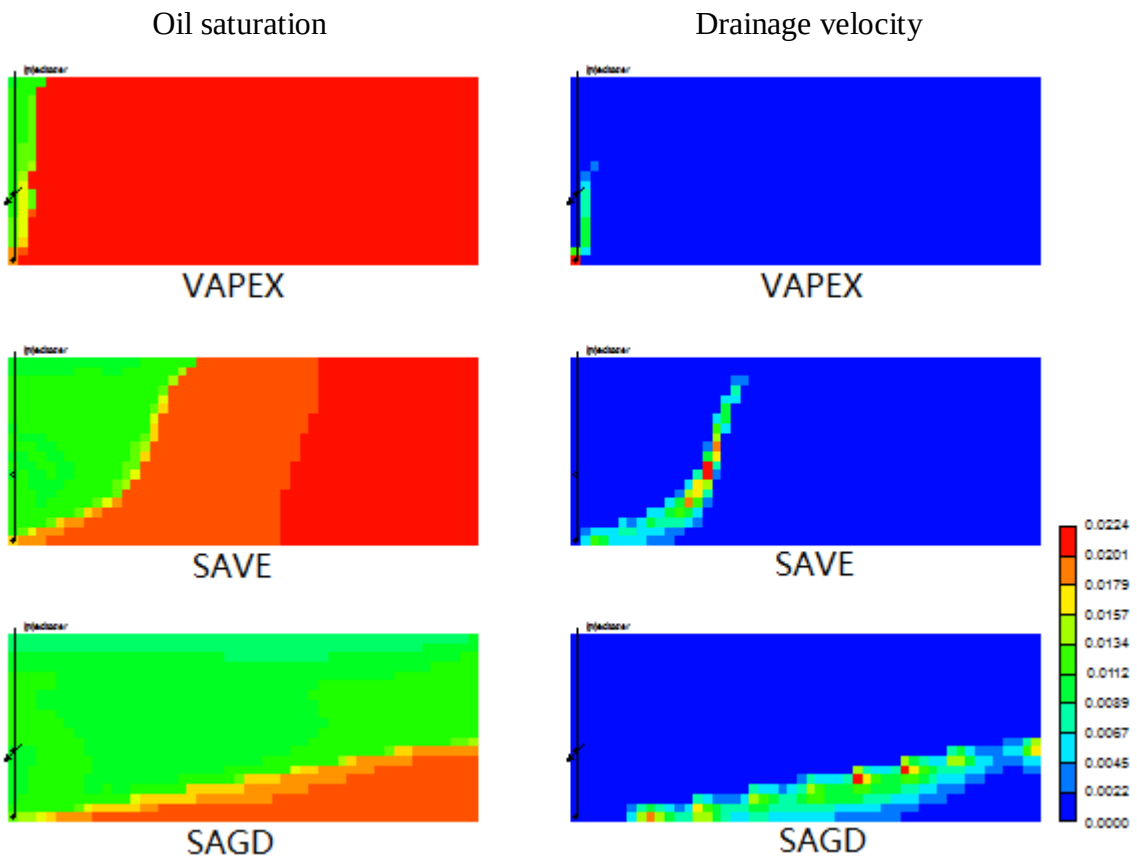

Figure 6.7 Comparison of oil-saturation and oil-velocity distributions over reservoir of VAPEX, SAVE, and SAGD at t = 360 days.

6.3.2 SAVE vs SAGD/VAPEX

Figure 6.7 shows the distributions of oil saturation and oil velocity of three processes: a cold solvent-based recovery process (VAPEX), a thermal recovery process (SAGD), and a hybrid recovery process (SAVE). Obviously, the chamber is least developed in VAPEX and best developed in SAGD within a same time period. Also, it can be identified that the transition zone, or the mobile oil zone is the widest in SAGD and the thinnest in VAPEX.

Figure 6.8 further compares SAVE and SAGD performances in terms of cumulative oil production, cumulative steam injection, and cumulative steam-oil ratio. It can be seen that at t = 400 days, the oil recovery of SAVE (RF = 23.2%OOIP) is 33.03% of that of SAGD (RF = 70.1%OOIP) (**Figure 6.8a**). However, the cumulative steam injection of SAVE (Q_s = 12.02 m^3) is 12.32% of that of SAGD (Q_s = 95.8 m^3) (**Figure 6.8b**). In comparison, the cumulative steam-oil ratio of SAVE (SOR = 0.66 m^3/m^3) is 32.6% of that of SAGD (SOR = 1.79 m^3/m^3) (**Figure 6.8c**).

Figure 6.9 compares the cumulative oil production and steam-oil ratio of SAVE and SAGD for different pay-zone thickness scenarios. It is found that the slope of the linearly regressed line for SAGD is larger than that for SAVE. Quantitatively, the oil production rate for SAVE is 32.3% of that of SAGD at a thicker formation (h = 15 m), and 40.8% of that of SAGD at a thinner formation (h = 5 m) (**Figure 6.9a**). In addition, the steam-oil ratio of SAVE is 52.4% of that of SAGD at a thicker formation (h = 15 m), and 30.9% of that of SAGD at a thinner formation (h = 5 m) (**Figure 6.9b**). In short, SAVE performs relatively better than SAGD in heavy oil reservoirs with thinner pay-zones.

Figure 6.10 further compares SAVE and VAPEX performances in terms of cumulative oil production, cumulative steam injection, and cumulative solvent-oil ratio. It can be seen that at t = 400 days, the cumulative oil production of SAVE (Q_o = 23.15 m^3) is 7.16 times of that of VAPEX (Q_o = 3.23 m^3) (**Figure 6.10a**). Whereas the cumulative solvent injection of SAVE (Q_o = 554.06 m^3) is just 2.12 times of that of VAPEX (Q_o = 261.79 m^3) (**Figure 6.10b**). In comparison, cumulative solvent-oil ratio of SAVE (SOR = 127 m^3/m^3) is only 26.02% of that of VAPEX (SOR = 66.41 m^3/m^3) (**Figure 6.10c**).

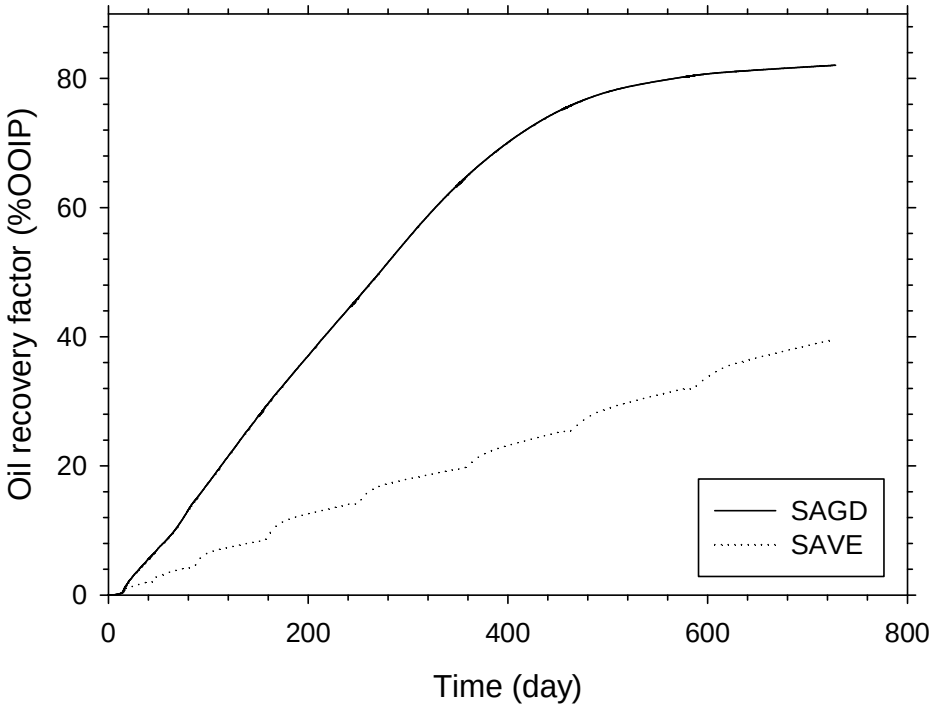
Oil recovery factor (%OOIP)
0
20
40
60
80
0
200
400
600
800
Time (day)
SAGD
SAVE

(a)

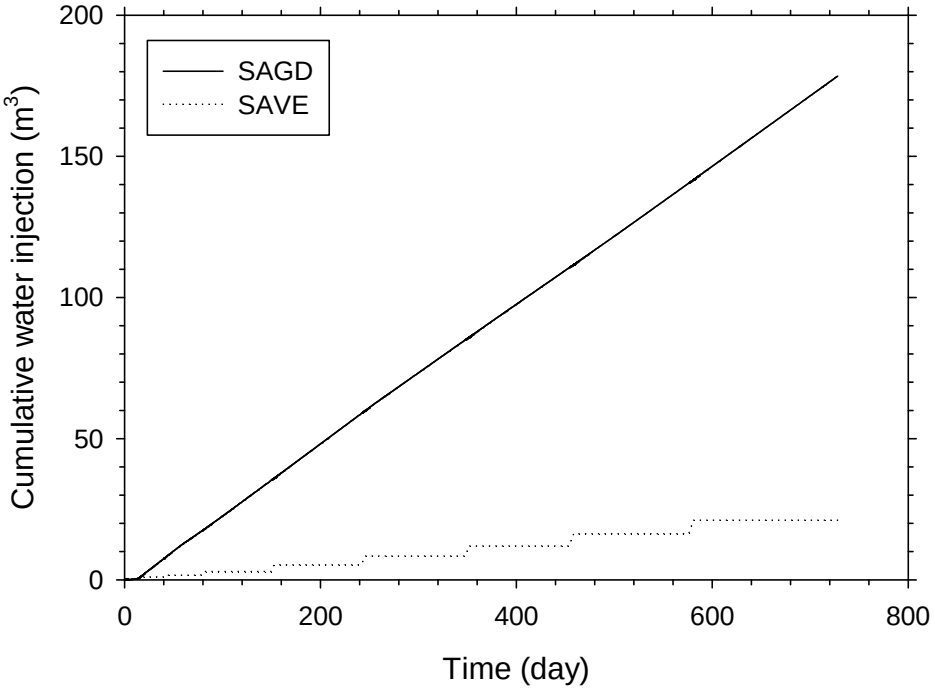
Cumulative water injection (m3)
0
50
100
150
200
0
200
400
600
800
Time (day)
SAGD
SAVE

(b)

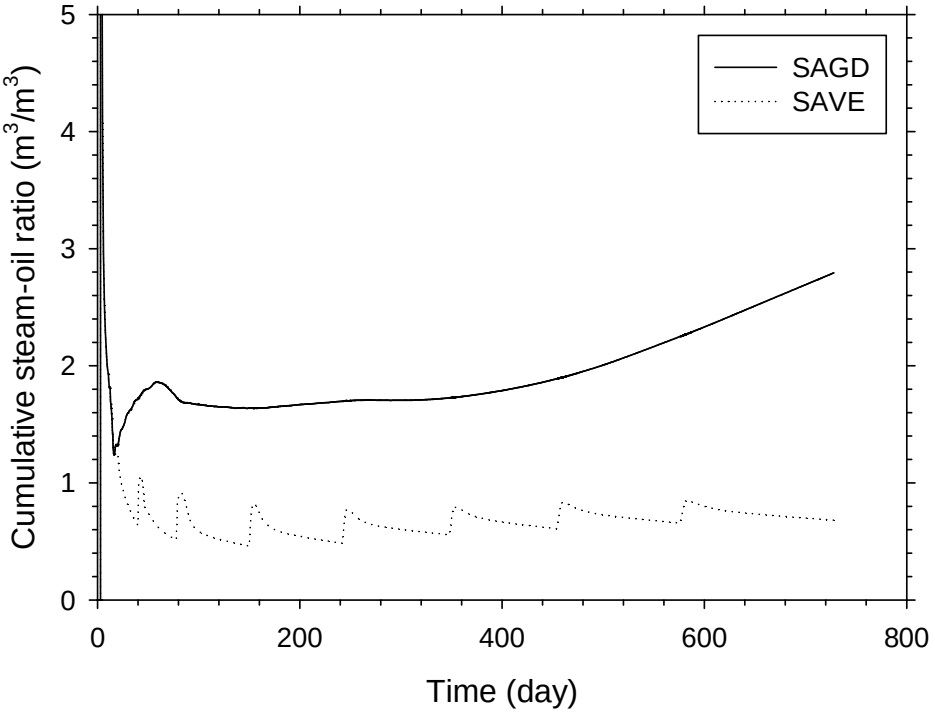

(c)

Figure 6.8 SAVE vs. SAGD in terms of **(a)** cumulative oil production, **(b)** cumulative steam injection, and **(c)** cumulative steam-oil ratio for the base case.

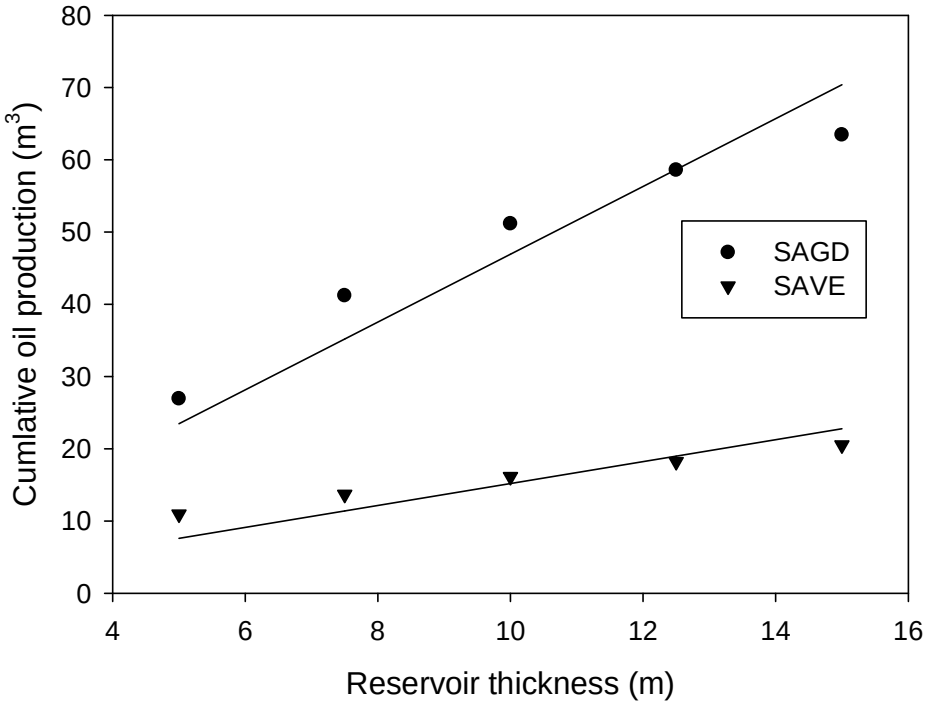

(a)

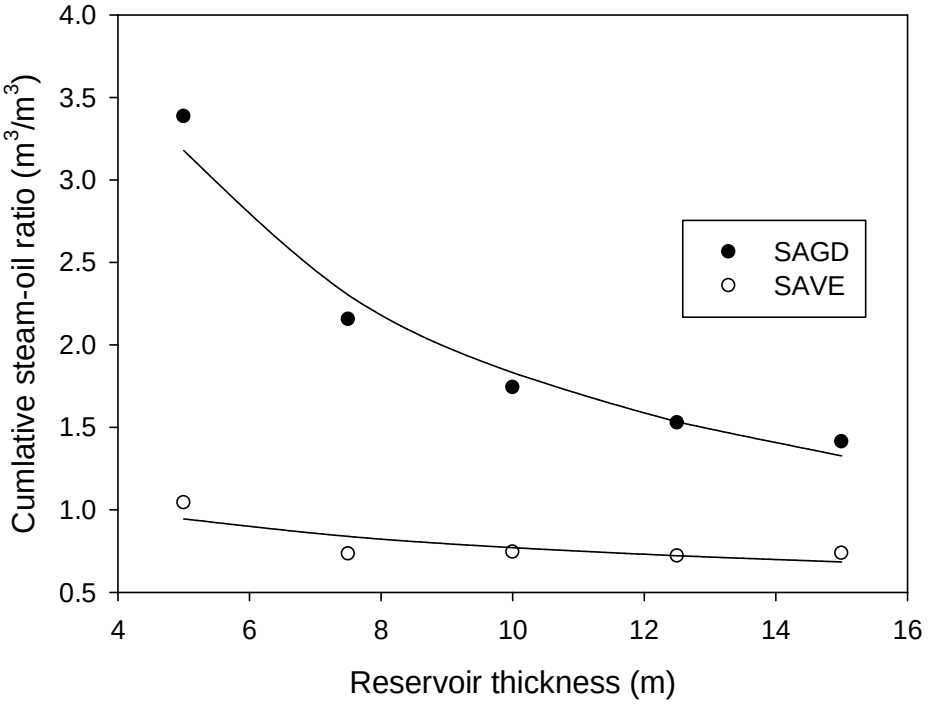

(b)

Figure 6.9 (a) Cumulative oil production and **(b)** cumulative steam-oil ratio of SAVE and SAGD for five different pay-zone thicknesses at t = 360 days.

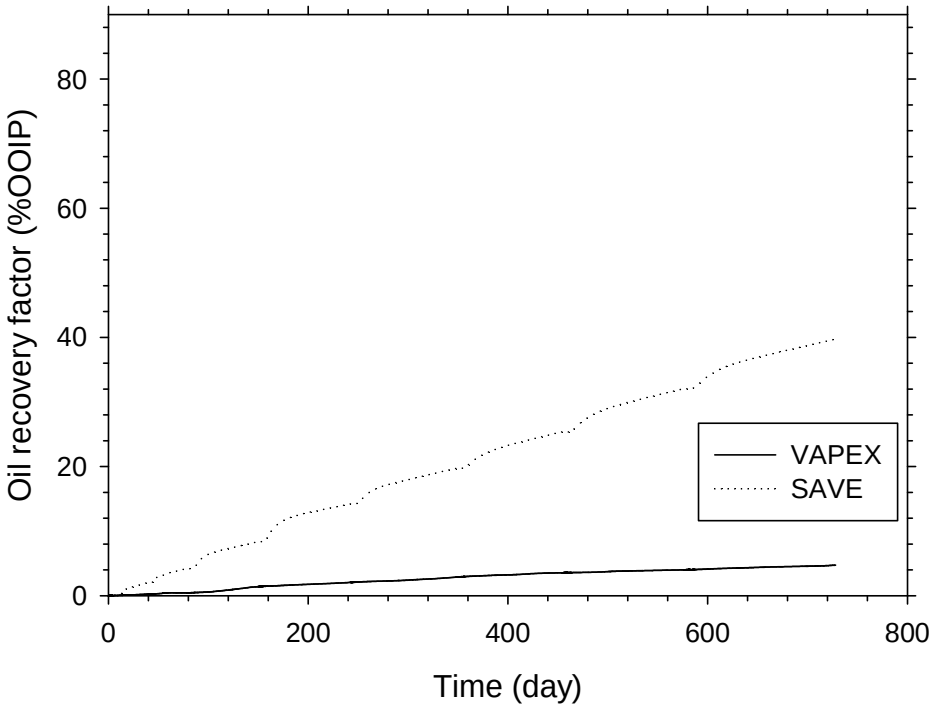
Oil recovery factor (%OOIP)
Time (day)
VAPEX
SAVE
0
20
40
60
80
0
200
400
600
800

(a)

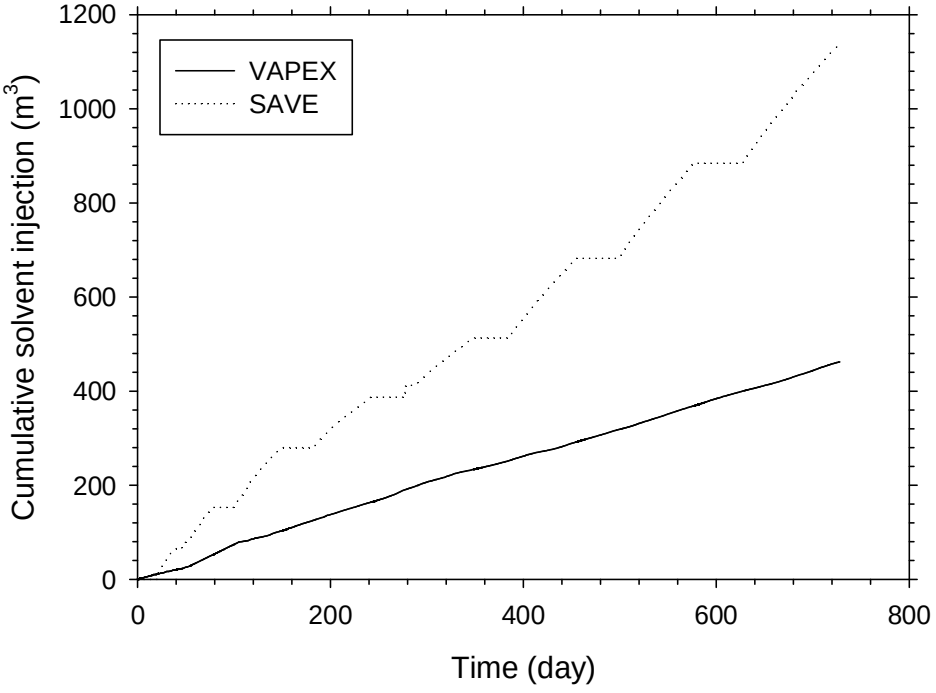
Cumulative solvent injection (m3)
Time (day)
VAPEX
SAVE
0
200
400
600
800
1000
1200
0
200
400
600
800

(b)

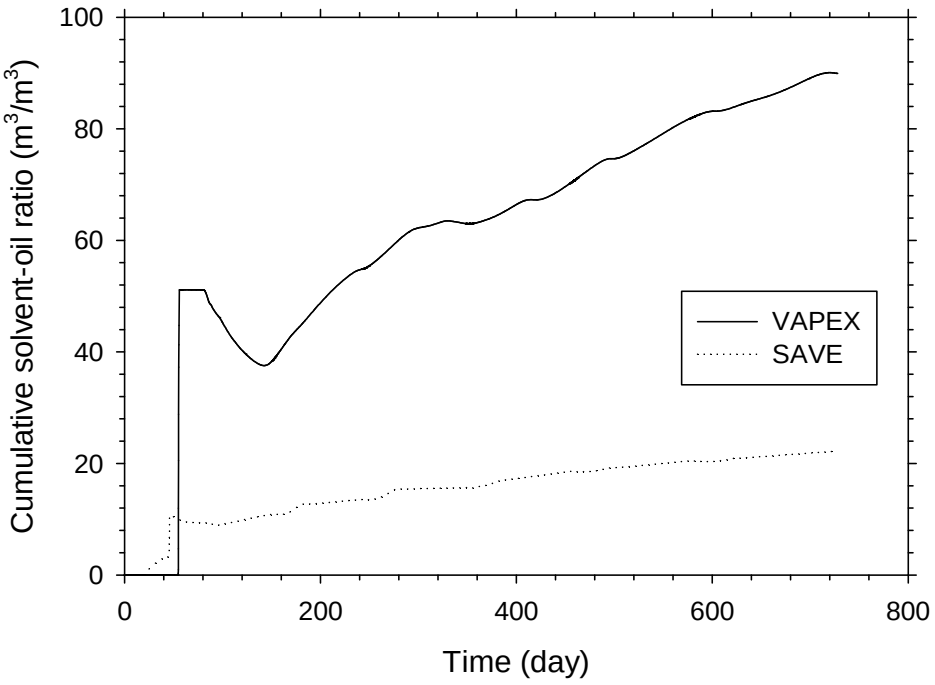

(c)

Figure 6.10 SAVE vs. VAPEX in terms of **(a)** cumulative oil production, **(b)** cumulative solvent injection, and **(c)** cumulative solvent-oil ratio for the base case.

Figure 6.11 compares the cumulative oil production and steam-oil ratio of SAVE and VAPEX for different pay-zone thickness scenarios. It is found that the slope of the linearly regressed line for SAVE is larger than that for VAPEX. Quantitatively, the oil production rate of SAVE is 6.3 times of that of VAPEX at a thicker formation (h = 15 m), and 11.0 times at a thinner formation (h = 5 m) (**Figure 6.11a**). In addition, the solvent-oil ratio of SAVE is just 24.3% of that of VAPEX at a thicker formation (h = 15 m), and 11.2% at a thinner formation (h = 5 m) (**Figure 6.11b**). In short, SAVE performs relatively better than VAPEX in heavy oil reservoirs with thinner pay-zones

For a process involving both steam and solvent, steam-oil ratio or solvent-oil ratio alone is no longer the measure of economics. Instead, this study use the cost per bbl oil as the parameter for comparison. Again, SAVE and VAPEX both inject cold solvent at the surface, and both SAVE and SAGD infuse steam at the surface. The cost of SAVE can be roughly estimated by considering the cost of SAGD and VAPEX and the solvent-/steam-oil ratios. Suppose the solvent-oil ratio of SAVE is 1/4 of that of VAPEX, and the steam-oil ratio of SAVE is 1/3 of that of SAGD, the cost of SAVE is the addition of the 1/4 of the VAPEX cost plus the 1/3 of the SAGD cost, as shown in **Table 6. 3**. For the SAGD cost range of 10–30 CAN.$/bbl and the VAPEX cost range of 30–50 CAN.$/bbl, SAVE is cheaper in most cases. It is always better than VAPEX, but confronts more challenges by low-cost SAGD.

6.3.3 Injection pressure

Figure 6.12 investigates the effect of chamber pressure during the solvent injection period on the cumulative oil production, cumulative steam-oil ratio, and cumulative solvent-oil ratio. It is found that higher chamber pressure (p_{inj} = 1,200 kPa) produces 3.76% of OOIP more oil than a lower chamber pressure (p_{inj} = 800 kPa) (**Figure 6.12a**). Meanwhile, a higher pressure has a 0.136 lower cumulative steam-oil ratio than a lower pressure (**Figure 6.12b**). Furthermore, the cumulative solvent-oil ratio for the three pressures is almost the same after 400 days of production (**Figure 6.12c**).

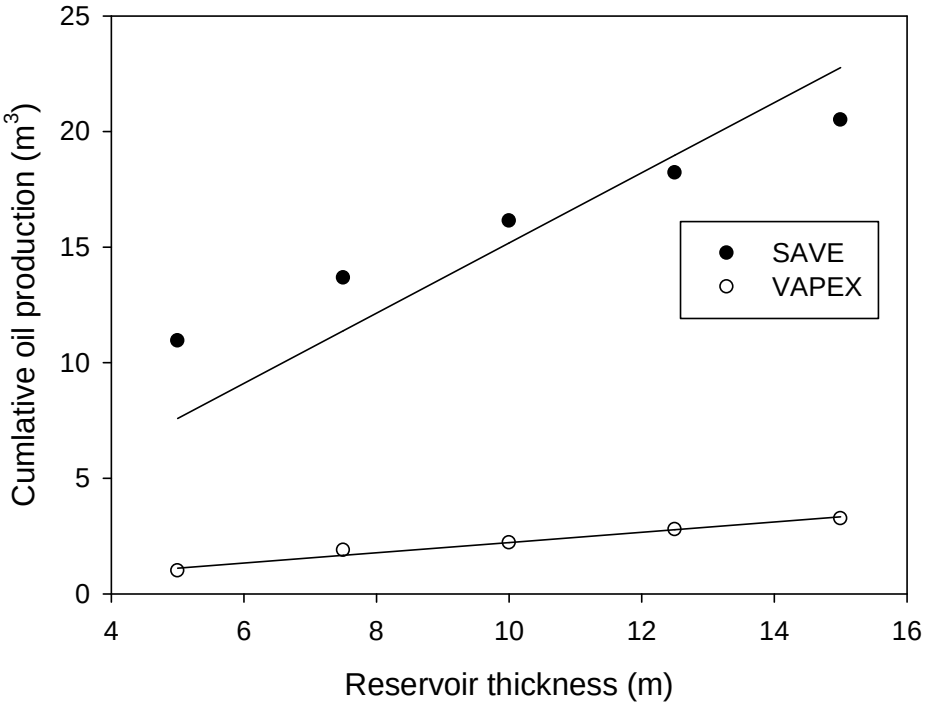

(a)

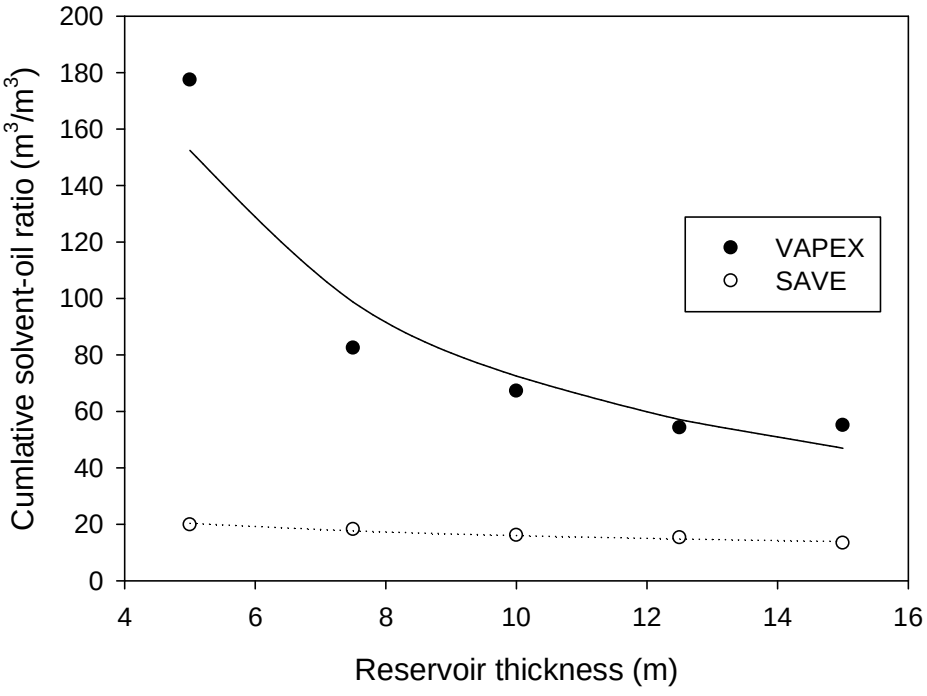

(b)

Figure 6.11 (a) Cumulative oil production and **(b)** cumulative solvent-oil ratio of SAVE and VAPEX for five different pay-zone thicknesses at t = 360 days.

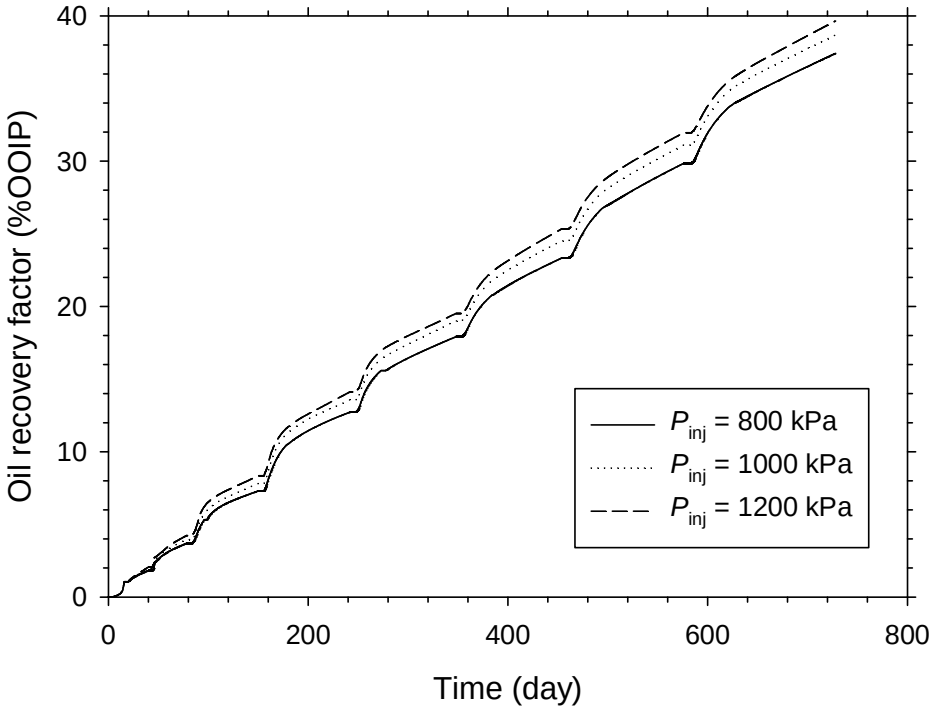
Oil recovery factor (%OOIP)
Time (day)
P_{inj} = 800 kPa
P_{inj} = 1000 kPa
P_{inj} = 1200 kPa
0
10
20
30
40
0
200
400
600
800

(a)

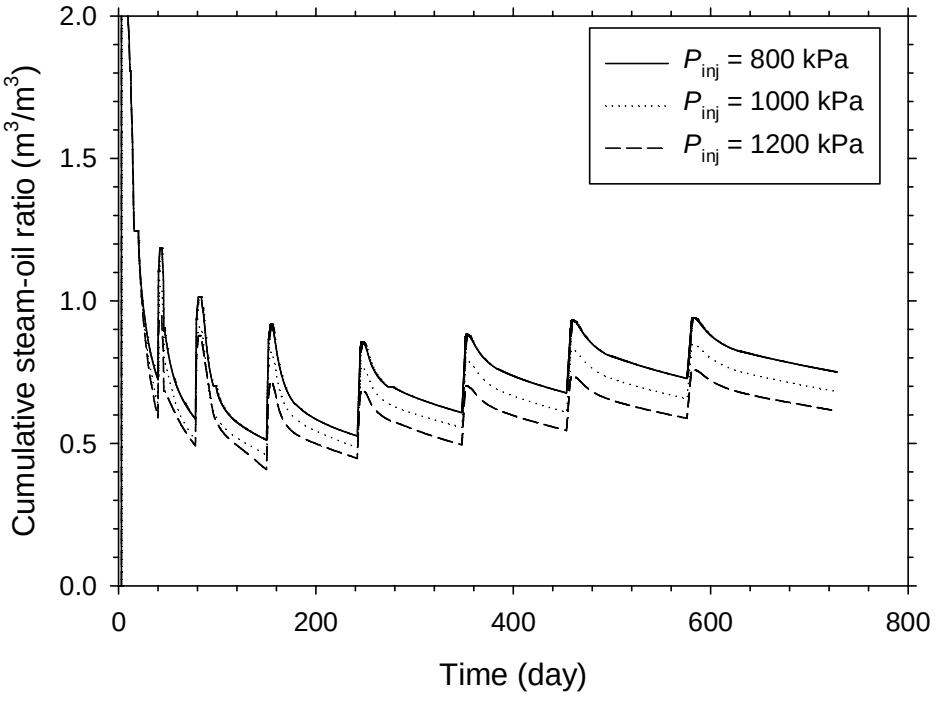
Cumulative steam-oil ratio (m^3/m^3)
Time (day)
P_{inj} = 800 kPa
P_{inj} = 1000 kPa
P_{inj} = 1200 kPa
0.0
0.5
1.0
1.5
2.0
0
200
400
600
800

(b)

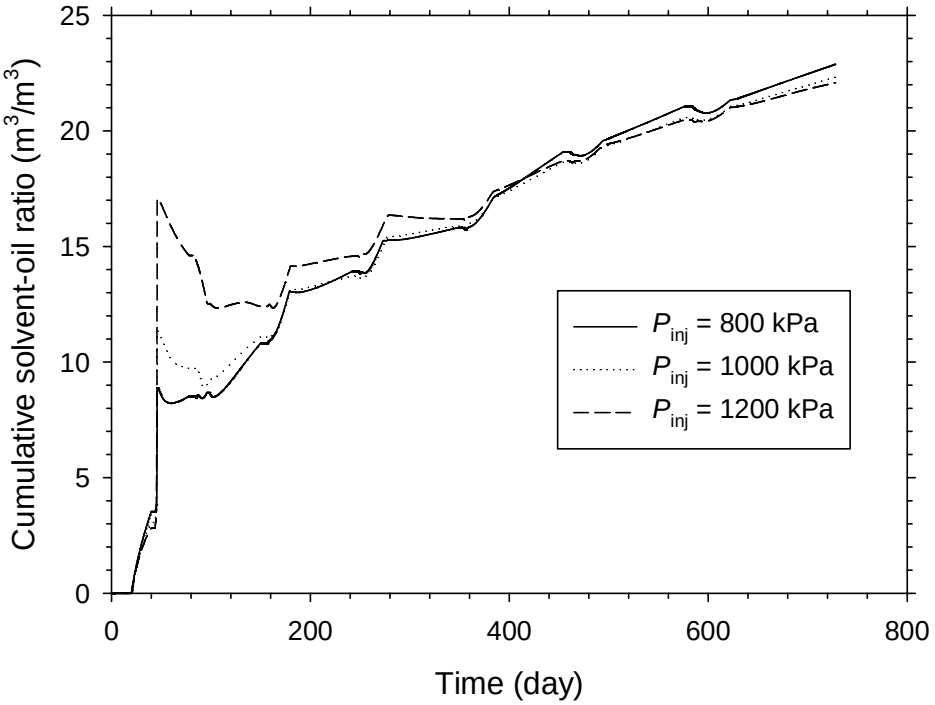

(c)

Figure 6.12 Effect of injection pressure on SAVE simulation results: **(a)** cumulative oil production, **(b)** cumulative steam-oil ratio, and **(c)** cumulative solvent-oil ratio.

6.3.4 Permeability

Permeability is one of the most important geological properties of a reservoir. **Figure 6.13** compares the SAVE performance in heavy oil reservoir with four matrix permeabilities: k = 3, 5, 7, and 9 Darcy. These values are chosen to be consistent with the experimental permeability ranges in the literature. As expected, SAVE extracts oil faster in more permeable formations. The k = 7 Darcy case achieves 21.5% of OOIP more than the k = 3 Darcy case. In addition, it is found that the cumulative steam-oil ratios remain almost the same for the three cases. However, the corresponding solvent-oil ratios are rather different. SAVE uses much more solvent to extract per unit volume of oil in a tighter formation than that in a more porous media.

6.4 Chapter Summary

This chapter proposes and investigates a new recovery technique through numerical simulation for heavy oil production in thin reservoirs. Throughout a SAVE process, steam and solvent are alternately injected to extract heavy oil in a cyclic manner. Simulation results show that the cumulative steam-oil ratio of SAVE is 32.6% of that of SAGD. In comparison with VAPEX, SAVE (Q_o = 23.15 m^3) produces oil about 7.16 times faster than VAPEX but its cumulative solvent-oil ratio is only 26.02% of that of VAPEX. SAVE performs relatively better in thinner formations than in thicker formations. Besides, SAVE performs relatively better than SAGD and VAPEX in heavy oil reservoirs with thinner pay-zones. Moreover, it is found that a higher chamber pressure can have a better performance than a lower chamber pressure.

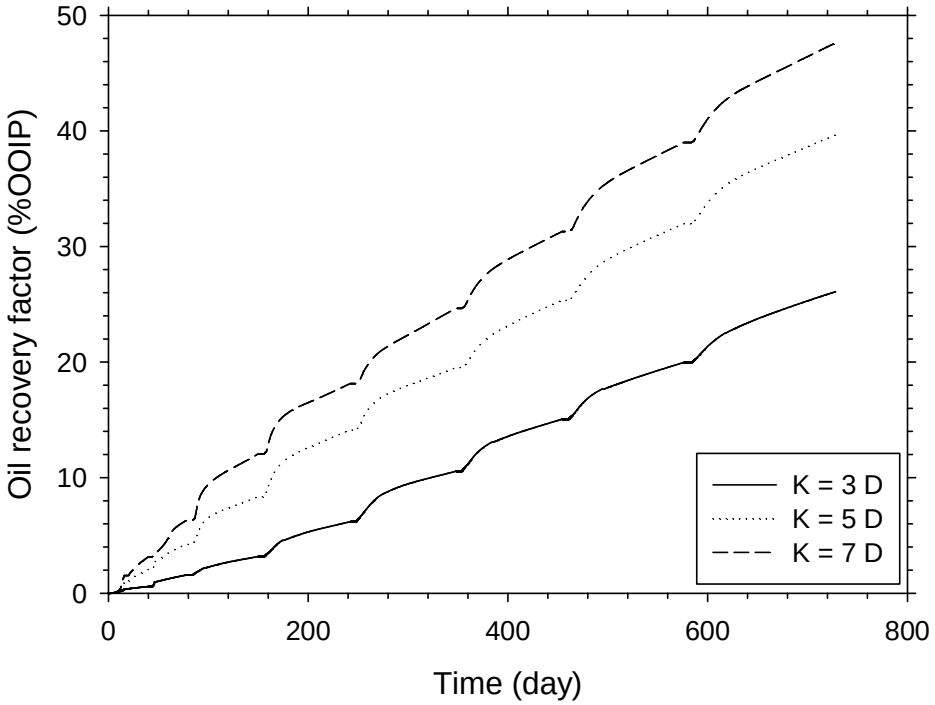
Oil recovery factor (%OOIP)
Time (day)
K = 3 D
K = 5 D
K = 7 D
0
10
20
30
40
50
0
200
400
600
800

(a)

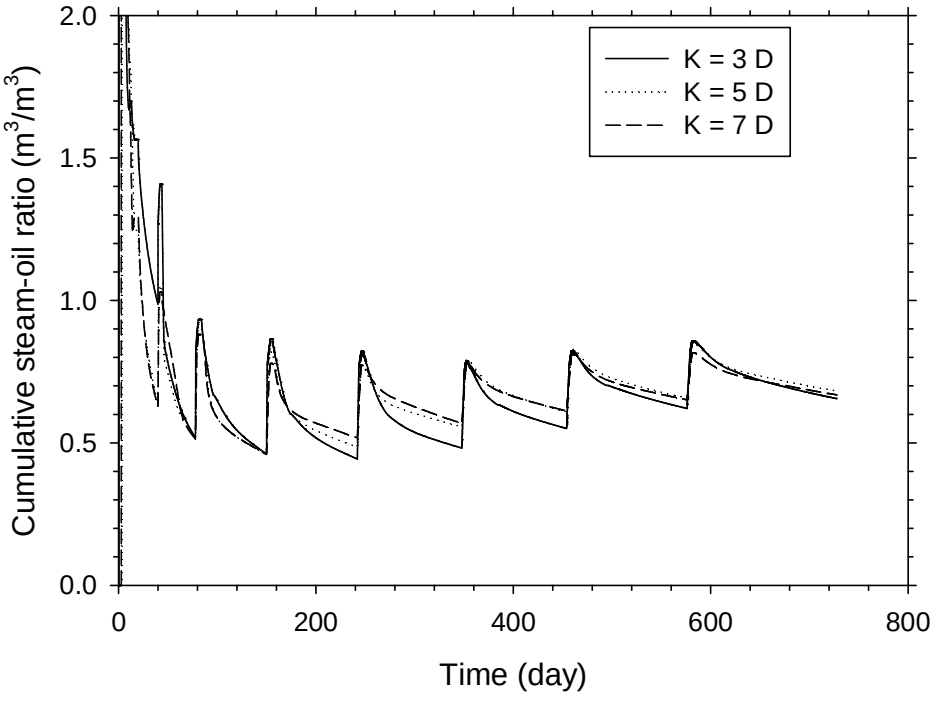
Cumulative steam-oil ratio (m3/m3)
Time (day)
K = 3 D
K = 5 D
K = 7 D
0.0
0.5
1.0
1.5
2.0
0
200
400
600
800

(b)

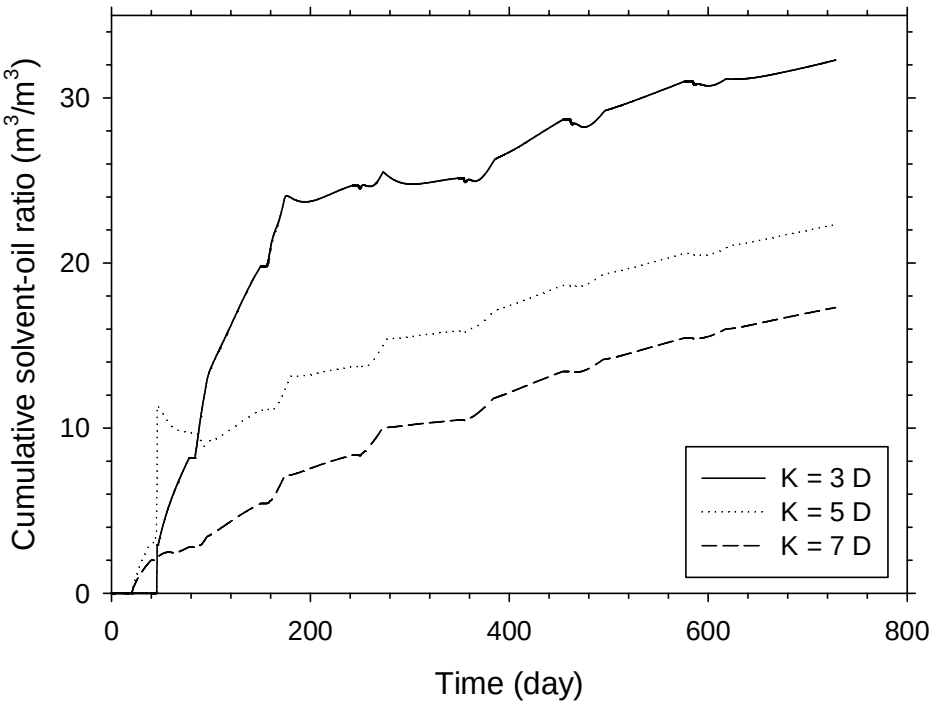

(c)

Figure 6.13 Effect of absolute permeability on SAVE simulation results: **(a)** oil recovery factor, **(b)** cumulative steam-oil ratio, and **(c)** cumulative solvent-oil ratio.

CHAPTER 7 CONCLUSIONS AND RECOMMENDATIONS

7.1 Conclusions

This thesis conducts some theoretical modeling of the cold and hot solvent-based heavy oil recovery processes and proposes a new steam–solvent hybrid scheme to improve heavy oil production rates. Through this study, major conclusions are summarized as follows:

VAPEX

Solvent concentration in the transition zone of VAPEX grows slower at the top than at the bottom while rather stable at the middle along the drainage surface. The stabilized oil production rate depends linearly on the square root of drainage height at both lab- and field-scales. In addition, the newly developed VAPEX model can accurately describe the relationship between an oil production rate and a diffusion coefficient in various scales thanks to the absence of numerical dispersion. Furthermore, the numerical dispersion is estimated to increase with an increase in gridblock sizes but decrease with an increase in physical diffusivity.

Diffusivity

Diffusivity is determined through history matching the theoretically predicted and experimentally measured oil production rate. Although both constant and variable diffusivities can achieve a fairly good fit in cumulative oil production data, their respective characterizations of the fluid properties in the transition zone are rather different. Variable diffusivity estimates the mobile zone as about 1 cm thick in the middle part of solvent chamber, whereas constant diffusivity prediction doubles thickness and is much wider than physical experimental analysis. Constant diffusivity can be converted to equivalent variable diffusivity by using some correlations regressed in this study. Moreover, the back-calculated effective diffusivity is about 10–30 times the measured molecular diffusivity in laboratory.

Warm VAPEX

Elevating solvent injection temperature can reduce oil viscosity and improve diffusivity by orders. An oil production rate increases exponentially with temperature. The oil production rate is almost tripled by elevating temperature from T = 20 to 90°C. SOR shows three stages throughout a warm-VAPEX process: it is initially high, remains nearly constant in the middle stage, and increases slightly in the late stage. About 90% of the injected solvent is produced with oil, only about 4% is filled in the solvent chamber, and the rest is mixed with oil in the transition zone. An oil production rate increases linearly with the square root of permeability and the square root of pay-zone thickness, respectively. With an increase in crude oil viscosity, the oil production rate decreases logarithmically and SOR increases linearly.

SAVE

SAVE is a new hybrid recovery process, in which steam and solvent are alternately injected to extract heavy oil in a cyclic manner. The cumulative steam-oil ratio of SAVE is 37.26% of that of SAGD. In comparison with VAPEX, SAVE produces oil 8.4 times faster than VAPEX but its cumulative steam-oil ratio is only 25% of that of VAPEX. SAVE performs relatively better in thinner formations than in thicker ones. In addition, it is found that a higher chamber pressure can have a better performance than a lower one. Moreover, the oil production rate is found to be linearly dependent on the square root of permeability.

7.2 Recommendations

The following research topics may need more efforts to be made in the future:

Coupled modeling of mass and heat transfer

In the present mass transfer model in Chapter 5, transient heat transfer is simplified as a constant temperature profile close to the boundary of a solvent chamber. To accurately model the mass transport process, a transient mass and heat transfer model needs to be reasonably coupled.

Coupled modeling of mass transfer and pressure diffusion

This thesis considers the chamber pressure as maintained constant. However, in some solvent-based recovery processes, pressure is raised and dropped. For such processes, mass transfer and pressure diffusion need to be reasonably coupled to accurately characterize the solvent dissolution and exsolution in the heavy oil.

Economic evaluation of SAVE

The simulation study proves that SAVE has advantages over both VAPEX and SAGD in some respects. Meanwhile, it has some shorting comings as well. For example, it injects two materials (steam and solvent) instead of one (steam or solvent). To evaluate its potential for field applications, it is necessary to conduct a more detailed economic evaluation of this new process.

REFERENCE

Abramowitz, M. and Stegun, I.A. 1970. Handbook of mathematical functions with formulas, graphs, and mathematical tables. Dover Publications, New York.

Akin, S., 2005. Mathematical modeling of steam-assisted gravity drainage. SPE Res. Eval. & Eng. 8 (5), 372–376.

Al-Bahlani, A.M., Babadagli, T., 2009. SAGD laboratory experimental and numerical simulation studies: a review of current status and future issues. J. Petrol. Sci. & Eng. 68 (3–4), 135–150.

Ali, S.M.F. 2003. Heavy oil–ever more mobile. J Pet Sci Eng 37 (1–2): 5–9. doi: 0920-4150/02.

Alkindi, A.S., Al-Wahaibi, Y.M., and Muggeridge, A.H. 2012. Experimental and numerical investigation of oil-drainage rate during Vapex process. SPE Journal 16 (2): 343–357. doi: 10.2118/141053-PA.

Allen J.C., Gillespie, R.E. and Burnett, D.B. 1984. Superheated solvent method for recovering viscous petroleum. US Patent No. 4,450,913.

Allen, J.C. 1973. Method for recovering viscous oils by solvent extraction. Canadian Patent No. 1,008,361.

Allen, J.C. 1974. Gaseous solvent heavy oil recovery. Canadian Patent No. 1,027,851.

Allen, J.C. and Redford, D.A. 1978. Combination solvent-noncondensible gas injection method for recovering petroleum from viscous petroleum-containing formations including tar sand deposits. US Patent No. 4,109,720.

Allen, J.C., Woodward, C.D., and Brown, A. 1976. Multiple solvent heavy oil recovery method. US Patent No. 3,954,141.

Al-niami, A.N.S. and Rushton, K.R. 1978. Radial dispersion to an abstract well. Journal of Hydrology 39 (3−4): 287−300.

Alston, R.B. 1981. Enhanced oil recovery employing blend of carbon dioxide, inert gas and intermediate hydrocarbons. US Patent No. 4,299,286.

ALvestad, J., Lagisquet, A., and Gilje, E. 2013. Solvent injection recovery process. US Patent No. 2013/0000894 A1.

Awang, M. and Farouq Ali, S.M., Hot-Solvent Miscible Displacement; paper 80-31-29 presented at the 31st Annual Technical Meeting of the Petroleum Society of CIM, Calgary, AB, 25−28 May 1980.

Ayodele, O.R., Nasr, T. N., Ivory, J. Beaulieu, G., and Heck, G. 2010. Testing and History Matching ES-SAGD (Using Hexane). Paper 134002-MS presented at SPE Western Regional Meeting, Anaheim, USA 27−29 May.

Azad, A., Chalaturnyk, R.J., 2010. A mathematical improvement to SAGD using geomechanical modelling. J. Can. Pet. Technol. 49 (10), 53–64.

Bergman, T.L., Lavine, A.S., Incropera, F.P., DeWitt, D.P., 1990. Fundamentals of heat and mass transfer. John Wiley & Sons.

Bird, R.B., Stewart, W.E., and Lightfoot, E.N. 2001. Transport Phenomena (Second Edition ed.). John Wiley and Sons. ISBN 0-471-41077-2.

Birrell, G., 2001. Heat transfer ahead of a SAGD steam chamber: a study of thermocouple data from phase B of the underground test facility (Dover project).

Presented at the Pet. Soc. Of CIM's Canadian International Petroleum Conference, Calgary, Alberta, Canada.
Boustani, A. and Maini, B.B. 2001. The role of diffusion and convective dispersion in vapour extraction process. J Can Pet Technol 40 (4): 68−77. doi: 10.2118/01-04-05.
Brooks, R.H., Corey, A.T., 1964. Hydraulic properties of porous media. Hydrology papers, No. 3, Colorado State U., Fort Collins, Colorado.
Buckley, J.S. 1991. Multiphase Displacements in Micromodels. In Interfacial Phenomena in Oil Recovery, N.R. Morrow, ed., Marcel Dekker, Inc., New York City, 157−189.
Buckley, S. E. and Leverett, M.C. 1942. Mechanism of Fluid Displacements in Sands. Transactions of the AIME 146: 107–116.
Butler, R.M. and Mokrys, I.J. 1993. Recovery of Heavy Oils using Vapourized Hydrocarbon Solvents: Further Development of the VAPEX Process. J Can Pet Technol 32 (6): 56–62. doi: 10.2118/93-06-06.
Butler, R.M. and Mokrys, I.J. 1998. Closed-loop Extraction Method for the Recovery of Heavy Oils and Bitumens Underlain by Aquifers the VAPEX Process. J Can Pet Technol 37 (4): 41−50. doi: 10.2118/98-04-04.
Butler, R. M. 1997b. The Steam and Gas Push (SAGP). Paper presented at the Petroleum Society 48th Annual Technical Meeting, Calgary, Alberta, 8−11 June. 26.
Butler, R.M. 1985. A New Approach To The Modeling Of Steam-Assisted Gravity Drainage J Can Pet Technol 24 (3): 42–51. JCPT-85-03-01. doi: 10.2118/85-03-01.
Butler, R.M. 1985. A New Approach to the Modelling of Steam-Assisted Gravity Drainage. J. Can. Pet. Tech. 24(3): 42−51.
Butler, R.M. 1994. Horizontal Wells for the Recovery of Oil, Gas, and Bitumen. The Petroleum Society of the Canadian Institute of Mining, Metallurgy and Petroleum, Calgary Section Monograph 2, 169−199.
Butler, R.M. 1997. Process and apparatus for the recovery of hydrocarbons from a reservoir of hydrocarbon. US Patent No. 5,607,016.
Butler, R.M. 1997a. Thermal Recovery of Oil and Bitumen. GravDrain Inc., Calgary, AB, ISBN 0-9682563-0-9. 25.
Butler, R.M. 1999. The Steam and Gas Push (SAGP). J. Can. Pet. Tech. 38: 54−61, March. 24.
Butler, R.M. and Jiang, Q. 2000. Improved recovery of heavy oil by Vapex with widely spaced horizontal injectors and producers. J Can Pet Technol 39 (1): 48−56. doi: 10.2118/00-01-04.
Butler, R.M. and Mokrys I.J. 1995. Process and apparatus for the recovery of hydrocarbons from a hydrocarbon deposit. US Patent No. 5,407,009
Butler, R.M. and Mokrys, I.J. 1989. Solvent Analogue Model of Steam-assisted Gravity Drainage. AOSTRA Journal of Research. 5 (1): 17−32.
Butler, R.M. and Mokrys, I.J. 1991. A New Process (VAPEX) for Recovering Heavy Oils using Hot Water and Hydrocarbon Vapour. J Can Pet Technol 30 (1), 97−106. doi: 10.2118/91-01-09.
Butler, R.M. and Stephens, D. J. 1981. The Gravity Drainage of Steam-heated Heavy Oil to Parallel Horizontal Wells. J. Can. Pet. Tech. 20(2): 90−96.
Butler, R.M. and Yee, C.T. 1986. A Theoretical Study of Steam Condensation in the Presence of Non-Condensable Gases. AOSTRA J. Res. 3:1−13.
Butler, R.M., and Mokrys, I.J. 1989. Solvent Analog Model of Steam-Assisted Gravity

Drainage. AOSTRA J. Res. 5: 17−32.
Butler, R.M., Jiang and Yee, Chi-Tak. 2000b. Steam and Gas Push (SAGP). J. Can. Pet. Tech. 39(8): 51−60, August. 23.
Butler, R.M., McNab, G.S., and Lo, H.Y. 1981. Theoretical Studies on the Gravity of Heavy Oil during Steam Heating. Can. J. Chem. Eng. 59(4): 455−460.
Carslaw H.S., Jaeger J.C., 1959. Conduction of heat in solids. Oxford university press.
Chakrabarty, T. 2010. Solvent for extracting bitumen from oil sands. US Patent No. 2010/0130386 A1.
Chen, Z., 2006a. Heavy oils, Part I, *SIAM News*, Vol. 39/Number 3, April, pages 1 and 8.
Chen, Z., 2006b. Heavy oils, Part II, *SIAM News*, Vol. 39/Number 4, May, pages 5 and 8.
Chen, Z., G. Huan and Ma, Y., 2006. Computational Methods for Multiphase Flows in Porous Media. Computational Science and Engineering Series, Vol. 2, SIAM, Philadelphia.
Chen, Z. 2007. Reservoir simulation: mathematical techniques in oil recovery. Society of Industrial and Applied Mathematics, Phyladelphia, PA.
Christiansen, R.L. and Smith, S.R. 1993. Sequentially flooding a subterranean hydrocarbon-bearing formation with a repeating cycle of immiscible displacement gases. US Patent No. 5,232,049.
Chuang, B.C., Bose, M., Morton, S.A., Elkow, K.J., Erlendson, E. 2009. Methods of improving heavy oil production. US Patent No. 7,527,096 B2.
CMG, STARS manual, Version 2009.
Cohen, Y. and Metzner, A.B. 1981. Wall effects in laminar flow of fluids through packed beds. AIChe J. 27 (5):705−715. doi: 10.1002/aic.690270502.
Corey, A.T. 1954. The Interrelation between Gas and Oil Relative Permeabilities. Prod. Monthly 19(1): 38−41.
Cuthiell, D. and Edmunds, N. 2012. Thoughts on simulating the VAPEX process. Paper SPE-158499 presented at the SPE heavy oil conference, Calgary Canada, 12−14 June.
Cuthiell, D., Kissel, G., Jackson, C., Frauenfeld, T., Fisher, D., and Rispler, K. 2006. Viscous Fingering Effects in Solvent Displacement of Heavy Oil. J Can Pet Technol 45 (7): 29–39. doi: 10.2118/06-07-02.
Cuthiell, D., McCarthy, C, Kissel, G., and Cameron, S. 2006. The role of capillary in VAPEX. Paper PETSOC 2006-073, presented at the Canadian International Petroleum Conference, Calgary, Alberta, 13−15 June. doi: 10.2118/2006-073.
Cuthiell, D., Mccarthy, C., Frauenfeld, T., Cameron, S., and Kissel, G. 2003. Investigation of the VAPEX process using CT scanning and numerical simulation. J Can Pet Technol 42 (2): doi: 10.2118/03-02-04.
Darvish, M.P., and Firoozabadi, A. 1999. Solution-gas Drive in Heavy Oil Reservoirs. J Can Pet Technol 38 (4): 54–61. doi: 10.2118/99-04-06.
Das, S.K. 1998. VAPEX: an efficient process for the recovery of heavy oil and bitumen. SPE Journal 3 (3): 232–237. doi: 10.2118/50941-PA.
Das, S.K. 2005. Diffusion and dispersion in the simulation of VAPEX process. Paper SPE-97924 presented at the 2005 SPE International Thermal Operation and Heavy Oil symposium, Calgary, Canada, 1−3 November.

Das, S.K. and Butler, R.M. 1994. Effect of aphalentene deposition on Vapex process a preliminary investigation using a Hele-Shaw cell. J Can Pet Technol 33 (6): 39–45.

Das, S.K. and Butler, R.M. 1996. Diffusion coefficients of propane and butane in Peace River bitumen. Can J Chem Eng 74 (6): 985−992.

Das, S.K., Butler, R.M. 1998. Mechanism of the vapour extraction process for heavy oil and bitumen. J Pet Sci Eng 21 (1): 43−59. doi: 0920-4105/98.

Denbina, E.S., Boberg, T.C., and Rottor, M.B. 1991. Evaluation of Key Reservoir Drive Mechanisms in the Early Cycles of Steam Stimulation at Cold Lake SPE Reservoir Engineering 6 (2): 207−211. SPE-16737-PA. doi: 10.2118/16737-PA.

Dong, M., Huang, S., and Hutchence, K. 2006. Methane Pressure-Cycling Process With Horizontal Wells for Thin Heavy-Oil Reservoirs. SPE Reservoir Evaluation & Engineering 9 (2): 154–164. doi: 10.2118/88500-PA.

Dunn, S.G., Nenniger, E.H., and Rajan, V.S.V. 1989. A study of bitumen recovery by gravity drainage using low temperature soluble gas injection. Can J Chem Eng 67 (6): 978-991. doi: 10.1002/cjce.5450670617.

Dusseault, M.B. 2001. Comparing Venezuelan and Canadian Heavy oil and Tar Sands, Presented at the 2nd Canadian International Petroleum Conference, Calgary, Alberta.

Edmunds, N. R. 2007. Effect of Solution Gas on 1D Steam Rise in Oil Sands. J. Can. Pet. Tech., 46(1).

Edmunds, N., 1999. On the difficult birth of SAGD. J Can Pet Technol 38 (1), 14−24.

Edmunds, N.R. and Chhina Harbir. 2001. Economic Optimum. Operating Pressure for SAGD Projects in Alberta. J. Cdn. Pet. Tech. Distinguished Authors Series 40 (12): 14−17.

Etminan, S.R., Maini, B.B., Chen, Z., and Hassanzadeh, H.S.R. 2010. Constant-Pressure Technique for gas diffusivity and solubility measurements in heavy oil and bitumen. Energy & Fuels 24 (1): 533−549. doi: 10.1021/ef9008955.

Fang, W. and Wheeler, T.J. 2012. Method for accelerating start-up for steam-assisted gravity drainage (SAGD) operations. US Patent No. 2012/0227965 A1.

Farouq Ali, A., Abad, B. 1976. Bitumen Recovery from Oil Sands, Using Solvents in Conjunction with Steam. J. Cdn. Pet. Tech. 15(3): 80-90.

Farouq Ali, S.M. 2008. Practical Heavy Oil Recovery. ENCH 647 Lecture Notes, Dept. of Chem. and Pet. Eng., University of Calgary.

Farouq Ali, S.M. and Snyder, S.G., Miscible Thermal Methods Applied to a Two-Dimensional, Vertical Tar Sand Pack, With Restricted Fluid Entry; Journal of Canadian Petroleum Technology, Vol. 12, No. 4, pp. 20−26, October-December 1973.

Farouq Ali, S.M., 2003. Heavy oil - evermore mobile. Journal of Petroleum Science and Engineering, 37 (1–2): 5–9.

Farouq Ali, S.M., 1997. Is there life after SAGD? J. Can. Pet. Technol. 36 (6), 20−24.

Fick, A., Poggendorff's Annalen, 94 (1855) 59-86. (in English) Phil. Mag. 10 (4) 30–39.

Firouz A.Q. and Torabi, F. 2012. Feasibility study of solvent-based huff-n-puff method (Cyclic solvent injection) to enhance heavy oil recovery. Paper SPE 157853 presented at the SPE Heavy Oil Conference Canada, Calgary, Alberta, 12−14 June. doi: 10.2118/157853-MS.

Franenfeld, T.J.W. and Lillico, D.A. 1999. Solvent-assisted method for mobilizing viscous heavy oil. US Patent No. 5,899,274.

Frauenfeld, T., Jossy, C., and Wang, X. 2007. Experimental studies of thermal solvent oil recovery process for live heavy oil. J Can Pet Technol 46 (11): 41−46. doi: 10.2118/07-11-03.

Frauenfeld, T., Jossy, C., Rispler, K., and Kissel, G. 2006. Evaluation of the bottom water reservoir VAPEX process. J Can Pet Technol 45 (9): 29−35. doi: 10.2118/06-09-02.

Frauenfeld, T., Lillico, D., Jossy, C., Vilcsak, G., Rabeeh, S., and Singh, S. 1998. Evaluation of Partially Miscible Processes for Alberta Heavy Oil Reservoirs. J Can Pet Technol 37 (4): 17−24. JCPT 98-04-01. doi: 10.2118/98-04-01.

Frauenfeld, T.W., Deng, X. and Jossy, C., Economic Analysis of Thermal Solvent Processes; paper 2006-164 presented at the Petroleum Society's 7th Canadian International Petroleum Conference (57th Annual Technical Meeting), Calgary, AB, 13−15 June 2006.

Gates, I.D. 2007. Oil phase viscosity behaviour in expanding solvent steam-assisted gravity drainage. J. Pet. Sci. Eng. 59:123−134.

Gates, I.D. and Bunio, G. 2008. In situ process to recover heavy oil and bitumen. US Patent No. 2008/0017372 A1.

Gates, I.D. and Chakrabarty, N. 2008. Design of the Steam and Solvent Injection Strategy in Expanding-Solvent Steam-Assisted Gravity Drainage. J. Can. Pet. Tech. 47(9):12−19.

Gupta, S. and Gittins, S. 2005. Christina Lake Solvent Aided Process Pilot. Paper No. 2005-190, Can. Intl. Pet. Conf., Calgary, Canada, 7−9 June.

Gupta, S., Gittins, S., and Picherack, P. 2005. Field Implementation of Solvent Aided Process. J. Can. Pet. Tech. 44(11): 8−13.

Gupta, S.P. and Greenkorn, R.A. 1974. An Experimental Study of Immiscible Displacement with an Unfavorable Mobility Ratio in Porous Media. Water Resources Res 10 (2): 371−374. 72. Hill, S. 1952. Channeling in Packed Columns. Chem. Eng. Sci. 1(6), 247−253.

Gutek, A.M.H., Harschnitz, B., Myers, R.D., and Okazawa, T. 2003. Combined steam and vapour extraction process (SAVEX) for in situ bitumen and heavy oil production. US Patent No. 6,662,872 B2.

H. Darcy, Les Fontaines Publiques de la Ville de Dijon, Dalmont, Paris, 1856.

Haghighat, P. and Maini, B.B. 2010. Role of asphaltene precipitation in vapex process. J Can Pet Technol 49 (3) 14−21. doi: 10.2118/134244-PA.

Hayduk, W., and Cheng, S.C. 1971. Review of relation between diffusivity and solvent viscosity in dilute liquid solutions. Chem. Eng. Sci., 26 (5): 635–646.

Hayduk, W., Castaneda, R., Bromfield, H., Perras, R.R. 1973. Diffusivities of propane in normal paraffin, Chlorobenzene, and Butanol solvents. AIChE Journal 19 (4), 859–861. doi: 10.1002/aic.690190432.

Hayduk, W., Minhas, B.S. 1982. Correlations for Prediction of molecular diffusivities in liquids. Can. J. Chem. Eng., 60 (2): 295−299. doi: 10.1002/cjce.5450600213.

Hoier, L., Alvestad, J., Lagisquet, A., and Gilje, E. 2013. Solvent and gas injection recovery process. US Patent No. 2013/0025858 A1.

Holm, L.W. and Josendal, V.A. 1974. Mechanisms of oil displacement by carbon dioxide. J. Pet. Tech. 26 (12): 1427–1436. DOI:10.2118/4736-PA.

Huang, W.S. and Chien, S.F. 1986. Method and apparatus for producing viscous hydrocarbons from a subterranean formation. US Patent No. 4,577,691.

Irani, M., Gates, I., 2013. Understanding the convection heat-transfer mechanism in steam-assisted-gravity-drainage process. SPE J. 18 (06), 1202−1216.

Ito, Y., Hirata, T., 1999. Numerical simulation study of a well in the JACOS Hangingstone steam pilot projects near Fortmcmurray. J. Can. Pet. Technol. 38 (13), 29−36.

Ito, Y., Ichikawa, M., and Hirata, T. 2001. The Effect of Gas Injection on Oil Recovery During SAGD Projects J Can Pet Technol 40 (1): 38−43. JPCT-01-01-03. doi: 10.2118/01-01-03.

Ito,Y., Suzuki, S., 1999. Numerical simulation of the SAGD Process in the Hangingstone oil sands reservoir. J. Can. Pet. Technol. 38 (9), 27−35.

Ivory, J, Chang, J, Coates, R, and Forshner, K. 2010. Investigation of cyclic solvent injection process for heavy oil recovery. J Can Pet Technol 49 (9): 22−33. doi: 10.2118/140662-PA.

Jamaloei, B.Y., Dong, M.Z., Mahinpey, N., and Maini, B.B. 2012. Enhanced cyclic solvent process (ECSP) for heavy oil and bitumen recovery in thin reservoirs. Energy & Fuels 26 (5): 2865−2874. doi: 10.1021/ef300152b.

James, L.A., Rezaei, N., and Chatzis, I. 2009. VAPEX, Warm VAPEX and Hybrid VAPEX - The State of Enhanced Oil Recovery for In Situ Heavy Oils in Canada. J Can Pet Technol 47 (4): 1−7. doi: 10.2118/08-04-12-TB.

Javaheri, M. and Abedi, J. 2008. Modeling Mass Transfer Boundary Layer Instability in the CO_2-Based VAPEX Process. J Can Pet Technol 48 (8): 42−48. JPCT-2008-089. doi: 10.2118/09-08-42.

Jensen, E.M., Uhrich, K.D., and Hassan, D.J. 1998. Single well vapor extraction process. US Patent No. 5,771,973.

Jia, X., Jiang, T., Zeng, F., and Gu, Y. 2013. Enhanced vapor extraction through foamy oil flow. Presentated at the SPE Heavy Oil Conference Canada held in Calgary, Alberta, Canada, 11−13 June 2013.

Jia, X., Zeng, F., and Gu, Y. 2014. A New Mathematical Model for the Solvent Chamber Evolution in the Vapour Extraction (VAPEX) Process. Journal of Porous Media, 17 (12): 1093-1108.

Jiang, Q. and Butler, R.M. 1996. Experimental Studies on Effects of Reservoir Heterogeneity on the Vapex Process. J Can Pet Technol 35 (10): 46−54. doi: 10.2118/96-10-04.

Jiang, T., Jia, X., Zeng, F., and Gu, Y. 2013. A novel solvent injection technique for enhanced heavy oil recovery: cyclic production with continuous solvent injection. Paper SPE 165455 presented the SPE Heavy Oil Conference Canada, Calgary, Alberta, 11−13 June. doi: 10.2118/165455-MS.

Jimenez, J., 2008. The field performance of SAGD projects in Canada. Presented at the International Petroleum Technology Conference, Kuala Lumpur, Malaysia.

Kapadia, R.A., Upreti, R.S., Lohi, A., and Chatzis, I. 2006. Determination of gas dispersion in vapor extraction of heavy oil and bitumen. J Pet Sci Eng 51 (3−4): 214–222. doi: 10.1016/j.petrol.2006.01.001.

Karmaker, K. and Maini, B.B., Experimental Investigation of Oil Drainage Rates in the Vapex Process for Heavy Oil and Bitumen Reservoirs; paper SPE 84199 presented at the SPE Annual Technical Conference and Exhibition, Denver, CO, 5-8 October 2003.

Karnaker, K. and Maini, B.B., Applicability of Vapor Extraction Process to Problematic Viscous Oil Reservoirs; paper SPE 84034 presented at the SPE Annual Technical Conference and Exhibition, Denver, CO, 5-8 October 2003.

Knorr, K.D. and Imran, M. 2011. Extension of Das and Butler Semi-analytical Flow Model. J Can Pet Technol 50 (6): 53−60. doi: 10.2118/148944-PA.

Knorr, K.D. and Imran, M. 2012. Solvent-chamber development in 3D-physical-model experiments of solvent-vapor extraction (SVX) processes with various permeabilities and solvent-vapour qualities. J Can Pet Technol 51 (6): 425−436. doi: 10.2118/149190-PA.

Kumar, R. and Mahadevan, J. 2012. Well-Performance Relationships in Heavy-Foamy-Oil Reservoirs. SPE Production & Operation 27 (1): 94−105. doi: 10.2118/117447-PA.

Kumer, A., Jaiswal, D.K., and Kumer, N. 2009. Analytical solutions of one dimensional convection−diffusion equation with variable coefficient in a finite domain. J. Earth Sys. Sci. 118 (5), 539−549. doi: 10.1007/S12040-009-0049-Y.

Leaute, R.P. and Carey, B.S. 2005. Liquid Addition to Steam for Enhancing Recovery (LASER) of Bitumen with CSS: Results from the First Pilot Cycle. Paper Number 2005-161, Can. Intl. Pet. Conf. , Calgary, Canada, 7-9 June.

Lederer, E.L. 1933. Proc. World Pet. Cong. (London) 2, (1933): 526−528.

Lewis, E. and Mohanty, K.K. 2011. Partially miscible VAPEX displacement of a moderately viscous oil. J Pet Sci Eng 77 (1): 104−110. doi: 10.1016/j.petrol.2011.02.008.

Leyva-Gomez, H., and Babadagli, T., 2017. High-Temperature Solvent Injection for Heavy-Oil Recovery from Oil Sands: Determination of Optimal Application Conditions Through Genetic Algorithm. Society of Petroleum Engineers. SPE REE. 20(2): 372-382.

Lim, G.B., Kry, R.P., Harker, B.C., and Jha, K.N. 1995. Cyclic stimulation of Cold Lake oil sand with supercritical ethane. Paper SPE 30298 presented at the International Heavy Oil Symposium, Calgary, Alberta, 19–21 June. doi: 10.2118/30298-MS.

Lim, G.B., Kry, R.P., Harker, B.C., and Jha, K.N. 1996. Three-dimensional scaled physical modeling of solvent vapour extraction of Cold Lake bitumen. J Can Pet Technol 35 (4): 32−40. doi: 10.2118/96-04-03.

Lin L, Zeng F, Gu Y. A circular solvent chamber model for simulating the VAPEX heavy oil recovery process. J Pet Sci Eng 2014;118 :27–39.

Luhning, R.W., Das, S.K., Fisher, L.J., Bakker, J., Grabowski, J., Engleman, J.R., Wong, S., Sullivan, L.A., and Boyle, H.A. 2003. Full Scale VAPEX Process-Climate Change Advantage and Economic Consequences A. J Can Pet Technol 42 (2): 29−34. doi: 10.2118/03-02-02.

Hongze Ma, Gaoming Yu, Yuehui She, Yongan Gu, 2017. A parabolic solvent chamber model for simulating the solvent vapor extraction (VAPEX) heavy oil recovery process, Journal of Petroleum Science and Engineering, 149(2017): 465-475.

Maini, B.B. 1996. Foamy Oil Flow in Heavy Oil Prodution. J Can Pet Technol 35 (6): 21−24. doi: 10.2118/96-06-01.

Maini, B.B. 2001. Foamy oil flow. Journal of Petroleum Technology 53 (10): 54−64. doi: 10.2118/68885-MS.

Maini, B.B., Sharma, H.K., and George, A.E. 1993. Significance of foam-oil behavior in primary production of heavy oils. J Can Pet Technol 32 (9): 50−54.

Mohammadpoor, M. and Torabi, F., 2015. Comprehensive Experimental Study and Numerical Simulation of Vapour Extraction (VAPEX) Process in Heavy Oil Systems. Journal of Canadian Chemical Engineering, 93:1929–1940.

Crank J. Free and moving boundary problems, Oxford: Clarendon Press; 1984.

Joshi M, Pani A, Sabnis S. Industrial mathematics. New Delhi: Narosa Publishing House; 2006.

Mohsen M, Baluch MH. An analytical solution of the diffusion convection equation over a finite domain. Applied Mathematical Modeling 1983;7(4):285–287.

Marino, M.A. 1974. Numerical and analytical solutions of dispersion in a finite, adsorbing porous medium. Journal of the American Water Resources Association. 10 (1): 81−90. doi**:** 10.1111/j.1752-1688.1974.tb00542.x.

McCain Jr., W.D., 1990. The properties of Petroleum Fluids, 2nd edition. PennWell Publishing Company, Tulsa, Oklahama.

McMillen, J.M. 1985. Method of solvent stimulation of heavy oil reservoirs. US Patent No. 4,531,586.

Moghadam, S., Nobakht, M., and Gu, Y. 2008. Theoretical and physical modeling of a solvent vapour extraction (VAPEX) process for heavy oil recovery. J Pet Sci Eng 69 (2009), 93−104. doi: 10.1016/j.petrol.2008.12.029.

Mokrys, I.J. 2001. Vapor extraction of hydrocarbon deposits. US Patent No. 6,318,464 B1.

Mokrys, I.J. and Butler, R.M. 1993. The rise of interfering solvent chambers: solvent analog model of steam-assisted gravity drainage. J Can Pet Technol 32 (3): 26−36. doi: 10.2118/93-03-02.

Moore, R.G., Laureshen, C.J., Belgrave, J.D.M., Ursenbach, M.G., Mehta, S.A., 1995. In-situ combustion in Canadian heavy oil reservoirs. Fuel 74 (8): 1169−1175.

Muller, K.E. 2001. Computing the confluent hypergeometric function, M(a, b, x). Numerical Mathematics 90 (1): 179–196. doi: 10.1007/s0022110100285.

Naar, J. and Wygal, R.J. 1961. Three-phase Imbibition Relative Permeability. Trans. AIME 222: 254−258.

Naar, J., Wygal, R. J., and Henderson, J. H. 1962. Imbibition Relative Permeability in Unconsolidated Porous Media. SPE Journal 2(1):13−17.

Nasr T.N. and Isaacs, E.E. 2001. Process for enhancing hydrocarbon mobility using a steam additive. US Patent No. 6,230,814 B1.

Nasr, T.N. and Isaacs, E. 2004. Process for enhancing HC on mobility using a steam additive Canadian Patent No. 2,323,029.

Nasr, T.N., Beaulieu, G., Golbeck, H., and Heck, G. 2003. Novel Expanding Solvent SAGD process (ES-SAGD), J. Can. Pet. Tech. 42(1):13−16.

Nenniger, E.H. 1979. Hydrocarbon recovery. Canadian Patent No. 1,059,432.

Nenniger, J. 2007. Method and apparattus for heavy oil production. Canadian Patent No. 2235085.

Nenniger, J. and Dunn, S. 2010. Situ extraction process for the recovery of hydrocarbons. US Patent No. 2010/0236783 A1.

Nenniger, J. and Nenniger, E. 2005. Method and apparatus for stimulating heavy oil production. US Patent No. 6,883,607 B2.

Nenniger, J.E. and Dunn, S.G. 2008. How fast is solvent based gravity drainage? Paper

PETSOC 2008-139 accepted for the Proceedings of the Canadian International Petroleum/SPE Gas Technology Symposium 2008 Joint Conference (Petroleum Society's 59th Annual Technical Meeting), Calgary, Alberta, 17−19 June. doi: 10.2118/2008-139.

Nghiem, L.X., Kohse, B.F., and Sammon, P.H. 2001. Compositional Simulation of the VAPEX Process. J Can Pet Technol 40 (8). 54−61. JCPT-01-08-05. doi: 10.2118/01-08-05.

Nukhaev, M., Pimenov, V., Shandrygin, A., Tertychnyi, V.V., 2006. A new analytical model for the SAGD production phase. Presented at the SPE Annual Technical Conference and Exhibition, San Antonio, Texas.

Ostos, A.N. and Maini, B.B. 2005. An Integrated Experimental Study of Foamy Oil Flow during Solution Gas Drive. J Can Pet Technol 44 (4): 43−50. doi: 10.2118/05-04-05.

Palmgren C., and Edmunds, N. 1995. High Temperature Naptha to Replace Steam in the SAGD Process. Paper SPE-30294-MS presented at the International Heavy Oil Symposium held in Calgary, Canada, 19−21 June 1995.

Rahnema, H., Kharrat, R. and Tostami, B. 2008. Experimental and numerical study of vapor extraction process (VAPEX) in heavy oil fractured reservoir. Petroleum Society Paper 2008-116 presented at Canadian International Petroleum Conference, Calgary, Alberta, June 17−19.

Rathmell, J.J., Stalkup, F.I., and hassinger, R.C. 1971. A laboratory investigation of miscible displacement by carbon dioxide. Paper SPE 3483 presented at Fall Meeting of the Society of Petroleum Engineers of AIME, 3−6 October 1971, New Orleans, Louisiana. doi: 10.2118/3483-MS.

Redford, D.A. and Luhning, R.W. 1999. In Situ Recovery from the Athabasca Oil Sands-Past Experience and Future Potential, Part II. J Can Pet Technol 38 (13): 1−13. doi: 10.2118/99-13-41.

Reis, J.C., 1992. A steam-assisted gravity drainage model for tar sands: linear geometry. J. Can. Pet. Technol. 31 (10), 14−20.

Richardson, W.C. and Kibodeaux, K.R. 2001. Chemically assisted thermal flood process. US Patent No. 6,305,472 B2.

Sayegh, S. and Maini, B.B. 1984. Laboratory evaluation of the CO_2 huff-n-puff process for heavy oil reservoirs. J. Can. Pet. Technol. **23** (3): 29−36.

Schmidt, T. 1989. Mass transfer by diffusion, in: AOSTRA Technical Handbook on Oil Sands, Bitumens and Heavy Oils, AOSTRA, Edmonton, Alberta.

Scott, A.S. and Jirka, G.H. 2002. Environmental fluid mechanisms part I: Mass transfer and diffusion. Karlsruhe, Germany.

Sharma, J. and Gates, I.D. 2010b. Steam Solvent Coupling at the Chamber Edge in an In Situ Bitumen Recovery Process. Proceedings of SPE Oil & Gas India Conference, Mumbai, India, 20−22 January.

Sharma, J. and Gates, I.D. 2011a. Convection at the Edge of a Steam-Assisted Gravity Drainage Steam Chamber. Paper SPE-142432-PA SPE Journal (in press).

Sharma, J. and Gates, I.D. 2011b. Interfacial Stability of In-Situ Bitumen Thermal Solvent Recovery Processes. SPE Journal 16(1): 55−64. SPE-130050-PA.

Sharma, J., Gates, I.D., 2010. Multiphase flow at the edge of a steam chamber. Can. J. Chem. Eng. 88 (3), 312−321.

Sharma, J., Gates, I.D., 2011. Convection at the edge of a steam-assisted-gravity-drainage steam chamber. SPE J. 16 (3), 503−512.

Shelton, J.L. and Morris, E.E. 1973. Cyclic Injection of Rich Gas into Producing Wells to Increase Rates from Viscous-Oil Reservoirs. Journal of Petroleum Technology 25 (8): 890−896. doi: 10.2118/4375-PA.

Shu, W.R. 1984. A viscosity correlation for mixtures of heavy oil, bitumen, and petroleum fractions. SPE Journal 24 (3): 227−282. doi: 10.2118/11280-PA.

Singhal, A.K., Das, S.K., Leggitt, S.M., Kasraie, M., and Ito, Y. 1997. Steam-Assisted Gravity Drainage and VAPEX Process Reservoir Screening. Journal of Petroleum Technology 1997: 1122−1124.

Smith, G.E. 1988. Fluid flow and sand production in heavy oil reservoirs under solution gas drive. SPE Production Engineering 3 (2): 169−180. doi: 10.2118/15094-PA.

Speight, J.G., 1990. Fuel science and technology handbook, Marcel Dekker, New York.

Sposito, G. and Weeks, S.W. 1998. Tracer convection by steady groundwater flow in a stratified aquifer. Water Resources Research 34 (5): 1051−1059.

Stalkup, I.F. 1978. Carbon dioxide miscible flooding: Past, present, and outlook for the future, Journal of Petroleum Technology 30(8): 1102-1112. doi: 10.2118/7042-PA

Stefan, J., 1891. Uber die theorie der eisbildung imbesondee uber die eisbindung im polarmeere, Ann. Phys. U. Chem. 42 (1891), 269−286.

Stehfest, H. 1970. Numerical inversion of Laplace transformation. Communications of the ACM 13 (1): 47−49.

Talbi K., Maini B.B., 2003. Evaluation of CO2-based VAPEX process for the recovery of bitumen from tar sand reservoirs. paper SPE-84868 presented at the International Improved Oil Recovery Conference in Asia Pacific, SPE 84868, Lumpur, Malaysia.

Soheil Talebi, Ali Abedini, Pushan Lele, Adriana Guerrero, David Sinton, 2017. Microfluidics-based measurement of solubility and diffusion coefficient of propane in bitumen, Fuel, 210 (2017): 23-31.

Tharanivasan, A.K. 2004. Measurements of Molecular Diffusion Coefficients of Carbon Dioxide, Methane and Propane in Heavy Oil Under Reservoir Conditions, Master Thesis, University of Regina, Regina, Saskatchewan (December 2004).

Tharanivasan, A.K., Yang, C., and Gu, Y. 2006. Measurements of Molecular Diffusion Coefficients of Carbon Dioxide, Methane and Propane in Heavy Oil under Reservoir Conditions. Energy & Fuels 20 (6): 2509−2517. Doi: 10.1021/ef060080d.Etminan,

Upreti, S.R. and Mehrotra, A.K. 2000. Experimental Measurement of Gas Diffusivity in Bitumen Results for Carbon Dioxide. Ind. Eng. Chem. Res. 39 (4): 1080−1087. doi: 10/1021/ie990635a.

Upreti, S.R. and Mehrotra, A.K. 2002. Diffusivity of CO2, CH4, C2H6 and N2 in Athabasca bitumen. Canadian Journal of Chemical Engineering 80: 116−125.

Upreti, S.R., Lohi, A., Kapadia, R.A., and El-Haj, R. 2007. Vapour extraction of heavy oil and bitumen: a review. Energy & Fuels 21 (3): 562−1574. doi: 10.1021/ef060341j.

Vittoratos, E., Scott, G.R., Beattie, C.I., 1990. Cold Lake cyclic steam stimulation: a multi-well process. SPE Res. Eng. 5 (1): 19−24.

Vogel, J.V. 1987. Gravity stabilized thermal miscible displacement process. US Patent No. 4,697,642.

Wheeler, M.F. and Dawson, C.N. 1992. An operator-splitting method for convection–diffusion–reaction problems. London: Academic Press.

Wong, Kenny and Hall, W.L. 1982. Viscous oil recovery method. US Patent No. 4,324,291.

Wong, R.C.K. 2003. Sand Production in Oil Sand under Heavy Oil Foamy Flow. J Can Pet Technol 42 (3): 56−61. doi: 10.2118/03-03-06.

Wu, X., Polokar, M., and Cunha, L.B. 2005. A numerical approach to simulate and design VAPEX experiments. Paper 2005-180 presented at the Petroleum Society 6th Canadian International Petroleum Conference, Calgary, Canada, June 7–9.

Xu, S., Zeng, F., Gu, Y., and Knorr, K.D. 2012. Upscaling study of Vapour Extraction through Numerical Study. Transp Porous Med 95 (3): 697−715. doi: 10.1007/s11242-012-0069-y.

Yang, C. and Gu, Y. 2006. Diffusion coefficients and oil swelling factors of carbon dioxide, methane, ethane, propane, and their mixtures in heavy oil. Fluid Phase Equilibria 243 (2006): 64−73.

Yazdani, A. and Maini, B.B. 2005. Effect of drainage height and grain size on production rates in the Vapex process: Experimental study. SPE Reservoir Evaluation & Engineering 8 (3): 205−213. doi: 10.2118/89409-PA.

Yazdani, A. and Maini, B.B. 2008. Modeling of the Vapex process in a very large physical model. Energy & Fuels 22 (1): 535−544. doi: 10.1021/ef700429h.

Yazdani, A. and Maini, B.B. 2009. Pitfalls and solutions in numerical simulation of Vapex experiments. Energy & Fuels 23 (8): 3981–3988. doi: 10.1021/ef900200f.

Zeng, F., Knorr, K.D., and Wilton, R.R. 2008a. Enhancing oil rate in solvent vapour extraction processes through Tee-well pattern. Paper SPE-117528 presented at the 2008 SPE International Thermal Operations, Calgary, Canada, 20−23, October.

Zhang, H., Luo, P., and Gu, Y. 2006. Physical modeling of heavy oil production rate in a vapour extraction process. Paper PETSOC 2006-142 presented at the Petroleum Society's 7th Canadian International Petroleum Conference (57th Annual Technical Meeting), Calgary, Alberta, 13−15 June. doi: 10.2118/2006-142.

Zhao, L. 2007. Steam Alternating Solvent Process. SPE Res Eval & Eng 10 (2): 185-190. SPE-86957-PA.

Zhao, L., Nasr, T.N., Huang, H., Beaulieu, G., Heck, G., and Golbeck, H. 2005. Steam alternating solvent process lab test and simulation. 44 (9): 37−43. doi: 10.2118/05-09-04.

Zill, D.G. 2001. A first course in differential equations with modeling applications. Pacific Grove: Brooks/Cole Pub Co.

APPENDIX

Simulation .dat file of a SAVE process.

```
RESULTS SIMULATOR STARS 201401

INUNIT SI
WSRF WELL 1
WSRF GRID TIME
WSRF SECTOR TIME
OUTSRF GRID FLUXRC FLUXSC PRES SG SO SW TEMP VELOCRC VELOCSC
OUTSRF WELL LAYER NONE
WPRN GRID 0
OUTPRN GRID NONE
OUTPRN RES NONE
**  Distance units: m
RESULTS XOFFSET           0.0000
RESULTS YOFFSET           0.0000
RESULTS ROTATION           0.0000  **  (DEGREES)
RESULTS AXES-DIRECTIONS 1.0 -1.0 1.0
**
**********************************************************************
****
** Definition of fundamental cartesian grid
**
**********************************************************************
****
GRID VARI 50 1 20
KDIR DOWN
DI IVAR
 50*0.5
DJ JVAR
 1
DK ALL
 1000*0.5
DTOP
 50*500
```

```
VATYPE CON            1
*MOD
  1:1 1:1 1:20   = 2
VAMOD 2 0.5 1 0.5 0.5
PERMI CON         5000
**  0 = null block, 1 = active block
NULL CON            1
POR CON         0.35
**  0 = pinched block, 1 = active block
PINCHOUTARRAY CON            1
PERMJ EQUALSI
PERMK EQUALSI * 0.5
END-GRID
ROCKTYPE 1
PRPOR 101
CPOR 1e-6


**********************************************************************
*********
** THE FOLLOWING KEYWORDS CAN BE USED IN THE INITIALIZATION SECTION IN
STARS
**********************************************************************
*********
** MFRAC_OIL 'C3H8' CON  7.8912E-02
** MFRAC_OIL 'C12toC24' CON  3.7206E-01
** MFRAC_OIL 'C25toC45' CON  2.5502E-01
** MFRAC_OIL 'C46+' CON  2.9401E-01
**********************************************************************
*********
** THE FOLLOWING SECTION CAN BE USED FOR THE COMPONENT PROPERTY INPUT
INTO STARS
**********************************************************************
*********
** PVT UNITS CONSISTENT WITH *INUNIT *SI
** Model and number of components
MODEL 5 5 5 1
COMPNAME 'WATER' 'C3H8' 'C12toC24' 'C25toC45' 'C46+'
**            --------   --------   --------   --------   --------
CMM
0 0.0441 0.2467 0.4191 0.6808
PCRIT
0 4245.52 1641.17 1019.89 714.8
TCRIT
0.00 96.65 481.41 608.34 874.62
** low/high pressure; low/high temperature
KVTABLIM 100 3100 23.9 223.9
**   73.900                                          <extrap.>
**  123.900
**  173.900
**  223.900
** Gas-liquid K Value tables
KVTABLE 'C3H8'
**
       12.798    1.7163   0.97283    1.3271
       30.202    3.0215    1.7128    1.7128
       54.023    5.3193    3.0158    2.2107
       80.765    7.8189    4.3595    3.1417
       106.71    10.197    5.6145    3.9948
**   73.900                                          <extrap.>
**  123.900
**  173.900
**  223.900
```

```
** Gas-liquid K Value tables
KVTABLE 'C12toC24'
**
     1.0253e-006  1.4619e-006  4.9628e-006  2.9826e-006
     9.3577e-005  2.5236e-005   5.036e-005   5.036e-005
       0.0022806   0.00043565   0.00051102   0.00085031
        0.023723    0.0036719    0.0033341    0.0039934
         0.13869     0.018742     0.014658     0.014872
**   73.900                                       <extrap.>
**  123.900
**  173.900
**  223.900
** Gas-liquid K Value tables
KVTABLE 'C25toC45'
**
     2.9549e-012  3.1846e-011    5.27e-010  1.5788e-010
     4.9803e-009  3.2388e-009  1.9522e-008  1.9522e-008
      9.672e-007  3.2939e-007  7.2316e-007  2.4138e-006
     4.6623e-005  1.0826e-005  1.4915e-005  2.7442e-005
      0.00087697   0.00015962   0.00016816   0.00022988
**   73.900                                       <extrap.>
**  123.900
**  173.900
**  223.900
** Comparison of WinProp (W) and STARS K-value (S) phase split
calculations
** A = Aqueous, L = Liquid, V = Vapor
**                 Pressure,    kPa
** T, deg C    1.0000E+02  1.1000E+03  2.1000E+03  3.1000E+03
**   23.900   <W: LV,S: LV><W: L ,S: L ><W: L ,S: L ><W: L ,S: L >
**   73.900   <W: LV,S: LV><W: L ,S: L ><W: L ,S: L ><W: L ,S: L >
**  123.900   <W: LV,S: LV><W: LV,S: LV><W: L ,S: L ><W: L ,S: L >
**  173.900   <W: LV,S: LV><W: LV,S: LV><W: L ,S: L ><W: L ,S: L >
**  223.900   <W: LV,S: LV><W: LV,S: LV><W: LV,S: LV><W: L ,S: L >
** Gas-liquid K Value tables
KVTABLE 'C46+'
**
          1e-016       1e-016       1e-016       1e-016
          1e-016       1e-016       1e-016       1e-016
     2.0372e-014   2.289e-014  1.8508e-013  2.6587e-012
     2.1599e-011  1.1723e-011   3.888e-011  1.7785e-010
     4.4899e-009  1.5422e-009  3.0773e-009  8.0057e-009
** reference pressure,     corresponding to the density
PRSR 101
** reference temperature,  corresponding to the density
TEMR 23.9
** pressure at surface,    for reporting well rates, etc.
PSURF 101.325
** temperature at surface, for reporting well rates, etc.
TSURF 15.556
** Surface conditions
SURFLASH KVALUE
MOLDEN
0 7404 3442 2172 1648
CP
0 1.714e-006 6.632e-007 4.65e-007 3.349e-007
CT1
0 1.585e-005 -2.787e-005 -1.808e-005 4.206e-005
CT2
0 3.295e-006 1.498e-006 9.997e-007 5.03e-007
CPT
0 -4.966e-008 2.145e-011 8.232e-011 4.231e-011
** T, deg C        'WATER'      'C3H8'  'C12toC24'  'C25toC45'
'C46+'
```

```
**              --------    --------    --------    --------    ------
--
VISCTABLE
  *ATPRES 100
**       temp
          23.9         0  0.027871    6.6767    742.49  1.5462e+010
          73.9         0  0.057351    1.8284    36.813  2.3424e+006
         123.9         0  0.092412   0.88557    6.6257        13235
         173.9         0   0.12774   0.56848    2.3481       525.94
         223.9         0   0.15871   0.42194    1.2206       64.579
  *ATPRES 1100
**       temp
          23.9         0  0.057288     6.434    731.59  1.5609e+010
          73.9         0  0.057732    1.8778    38.701  2.5539e+006
         123.9         0  0.092992   0.90998    6.9536        14549
         173.9         0   0.12896   0.58488    2.4612          579
         223.9         0   0.16099   0.43566    1.2826       70.948
  *ATPRES 2100
**       temp
          23.9         0  0.058409    6.5815    764.82  1.6717e+010
          73.9         0  0.057376    1.9277     40.64  2.7796e+006
         123.9         0  0.092178   0.93469    7.2894        15954
         173.9         0   0.12833   0.60144    2.5762       635.45
         223.9         0   0.16159   0.44931    1.3447       77.661
  *ATPRES 3100
**       temp
          23.9         0  0.059496    6.7306    798.89  1.7888e+010
          73.9         0  0.042264    2.0296    43.733  3.0982e+006
         123.9         0  0.091486    0.9597    7.6317        17443
         173.9         0   0.12785   0.61824    2.6931       694.95
         223.9         0   0.16228   0.46309    1.4073       84.685

** The following is the complete WinProp fluid model description.

WINPROP *TITLE1     'Dead Oil Characterization'
WINPROP *TITLE2     ' '
WINPROP *TITLE3     ' '
WINPROP *INUNIT *SI
WINPROP *MODEL   *PR   *1978
WINPROP *NC        4      4
WINPROP *TRANSLATION 1
WINPROP *PVC3  9.2718124E-01
WINPROP *COMPNAME
WINPROP 'C3H8    ' 'C12toC24' 'C25toC45' 'C46+    '
WINPROP *HCFLAG
WINPROP   1  1  1  1
WINPROP *SG
WINPROP   5.0700000E-01  8.5590689E-01  9.1340605E-01  1.1155793E+00
WINPROP *TB
WINPROP  -4.2050000E+01  3.0876467E+02  4.5627503E+02  7.2356778E+02
WINPROP *PCRIT
WINPROP   4.1900000E+01  1.6197082E+01  1.0065497E+01  7.0545602E+00
WINPROP *VCRIT
WINPROP   2.0300000E-01  8.7276644E-01  1.4212364E+00  2.2557379E+00
WINPROP *TCRIT
WINPROP   3.6980000E+02  7.5456150E+02  8.8149188E+02  1.1477722E+03
WINPROP *AC
WINPROP   1.5200000E-01  7.3173783E-01  1.0909793E+00  1.4299325E+00
WINPROP *MW
WINPROP   4.4097000E+01  2.4665974E+02  4.1912816E+02  6.8083571E+02
WINPROP *VSHIFT
WINPROP  -9.9969361E-01  9.2877655E-02  2.1624836E-01  4.3726852E-01
WINPROP *VSHIF1
WINPROP   0.0000000E+00 -3.2838006E-04 -2.9184987E-04 -1.7951633E-04
```

```
WINPROP *TREFVS
WINPROP   1.5556000E+01  1.5555560E+01  1.5555560E+01  1.5555560E+01
WINPROP *ZRA
WINPROP   2.7630000E-01  2.5133403E-01  2.3387185E-01  2.0068501E-01
WINPROP *VISVC
WINPROP   2.0300000E-01  8.7755143E-01  1.4253402E+00  2.2557379E+00
WINPROP *VISCOR *MODPEDERSEN
WINPROP *VISCOEFF
WINPROP   1.0432000E-04  2.2237278E+00  8.8536000E-03  2.2163000E+00
4.4191650E-01
WINPROP *OMEGA
WINPROP   4.5723553E-01  4.5723553E-01  4.5723553E-01  4.5723553E-01
WINPROP *OMEGB
WINPROP   7.7796074E-02  7.7796074E-02  7.7796074E-02  7.7796074E-02
WINPROP *PCHOR
WINPROP   1.5030000E+02  6.4624575E+02  9.4846676E+02  1.1679174E+03
WINPROP *HREFCOR *HARVEY
WINPROP *IGHCOEF
WINPROP   6.8715000E-01  1.6030400E-01  1.2608400E-04  1.8143000E-07 -
9.1891300E-11  1.3548500E-14  2.6090300E-01
WINPROP   0.0000000E+00 -3.3271753E-02  4.1307829E-04 -6.0883574E-08
0.0000000E+00  0.0000000E+00  0.0000000E+00
WINPROP   0.0000000E+00 -1.9514732E-02  4.0156210E-04 -5.7411291E-08
0.0000000E+00  0.0000000E+00  0.0000000E+00
WINPROP   0.0000000E+00 -2.3702321E-02  3.5009525E-04 -5.1369391E-08
0.0000000E+00  0.0000000E+00  0.0000000E+00
WINPROP *HEATING_VALUES
WINPROP   2.1051600E+03  0.0000000E+00  0.0000000E+00  0.0000000E+00
WINPROP *COMPOSITION *PRIMARY
WINPROP   0.0000000E+00  4.0393012E-01  2.7686997E-01  3.1919991E-01
WINPROP *COMPOSITION *SECOND
WINPROP   1.0000000E+00  0.0000000E+00  0.0000000E+00  0.0000000E+00
ROCKFLUID
RPT 1 WATWET
**        Sw         krw       krow
SWT
          0.1           0      0.948
         0.15  0.00037325  0.8706085
          0.2    0.005068   0.691624
         0.25  0.01498125  0.5332125
          0.3    0.030113   0.395374
         0.35  0.05046325  0.2781085
          0.4    0.076032   0.181416
         0.45  0.10681925  0.1052965
          0.5    0.142825    0.04975
         0.55  0.18404925  0.0147765
          0.6    0.230492      0.008
         0.65  0.28215325      0.006
          0.7    0.339033      0.005
         0.75  0.40113125      0.004
          0.8    0.468448      0.003
         0.85  0.54098325      0.002
          0.9    0.618737      0.001
         0.95  0.70170925          0
            1      0.7899          0
**        Sl         krg       krog
SLT
          0.1    0.214753          0
         0.15  0.19025175          0
          0.2    0.167232     0.0002
         0.25  0.14569375     0.0004
          0.3    0.125637     0.0006
         0.35  0.10706175  0.0008655
          0.4    0.089968   0.010368
```

```
          0.45  0.07435575  0.0304295
           0.5    0.060225    0.06105
          0.55  0.04757575  0.1022295
           0.6    0.036408   0.153968
          0.65  0.02672175  0.2162655
           0.7    0.018517   0.289122
          0.75  0.01179375  0.3725375
           0.8    0.006552   0.466512
          0.85  0.00279175  0.5710455
           0.9    0.000513   0.686138
          0.95      0.0003  0.8117895
             1           0      0.948
INITIAL
VERTICAL OFF

INITREGION 1
PRES CON          650
TEMP CON         23.9
SW CON         0.10
MFRAC_OIL 'C46+' CON       0.3192
MFRAC_OIL 'C25toC45' CON      0.27687
MFRAC_OIL 'C12toC24' CON      0.40393
NUMERICAL
CONVERGE TOTRES TIGHTER
DTMAX 2
NORTH 200
ITERMAX 200


RUN
DATE 2014 1 1
DTWELL 0.0001

**
WELL  'injector'  FRAC  0.5
INJECTOR MOBWEIGHT IMPLICIT 'injector'
INCOMP  WATER  1.0  0.0  0.0  0.0  0.0
TINJW  212.0
QUAL  0.9
OPERATE  MAX  BHP  2000.0  CONT
OPERATE  MAX  STW  2.0  CONT
** UBA     ff   Status  Connection
**          rad  geofac  wfrac  skin
GEOMETRY  K  0.086  0.249  1.0  0.0
PERF  GEOA  'injector'
** UBA      ff   Status  Connection
    1 1 13  1.0  OPEN    FLOW-FROM  'SURFACE'

**
WELL  'producer'  FRAC  0.5
PRODUCER 'producer'
OPERATE  MIN  BHP  1500.0  CONT
OPERATE  MAX  STW  0.5  CONT
**          rad  geofac  wfrac  skin
GEOMETRY  K  0.086  0.249  1.0  0.0
PERF  GEOA  'producer'
** UBA      ff   Status  Connection
    1 1 20  1.0  OPEN    FLOW-TO  'SURFACE'


HTWELL 'injector'
   HTWTEMP 250
HTWELL 'producer'
   HTWTEMP 250
```

```
DATE 2014 1  2.00000
DATE 2014 1  3.00000
DATE 2014 1  4.00000
DATE 2014 1 16.00000
DATE 2014 1 17.00000
HTWELL 'injector' OFF
HTWELL 'producer' OFF
SHUTIN 'injector'
SHUTIN 'producer'
DATE 2014 1 18.00000
DATE 2014 1 19.00000
DATE 2014 1 20.00000
DATE 2014 1 21.00000
INJECTOR MOBWEIGHT IMPLICIT 'injector'
INCOMP  GAS  0.0  1.0  0.0  0.0  0.0
TINJW  24.0
OPERATE  MAX  BHP  1000.0  CONT
OPERATE  MAX  STG  50.0  CONT
OPEN 'injector'
PRODUCER 'producer'
OPERATE  MIN  BHP  950.0  CONT
OPERATE  MAX  STG  0.5  CONT
OPEN 'producer'
DATE 2014 1 22.00000
DATE 2014 2 10.00000
**----------------------------------------cycle - 1
INJECTOR MOBWEIGHT IMPLICIT 'injector'
INCOMP  WATER  1.0  0.0  0.0  0.0  0.0
TINJW  212.0
QUAL  0.9
OPERATE  MAX  BHP  2000.0  CONT
OPERATE  MAX  STW  2.0  CONT
SHUTIN 'producer'
DATE 2014 2 11.00000
DATE 2014 2 12.00000
SHUTIN 'injector'
DATE 2014 2 13.00000
DATE 2014 2 14.00000
PRODUCER 'producer'
OPERATE  MAX  STW  0.5  CONT
DATE 2014 2 15.00000
DATE 2014 2 16.00000
INJECTOR MOBWEIGHT IMPLICIT 'injector'
INCOMP  GAS  0.0  1.0  0.0  0.0  0.0
TINJW  24.0
OPERATE  MAX  BHP  1000.0  CONT
OPERATE  MAX  STG  50.0  CONT
OPEN 'injector'
PRODUCER 'producer'
OPERATE  MIN  BHP  950.0  CONT
OPERATE  MAX  STG  0.5  CONT
OPEN 'producer'
DATE 2014 2 17.00000
DATE 2014 2 18.00000
DATE 2014 2 19.00000
DATE 2014 2 20.00000
DATE 2014 2 25.00000
DATE 2014 3  1.00000
DATE 2014 3  5.00000
DATE 2014 3 10.00000
DATE 2014 3 15.00000
DATE 2014 3 20.00000
**----------------------------------------cycle - 2
```

```
INJECTOR MOBWEIGHT IMPLICIT 'injector'
INCOMP  WATER  1.0  0.0  0.0  0.0  0.0
TINJW  212.0
QUAL  0.9
OPERATE  MAX  BHP  2000.0  CONT
OPERATE  MAX  STW  2.0  CONT
SHUTIN 'producer'
DATE 2014 3 21.00000
DATE 2014 3 22.00000
DATE 2014 3 23.00000
SHUTIN 'injector'
DATE 2014 3 24.00000
DATE 2014 3 25.00000
DATE 2014 3 26.00000
PRODUCER 'producer'
OPERATE  MIN  BHP  850.0  CONT
OPERATE  MAX  STG  2  CONT
OPERATE  MAX  STW  1  CONT
OPEN 'producer'
DATE 2014 3 27.00000
DATE 2014 4  8.00000
DATE 2014 4  9.00000
DATE 2014 4 10.00000
INJECTOR MOBWEIGHT IMPLICIT 'injector'
INCOMP  GAS  0.0  1.0  0.0  0.0  0.0
TINJW  24.0
OPERATE  MAX  BHP  1000.0  CONT
OPERATE  MAX  STG  50.0  CONT
OPEN 'injector'
PRODUCER 'producer'
OPERATE  MIN  BHP  950.0  CONT
OPERATE  MAX  STG  1  CONT
OPEN 'producer'
DATE 2014 4 11.00000
DATE 2014 4 12.00000
DATE 2014 5 20.00000
DATE 2014 5 25.00000
DATE 2014 5 30.00000
**---------------------------------------cycle - 3
INJECTOR MOBWEIGHT IMPLICIT 'injector'
INCOMP  WATER  1.0  0.0  0.0  0.0  0.0
TINJW  212.0
QUAL  0.9
OPERATE  MAX  BHP  2000.0  CONT
OPERATE  MAX  STW  2.0  CONT
SHUTIN 'producer'
DATE 2014 6  1.00000
DATE 2014 6  2.00000
DATE 2014 6  3.00000
DATE 2014 6  4.00000
SHUTIN 'injector'
DATE 2014 6  5.00000
DATE 2014 6  6.00000
PRODUCER 'producer'
OPERATE  MIN  BHP  800.0  CONT
OPERATE  MAX  STG  4  CONT
OPERATE  MAX  STW  2  CONT
OPEN 'producer'
DATE 2014 6  7.00000
DATE 2014 6  8.00000
DATE 2014 6  9.00000
DATE 2014 6 10.00000
DATE 2014 6 15.00000
DATE 2014 6 20.00000
```

```
DATE 2014 6 25.00000
DATE 2014 6 30.00000
INJECTOR MOBWEIGHT IMPLICIT 'injector'
INCOMP  GAS  0.0  1.0  0.0  0.0  0.0
TINJW  24.0
OPERATE  MAX  BHP  1000.0  CONT
OPERATE  MAX  STG  50.0  CONT
OPEN 'injector'
PRODUCER 'producer'
OPERATE  MIN  BHP  950.0  CONT
OPERATE  MAX  STG  1  CONT
OPEN 'producer'
DATE 2014 7  1.00000
DATE 2014 7 30.00000
DATE 2014 8 30.00000

**---------------------------------------cycle - 4
INJECTOR MOBWEIGHT IMPLICIT 'injector'
INCOMP  WATER  1.0  0.0  0.0  0.0  0.0
TINJW  212.0
QUAL  0.9
OPERATE  MAX  BHP  2000.0  CONT
OPERATE  MAX  STW  2.0  CONT
SHUTIN 'producer'
DATE 2014 9  1.00000
DATE 2014 9  2.00000
DATE 2014 9  3.00000
DATE 2014 9  4.00000
SHUTIN 'injector'
DATE 2014 9  5.00000
DATE 2014 9  6.00000
PRODUCER 'producer'
OPERATE  MIN  BHP  800.0  CONT
OPERATE  MAX  STG  4  CONT
OPERATE  MAX  STW  2  CONT
OPEN 'producer'
DATE 2014 9  7.00000
DATE 2014 9  8.00000
DATE 2014 9  9.00000
DATE 2014 9 10.00000
DATE 2014 9 30.00000
DATE 2014 10  1.00000
DATE 2014 10  2.00000
DATE 2014 10  3.00000
DATE 2014 10  4.00000
DATE 2014 10  5.00000
INJECTOR MOBWEIGHT IMPLICIT 'injector'
INCOMP  GAS  0.0  1.0  0.0  0.0  0.0
TINJW  24.0
OPERATE  MAX  BHP  1000.0  CONT
OPERATE  MAX  STG  50.0  CONT
OPEN 'injector'
PRODUCER 'producer'
OPERATE  MIN  BHP  950.0  CONT
OPERATE  MAX  STG  1  CONT
OPEN 'producer'
DATE 2014 10  6.00000
DATE 2014 10  7.00000
DATE 2014 10  8.00000
DATE 2014 10  9.00000
DATE 2014 10 10.00000
DATE 2014 10 30.00000
DATE 2014 11 30.00000
DATE 2014 12 15.00000
```

```
**----------------------------------------cycle - 5
INJECTOR MOBWEIGHT IMPLICIT 'injector'
INCOMP  WATER  1.0  0.0  0.0  0.0  0.0
TINJW  212.0
QUAL  0.9
OPERATE  MAX  BHP  2000.0  CONT
OPERATE  MAX  STW  2.0  CONT
SHUTIN 'producer'
DATE 2014 12 16.00000
DATE 2014 12 17.00000
DATE 2014 12 18.00000
DATE 2014 12 19.00000
SHUTIN 'injector'
DATE 2014 12 20.00000
DATE 2014 12 21.00000
PRODUCER 'producer'
OPERATE  MIN  BHP  800.0  CONT
OPERATE  MAX  STG  4  CONT
OPERATE  MAX  STW  2  CONT
OPEN 'producer'
DATE 2014 12 22.00000
DATE 2014 12 30.00000
DATE 2015 1 20.00000
INJECTOR MOBWEIGHT IMPLICIT 'injector'
INCOMP  GAS  0.0  1.0  0.0  0.0  0.0
TINJW  24.0
OPERATE  MAX  BHP  1000.0  CONT
OPERATE  MAX  STG  50.0  CONT
OPEN 'injector'
PRODUCER 'producer'
OPERATE  MIN  BHP  950.0  CONT
OPERATE  MAX  STG  2  CONT
OPEN 'producer'
DATE 2015 1 21.00000
DATE 2015 1 30.00000
DATE 2015 2 28.00000
DATE 2015 3 31.00000
**----------------------------------------cycle - 6
INJECTOR MOBWEIGHT IMPLICIT 'injector'
INCOMP  WATER  1.0  0.0  0.0  0.0  0.0
TINJW  212.0
QUAL  0.9
OPERATE  MAX  BHP  2000.0  CONT
OPERATE  MAX  STW  2.0  CONT
SHUTIN 'producer'
DATE 2015 4  1.00000
DATE 2015 4  2.00000
DATE 2015 4  3.00000
DATE 2015 4  4.00000
DATE 2015 4  5.00000
SHUTIN 'injector'
DATE 2015 4  6.00000
DATE 2015 4  7.00000
PRODUCER 'producer'
OPERATE  MIN  BHP  800.0  CONT
OPERATE  MAX  STG  4  CONT
OPERATE  MAX  STW  2  CONT
OPEN 'producer'
DATE 2015 4  8.00000
DATE 2015 4  9.00000
DATE 2015 4 10.00000
DATE 2015 4 30.00000
DATE 2015 5 10.00000
```

```
INJECTOR MOBWEIGHT IMPLICIT 'injector'
INCOMP  GAS  0.0  1.0  0.0  0.0  0.0
TINJW  24.0
OPERATE  MAX  BHP  1000.0  CONT
OPERATE  MAX  STG  50.0  CONT
OPEN 'injector'
PRODUCER 'producer'
OPERATE  MIN  BHP  950.0  CONT
OPERATE  MAX  STG  2  CONT
OPEN 'producer'
DATE 2015 5 11.00000
DATE 2015 5 30.00000
DATE 2015 6 30.00000
DATE 2015 7 30.00000
**---------------------------------------cycle - 7
INJECTOR MOBWEIGHT IMPLICIT 'injector'
INCOMP  WATER  1.0  0.0  0.0  0.0  0.0
TINJW  212.0
QUAL  0.9
OPERATE  MAX  BHP  2000.0  CONT
OPERATE  MAX  STW  2.0  CONT
SHUTIN 'producer'
DATE 2015 8  1.00000
DATE 2015 8  2.00000
DATE 2015 8  3.00000
DATE 2015 8  4.00000
DATE 2015 8  5.00000
SHUTIN 'injector'
DATE 2015 8  6.00000
DATE 2015 8  7.00000
DATE 2015 8  8.00000
PRODUCER 'producer'
OPERATE  MIN  BHP  800.0  CONT
OPERATE  MAX  STG  4  CONT
OPERATE  MAX  STW  2  CONT
OPEN 'producer'
DATE 2015 8  9.00000
DATE 2015 8 10.00000
DATE 2015 8 30.00000
DATE 2015 9 15.00000
INJECTOR MOBWEIGHT IMPLICIT 'injector'
INCOMP  GAS  0.0  1.0  0.0  0.0  0.0
TINJW  24.0
OPERATE  MAX  BHP  1000.0  CONT
OPERATE  MAX  STG  50.0  CONT
OPEN 'injector'
PRODUCER 'producer'
OPERATE  MIN  BHP  950.0  CONT
OPERATE  MAX  STG  2  CONT
OPEN 'producer'
DATE 2015 9 16.00000
DATE 2015 9 30.00000
DATE 2015 10 30.00000
DATE 2015 11 30.00000
DATE 2015 12 30.00000
STOP
```